



UNIVERSITÀ
DEGLI STUDI
DI PADOVA

Sede Amministrativa: Università degli Studi di Padova

Dipartimento di Salute della Donna e del Bambino – SDB

CORSO DI DOTTORATO DI RICERCA IN:
MEDICINA DELLO SVILUPPO E SCIENZE DELLA PROGRAMMAZIONE SANITARIA
CURRICULUM: Emato-oncologia, genetica, malattie rare e medicina predittiva
CICLO XXXIV

**DEVELOPMENT AND CHARACTERIZATION
OF *IN VIVO* PRECLINICAL MODELS
FOR AN EFFECTIVE THERAPEUTIC STRATEGY
IN PEDIATRIC ACUTE MYELOID LEUKEMIA**

Coordinatore: Ch.mo Prof. Gianni Bisogno

Supervisore: Prof.ssa Martina Pigazzi

Dottoranda: Dott.ssa Ambra Da Ros

*“Ciò che è difficile attrae,
l'impossibile seduce,
ciò che è complicato spaventa,
ciò che è estremamente complicato innamora”*

INDEX

SUMMARY	3
CHAPTER 1	5
INTRODUCTION	5
1. ACUTE MYELOID LEUKEMIA	5
1.1 Pediatric AML genetic landscape.....	7
1.2 Pediatric AML classification	12
1.3 Pediatric AML diagnosis, treatment and outcome.....	15
1.4 Pitfalls of AML standard care and new therapeutic approaches for pediatric AML	18
2. AML PRECLINICAL MODELS.....	21
2.1 <i>In vitro</i> AML preclinical models	21
2.2 <i>In vivo</i> AML preclinical models	23
3. PRECISION MEDICINE AND PERSONALIZED TREATMENT APPROACHES	30
REFERENCES	34
CHAPTER 2	39
“DEVELOPMENT AND CHARACTERIZATION OF <i>IN VIVO</i> PRECLINICAL MODELS FOR AN EFFECTIVE THERAPEUTIC STRATEGY IN PEDIATRIC ACUTE MYELOID LEUKEMIA”	39
1. INTRODUCTION	39
2. AIM	40
3. MATERIALS AND METHODS	41
4. RESULTS.....	53
4.1 AML patient derived xenograft (PDX) establishment.....	53
4.1.1 AML-PDX generation timing	57

4.1.2 Variables associated with AML engraftment success.....	62
4.2 AML-PDXs characterization	64
4.2.1 PDXs genetic markers and immunophenotypic features	65
4.2.2 WHOLE EXOME SEQUENCING	68
AML variants, AML clonal composition and AML clonal dynamics <i>in vivo</i>	68
4.2.3 RNA SEQUENCING.....	86
PDXs' transcriptome analysis.....	86
Differential gene expression analysis	87
4.3 New targeted drugs identification and testing	88
4.3.1 Drug testing in AML cell lines.....	89
4.3.2 Testing of selected drugs on primary <i>ex vivo</i> cells	93
4.3.3 <i>In vivo</i> testing of the most promising drugs combinations	98
CHAPTER 3	101
APPLICATION OF ESTABLISHED PRECLINICAL AML MODELS	101
CHAPTER 4	109
DISCUSSION AND CONCLUSIONS	109
REFERENCES	119
ABOUT THE AUTHOR.....	127
ACKNOWLEDGEMENTS.....	133

SUMMARY

In pediatric acute myeloid leukemia (AML) chemotherapy is the standard of care, but more than 25% of patients still relapse and after a disease recurrence the survival probability is extremely low (<50%). There is an urgent need to discover new treatments to ameliorate patients' outcome. However, pediatric drug development is extremely reduced by the need of a better understanding of the adverse event profile of adult cancer indications in children, by the lack of pediatric-specific formulations, and by the reduced number of pediatric AML patients that can be included in clinical trials. Therefore, robust preclinical AML models to faithfully predict new drug efficacy is urgently needed to advance new drugs in clinical setting.

This PhD thesis aims at the development of more reliable preclinical models to improve treatments for children suffering from life threatening AML.

During my PhD I established patient derived xenograft models (PDX) of pediatric AML. Primary AML samples have been inoculated in NSG mice and, when engrafted, in 3 consequent mice recipients (namely P0, P1 and P2-PDXs). These models have been characterized for AML immunophenotypic profile and by RNA and whole-exome sequencing (WES). According to somatic mutations we determined AML clonal composition. These characterization allowed to select new drugs to be screened *in vitro* and *in vivo*. We finally generated 22 AML-PDXs mostly representing high-risk AML genetic markers such as t(5;11)*NUP98-NSD1*, t(3;5)*NPM1-MLF1*, t(16;16)*CBFA2T3-GLIS2*, t(16;21)*FUS-ERG*, *KMT2A* somatic translocations, or *FLT3ITD* mutation. We monitored the AML associated immunophenotype in PDXs finding it similar to that of the original AML. By WES we detected a consistent number of variants in each patient's AML (ranging from 28 to 69), confirming a high intra-tumoral AML heterogeneity. Furthermore, we did not find any mutation recurrence among models, underlining a high inter-tumoral heterogeneity. In all models we tracked clonal evolution from patients' AML to P2-PDXs highlighting that most variants were maintained, with very few variants acquired or lost during model development. Monitoring clonal dynamics we recognized a specific "founder" clone characterized by an average of 30 variants which are maintained up to P2 at the same allelic frequency, other small clones with an

average of 10 variants increasing the allelic frequencies in P2 and, in a restricted number of models some lost clones. By WES and transcriptome analysis we highlighted druggable mutations and pathways allowing the selection of novel targeted drugs. We screened their efficacy *in vitro* alone or combined with Venetoclax, using AML *ex vivo* cells and mesenchymal stromal cells in a 3D co-culture system for exploring their synergy in reducing AML proliferation. This refinement permitted to select two drugs currently under evaluation in AML-PDX models.

Overall, in this work we created a large series of paired AML and xenograft models for advancing pediatric AML therapeutics. Our models represent a concrete perspective for both the identification of new variants and pathways involved in AML progression to deepen into AML biology, as well as the possibility to perform novel drug screenings that will be further used to increase AML drug portfolio, with the final aim to translate new drugs into human clinical trials, contributing to cure pediatric AML.

CHAPTER 1

INTRODUCTION

1. ACUTE MYELOID LEUKEMIA

Hematopoiesis is a sophisticated cell differentiation process, that take place in the bone marrow (BM). All blood components are produced by single precursors, the pluripotent hematopoietic stem cells (HSCs), able to give rise to all mature circulating blood cells (erythrocytes, platelets, lymphocytes, monocytes/macrophages and neutrophilic, eosinophilic, and basophilic granulocytes). HSCs are at the center of lifelong blood cell production and are characterized by two fundamental properties including self-renewal ability, a cell division process that results in two HSCs, and multipotency referred to their differentiation capacity resulting into the production all mature blood lineages (Figure 1).

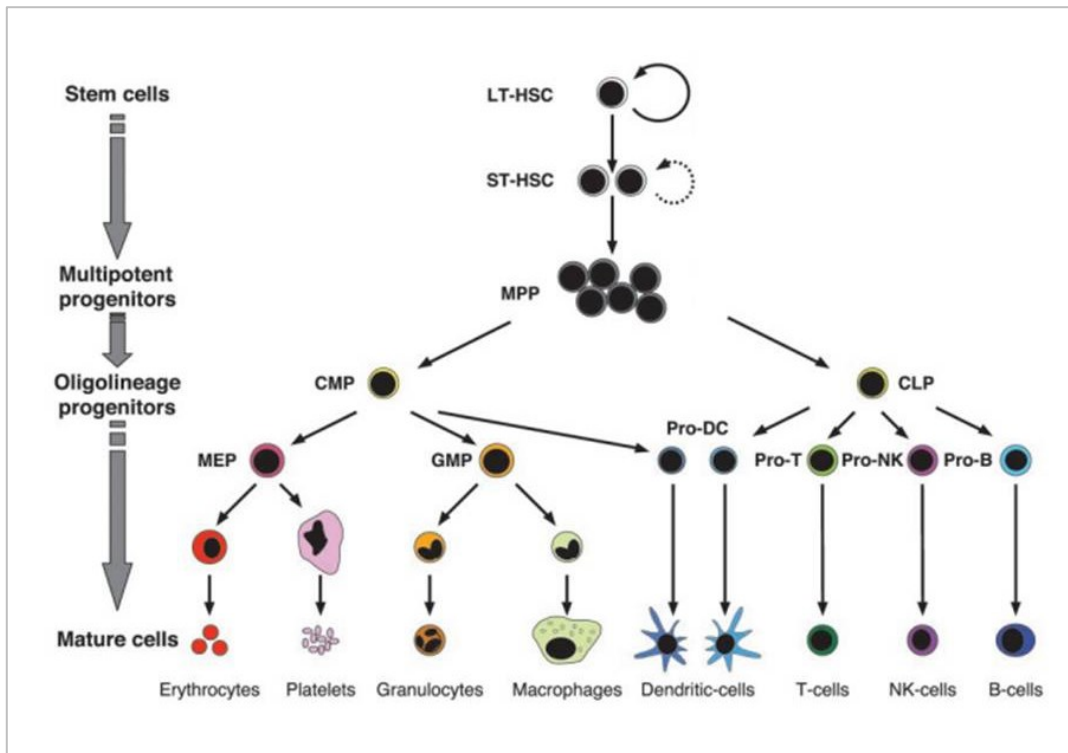


Figure 1. Hematopoiesis derives from an hematopoietic stem cells (HSCs) that differentiates into mature and specialized blood cells (adapted from¹).

The balance between self-renewal and maturation process is achieved thanks to cell intrinsic genetic differentiation programs and to a complex network of microenvironmental factors controlling cell fate decision within BM “niche”^{1,2}. The BM “niche” is populated by hematopoietic cells and by surrounding cells, such as mesenchymal stromal cells (MSCs) that are able to differentiate into osteoclasts, osteoblasts and adipocytes, endothelial cells, sympathetic neurons, and Schwann cells; signals from surrounding cells together with non-cellular components typical of BM niche like extracellular matrix (ECM) proteins, including collagen, fibronectin, laminin and hyaluronic acid are known to have important roles in the tight regulation of hematopoiesis (Figure 2)³⁻⁵.

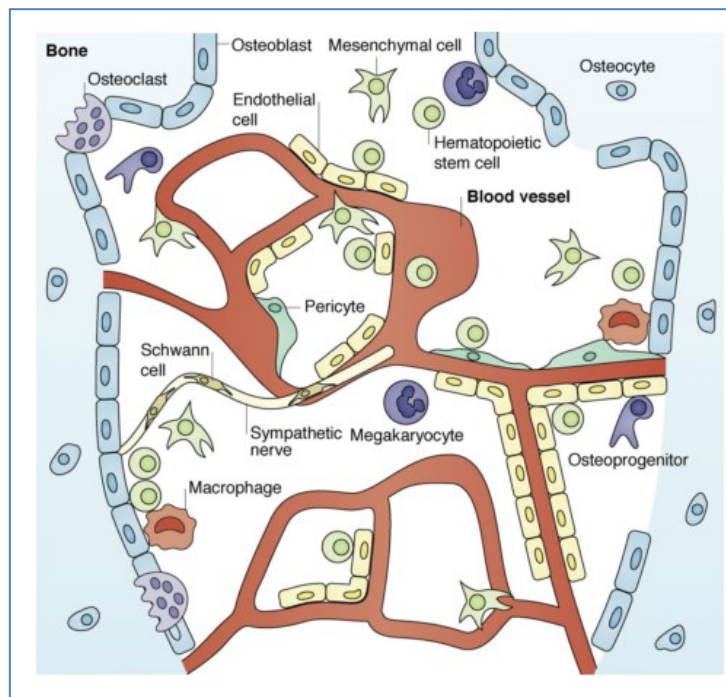


Figure 2. The hematopoietic BM niche where HSCs differentiate into blood cells such as macrophages and megakaryocytes, and surrounding composed by MSC, osteoblasts/osteocytes and osteoclasts, Schwann cells, and endothelial cells. All these cell types cooperate in the regulation of hematopoiesis (adapted from⁶).

Defects in hematopoietic process result in homeostatic imbalance in the production of mature blood cells, leading to hematological disorders including leukemia. Leukemia arises from genetic mutations occurring in a cell, called leukemic stem cell (LSC), that

acquires uncontrolled proliferation ability and lose its differentiation potential⁷. Depending on which progenitor is corrupted in differentiation and proliferation capabilities, it is possible to distinguish lymphoblastic leukemia, which arises from a lymphoid progenitor, or myeloid leukemia in which the precursor belongs to the myeloid lineage. In particular, Acute Myeloid Leukemia (AML) is characterized by the accumulation of myeloblasts with impaired differentiation capacity into the BM. These immature cells, called blasts, invade the BM, and repress the normal hematopoiesis resulting in patients symptoms like fatigue, bleeding, fever, anemia or thrombocytopenia, recurrent infections, pain in bones and joints, cutaneous manifestations and enlarged lymph nodes, liver and spleen. Leukemia can be defined as “acute” if patient’s BM aspirate presents at least 20% of blasts^{1,7}.

Acute leukemia is the most common cancer in childhood and in particular AML represent 15-20% of leukemia cases. The incidence of AML in childhood is 7-8 cases per million per year and every year in Italy there is an average of 70 new pediatric patients suffering from *de novo* AML. The majority of pediatric AML cases occur *de novo*, but in some cases AML can occur as a secondary malignancy⁷.

1.1 Pediatric AML genetic landscape

AML is a heterogeneous disease in term of morphology, immunophenotype cytogenetic and molecular genetics. This heterogeneity has been often associated with the wide spectrum of genetic mutations occurring in leukemogenesis. Historically, there are two main types of genetic aberrations namely type I mutations (occurring in genes such as *RAS*, *c-KIT*, *FLT3*) that confer proliferative advantages to cells, and type II mutations that lead to impaired hematopoietic differentiation process. An example of type II alteration is mutation at *KMT2A* (Lysine-specific MethylTransferase 2A) gene, which regulates the expression of crucial transcription factors involved in hematopoiesis control. *KMT2A* rearranges with multiple partners genes by chromosomal somatic translocation giving rise to chimeric transcripts with leukemogenic activity. The most common *KMT2A* partner genes are *MLLT3*, *MLLT10*, *AFDN* resulting in recurrent t(9;11)(p22;q23), t(10;11)(p12;q23) and t(6;11)(q27;q23) fusion genes. Other recurrent type II alterations involve core binding factors (CBF) genes giving rise to recurrent AML gene fusions namely t(8;21)(q22;q22) *RUNX1-RUNX1T1* or inv(16)(p13q22) *CBFB-MYH11*⁷. Type I and

Type II mutations combined randomly in AML cells, but selective mutational combinations have been observed (Figure 3), such as RAS mutations with *KMT2A*-rearrangements and *KIT* mutations with *CBF* rearrangements (Figure 3)⁷.

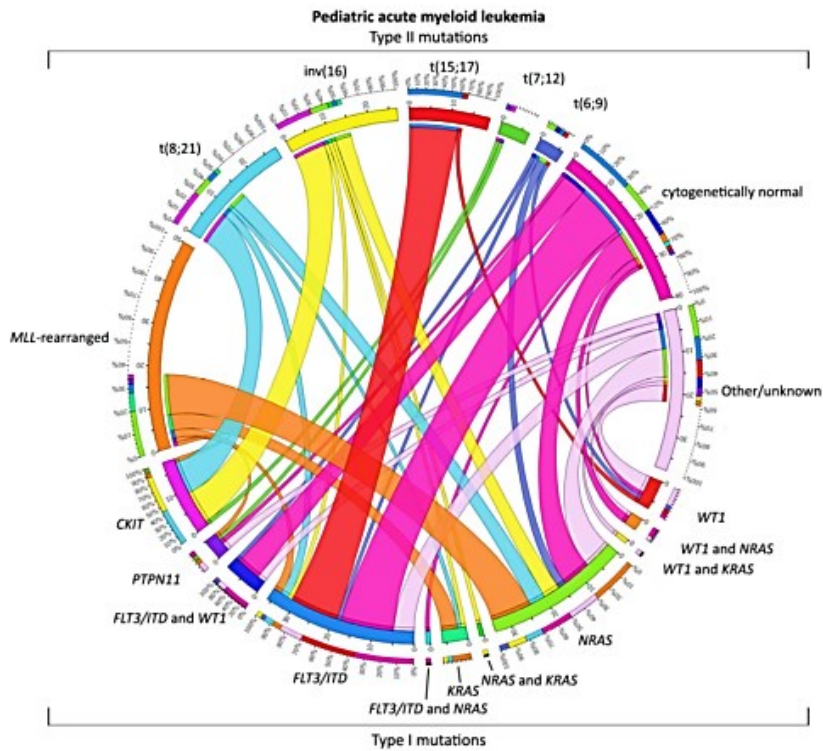


Figure 3. Distribution of type I and II abnormalities in pediatric AML. The circos plot depicts the frequency of type II mutations and the co-occurrence with type I mutations in de novo pediatric AML. The length of arch corresponds to the frequency of type II mutation and the width of the ribbon to the percentage of patients with a specific type I mutation or a combination of type I mutation (from⁷).

However, mutational landscape of AML increased, and the model of AML pathogenesis has been improved. In particular, additional categories of mutations has been described to cooperate in the onset of AML: class III mutations leading to defects in genes involved in epigenetic regulation, class IV mutations affecting cellular adhesion genes and genes regulating pathways related to migration and finally class V mutations altering genes that regulate DNA repair and splicing (Figure 4). The onset of these mutations, affecting different crucial process, suggest the disruption of a complex network that is fundamental for normal hematopoiesis, leading to leukemia onset.

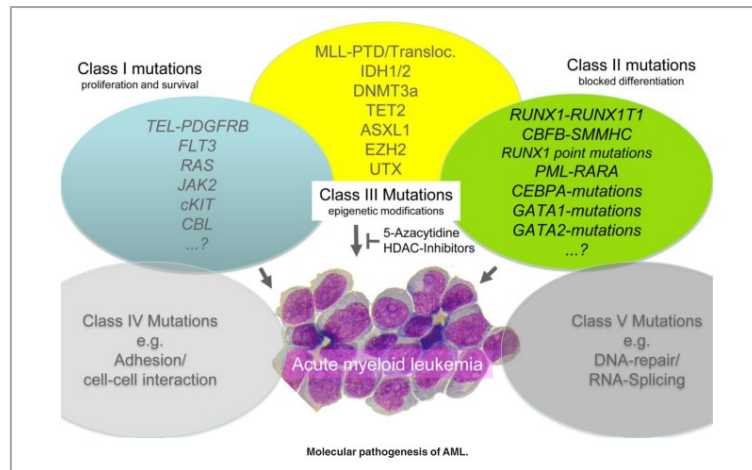


Figure 4. Schematic representation of AML pathogenesis theory based on five classes of mutations affecting genes involved in different pathways (from ⁸).

These recurrent AML mutations occur in a small pool of cells, defined as leukemic stem cells (LSCs), that could be immature or progenitor cells that re-acquire self-renewal ability in an aberrant form¹. LSCs acquiring one or more driver mutations proliferate in uncontrolled way, giving rise to the tumor founding clone. These cancer cells gain and accumulate additive mutations during time, evolving in genetically distinct sub-clones during the progression of the disease, under therapy pressure and at relapse. This process, known as “clonal evolution”, leads to a significant inter and intra-tumor heterogeneity. Clonal evolution is a term referred to the onset and in some cases to the selection and expansion of different leukemic subclones, originated from a single ancestral clone that, acquiring new mutations, give rise to genetically and functionally different subclones. It is possible to subdivide in primary/dominant mutations those typical of tumor founding clone and maintained during disease progression, and secondary alterations occurring later on in subclones, leading to changes in cancer composition during time. Several studies have been done to deeply characterize AML clonal evolution, in by studying clonal composition of coupled AML specimen at onset, at remission and at relapse by whole exome sequencing (WES) or whole genome sequencing (WGS)^{9–15} (examples and graphical representations of AML clonal evolution are reported in Figure 5 and Figure 6). As supported by Farrar et al., pediatric AML relapse seems to be associated to a clonal evolution from diagnosis, and this clonal

dynamics may be associated to chemotherapy pressure and to distinct subclones fitness of escaping therapy and re-emerge¹³.

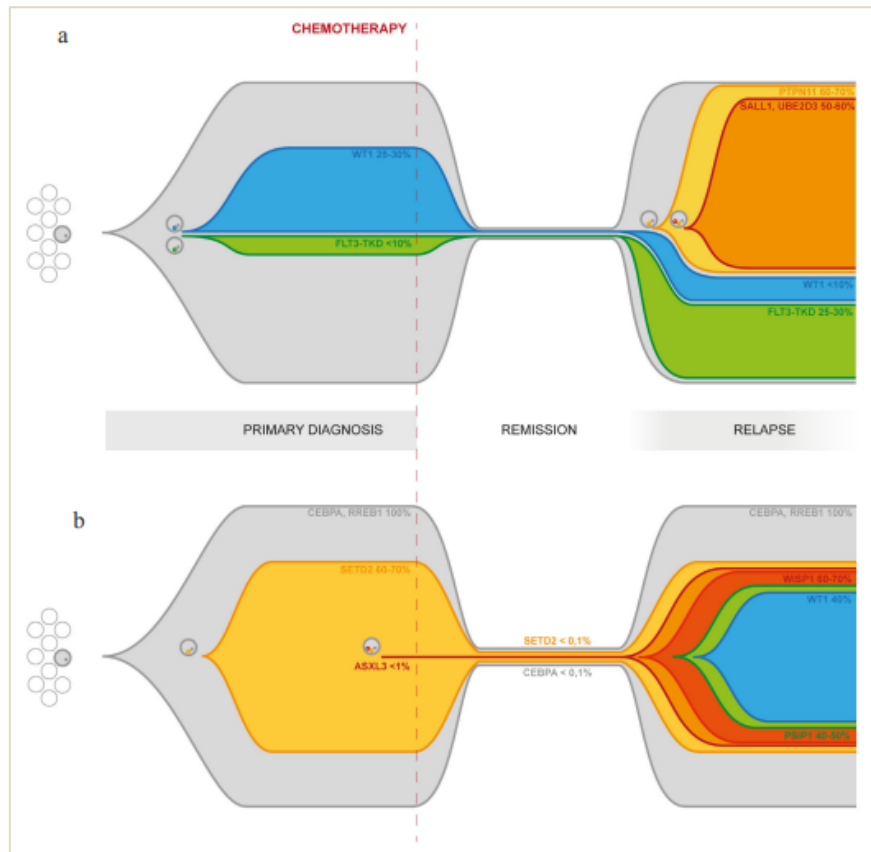


Figure 5. AML clonal evolution representation of two AML case where clones detected at diagnosis harbors different mutations with respect to clones detected at relapse indicating clonal composition modifications occurring during time (from⁹).

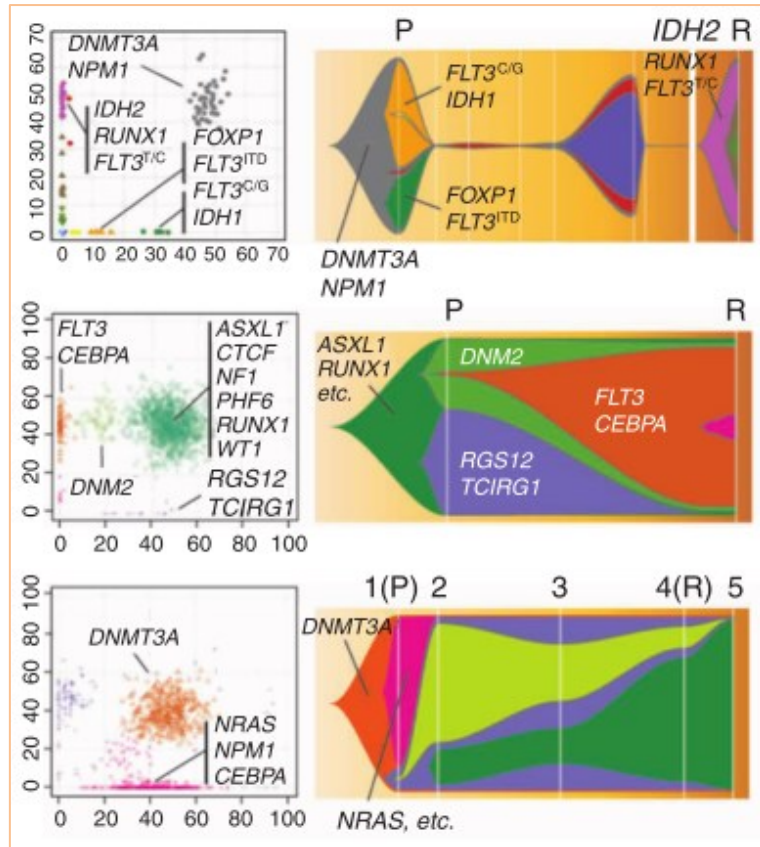


Figure 6. AML subclonal composition by WGS. Variant allele frequencies of each somatic mutations (represented by dots) in samples at diagnosis (P) and relapse(R); dot colors represent subclones, reported also in Fish plots where ribbons represent each subclone and respective height indicates the percentage of the tumoral cells within clones. Selected driver mutation genes are reported (adapted from ¹⁵).

In particular literature reported the detection of recurrent somatic mutations (in genes such as *FLT3*, *NRAS*, *PTPN11*, *WT1*, *TET2*, *DHX15*, *DHX30*, *KIT*, *ETV6*, *KRAS*) in pediatric AML samples at diagnosis, with variable persistence in AML samples at relapse, indicating that mutations characterized by significantly higher variant allele frequency (VAF) at diagnosis usually persist at relapse, compared with alterations with lower VAF that more frequently disappear in relapsed samples¹³. This clonal evolution pattern suggested that clones characterized by higher VAF mutations at diagnosis are probably represented also at relapse. Noteworthy, this complex clonal architecture is reflected into a functional heterogeneity, demonstrated by the acquisition of different clones

abilities, such as mice engraftment, *in vitro* expansion, therapy evasion, and recapitulating a disease relapse^{11,12}.

Overall, a lot of efforts in the dissection of AML clonal compositions and clonal dynamics during leukemia progression have been spent, and further work is needed for a better comprehension of the pathology. Indeed, studies on clonal evolution are still fundamental to unravel relations between gene mutations and subclones functionalities, helping to investigate molecular mechanisms involved in relapse and molecular clues for the identification of innovative therapeutic strategies, based on target selection¹⁰. The mutation profile, improved by VAF analysis, has important implications in treatment assignment, considering recently therapy decisions based on genomic rather than morphologic classification, and a deeper understanding of the contribution given by different mutations is critical to prioritize genomic events thus ameliorate treatment and patients' outcome.

1.2 Pediatric AML classification

Historically different subtypes of AML were defined according to FAB (French-American-British) classification based on morphological and cytochemical characteristics thus subdividing AML into 8 groups namely from M0 to M7 (Table 1)¹⁶.

FAB classification	Features
M0	AML with minimal differentiation
M1	Myeloblastic leukemia without maturation
M2	Myeloblastic leukemia with maturation
M3	Acute promyelocytic leukemia
M4	Acute myelomonocytic leukemia
M5	Acute monoblastic leukemia
M6	Acute erythroblastic leukemia
M7	Acute megakaryoblastic leukemia

Table 1. FAB classification of acute myeloid leukemia.

The FAB classification system was commonly used to group AML into subtypes, but while recognizing the morphological heterogeneity of the disease, it has limited power in reflecting the biological, genetic and clinical characteristics, resulting in limited prognostic significance. These considerations, in parallel with the progressive emergence of the great prognostic value of cytogenetic-molecular alterations, highlighted the revision of this classification that was published by the World Health Organization (WHO) in 2001¹⁷, then followed by two other revisions, in 2008¹⁸ and in 2016¹⁹. The first FAB classification remained relevant, but new WHO subcategories such as “not otherwise specified”, and several other specifications were included. In general, WHO classification is mainly based by morphology and recurrent chromosomal and genetic alterations with known prognostic significance, which better characterize disease biology. Starting from the WHO 2001 classification, the blasts threshold above which AML can be diagnosed was lowered from 30% to 20%, a part from the presence of neoplastic cells with recurrent genetic anomalies (t(8;21)RUNX1-RUNX1T1, inv(16)CBFB-MYH11, and t(15;17)PML-RARA chromosomal translocations) for whom diagnosis of AML is done regardless blasts threshold (Table 2, revision 2016).

2016 WHO classification of Acute Myeloid Leukemia (AML)	
AML with recurrent cytogenetic abnormalities	
	AML with t(8;21)(q22;q22.1) <i>RUNX1-RUNX1T1</i> ;
	AML with inv(16)(p13;q22) or t(16;16)(p13;q22) <i>CBFB-MYH1</i> ;
	APL with PML-RARA AML with t(9;11)(p21.3;q23.3) <i>MLLT3-KMT2A</i>
	AML with t(6;9)(p23;q34.1) <i>DEK-NUP214</i>
	AML with inv(3)(q21.3q26.2) or t(3;3)(q21.3;q26.2) <i>GATA2-MECOM</i>
	AML (megakaryoblastic) with t(1;22)(p13.3;q13.3) <i>RBM15-MKL1</i>
	Provisional entity: AML with <i>BCR-ABL1</i>
	AML with mutated <i>NPM1</i>
	AML with biallelic mutations of <i>CEBPA</i>
	Provisional entity: AML with mutated <i>RUNX1</i>
AML with myelodysplasia-related changes	
Therapy-related myeloid neoplasms	
AML, NOS	
	AML with minimal differentiation
	AML without maturation
	AML with maturation
	Acute myelomonocytic leukemia
	Acute monoblastic/monocytic leukemia
	Pure erythroid leukemia
	Acute megakaryoblastic leukemia
	Acute panmyelosis with myelofibrosis
	Acute basophilic leukemia
Myeloid sarcoma	
Myeloid proliferations related to Down syndrome	
	Transient abnormal myelopoiesis (TAM)

Table 2. WHO revised classification of acute myeloid leukemia (2016).

1.3 Pediatric AML diagnosis, treatment and outcome

According to the guidelines of the Associazione Italiana di Ematologia e Oncologia Pediatrica (AIEOP) AML diagnosis is based on the evaluation of different criteria of patients' BM aspirate: cells morphology, immunophenotype (analysis of the presence of specific surface markers typical of different lineage and different cell maturation steps), cytogenetic and molecular characterization. Morphological and cytochemical examination are necessary to determine the FAB subtype, immunophenotypic analysis for the characterization of the cellular lineage and maturation level of the neoplastic cells, cytogenetic and molecular biology investigations are fundamental for the evaluation of the presence of known prognostic abnormalities. Starting from 2002, the first risk stratification trial based on genetic abnormalities, the "AIEOP AML 2002/01 Protocol", was introduced by the AIEOP group. In particular, a molecular genetic screening was introduced for the evaluation of alterations known to be predictive of disease course, allowing a two-group risk stratification (high and low risk) ²⁰.

During this years, many other genetic mutations have been identified and associated with clinical risk²¹⁻²⁵. The continuous search for new genetic lesions is pursued by several groups for the improvement in AML stratification. This increased molecular genetic characterization was fundamental not only for a risk group refinement at diagnosis, but also to identify suitable markers for the monitoring of disease progression, indicative of both therapy response during treatment and of disease recurrence. Treatment response is evaluated by complete remission (CR) achievement and defined as blasts percentage minor then 5% by morphological analysis; nevertheless, the use of methods with higher sensitivity with respect to morphological analysis, in order to detect blasts persistence, is under evaluation. Minimal residual disease (MRD) monitoring has been taken into high consideration since this approach quantifies blasts after therapy by immunophenotypic evaluation by flow cytometry (multi-parameter flow cytometry, MFC) or by polymerase chain reaction (PCR) thanks to the presence of a molecular marker (molecular MRD)²⁶⁻²⁸.

Molecular MRD relies on genetic markers detected in AML samples at diagnosis, and allows following blasts clearance during therapy with high sensitivity and before clinical and morphological evidence, thus creating pre-emptive therapy opportunities.

Nowadays the molecular diagnostic screening of AML evaluates more than 40 genetic aberrations, most being somatic translocations or inversions, point mutations or internal repeats affecting different genes. On the basis of the improved genetic characterization, the “AIEOP AML Protocol 2013” started in 2015 introduced a new risk- based classification strategy. This protocol includes three risk classes defined as standard risk (SR), intermediate risk(IR) and high risk (HR) classes, that are based on genetic/cytogenetic abnormalities and early response to therapy, thanks to MRD evaluation by flow cytometry after induction therapy (Table 3) ²⁸. Patients’ stratification on three risk groups implies different therapeutic approaches. The induction therapy, relying on the use of Idarubicin, Cytarabine and Etoposide (ICE), is usually sufficient to reach a CR in patient of SR group, whereas subsequent different consolidation therapies are needed for IR-HR patients; in particular patients belonging to IR class, when in CR after consolidation cycles of chemotherapy are enrolled for the hematopoietic stem cell transplantation (HSCT) only in the presence of a family-matched donor, whereas the HSCT from any donor is considered for patients belonging to HR group^{20,29,30}.

RISK GROUP	PROGNOSTIC MARKERS
STANDARD RISK (SR)	<ul style="list-style-type: none"> • <i>CBFβ</i> rearrangements (without concomitant cytogenetic abnormalities) and MRD < 0.1% after first induction • t(8;21)(q22;q22) • inv(16)(p13q22) • t(16;16)(p13;q22) • Patients with normal karyotype and <i>NPM1</i> mutations with MRD < 0.1% after first induction
INTERMEDIATE RISK (IR)	<ul style="list-style-type: none"> • Normal Karyotype • t(9;11)(p22;q23) with no other concomitant cytogenetic abnormalities • t(1;11)(p32;q23) • t(11;19)(p13;q23) • t(16;21)(p11;q22)<i>FUS-ERG</i> • t(3;5)(q25;q34) • Other cytogenetic abnormalities • M7 harboring t(1;22), irrespectively of patient's age • Patients not belonging to SR nor HR groups • Patients with 0.1%<MRD>1% after first induction and MRD<0.1% after second induction
HIGH RISK (HR)	<ul style="list-style-type: none"> • Cytogenetic abnormalities associated with poor outcome: <ul style="list-style-type: none"> - Complex Karyotype (>3 abnormalities) - Monosomal Karyotype (-7, -5, other) - t(9;11)(p22;q23) associated with concomitant cytogenetic abnormalities - Cytogenetic abnormalities involving 11q23 not included in IR: t(11;17)(q23;q21), t(10;11)(p12;q23), t(4;11)(q21;q23), t(6;11)(q27;q23), t(X;11) -Rare cytogenetic abnormalities: t(6;9)(p23;q34), t(8;16)(p11;p13), t(9;22)(q34;q11) t(5;11)<i>NUP98-NSD1</i>, t(4;11)<i>KMT2A-ArgBP2</i> • <i>FLT3</i>-ITD • Cytogenetically normal AML expressing the chimeric transcript <i>CBFA2T3-GLIS2</i> FAB M0, M6, M7 without t(1;22) • Infants (excluding M7 AML harboring t(1;22)) • Patients with incomplete morphological remission after first induction • MRD>1% after first induction or MRD>0.1% after second induction • Patients not belonging to SR group and WBC>100.000/μL

Table 3: Stratification criteria according to AIEOP AML 2013/01 protocol.

The prognosis of Italian children affected by AML has been significantly improved over the last two decades. Currently, the Overall Survival (OS) and the Event Free Survival (EFS) at 8 years are estimated respectively of 68% and 55%²⁰. This progress can be attributed to a more precise patients stratification, an optimization of induction therapy, an increased supportive therapy, and to the wide use of HSCT^{20,31}.

1.4 Pitfalls of AML standard care and new therapeutic approaches for pediatric AML

Despite the improvement in patients' outcome, still 30% of children relapse and after disease recurrence the survival probability is extremely low (<50%)^{7,32}. The gold standard pharmacological treatment for pediatric AML is still based on the use of cytotoxic agents that induce cell and organs toxicity with severe late effects. The most frequent forms of toxicity due to chemotherapeutic agents include cardiotoxicity, gastrointestinal toxicity and neurotoxicity; neutropenia and disruption of skin and mucosal barriers are other complications that arise from intensive chemotherapy and that often lead to bacterial and fungal infections. Moreover, the wide use of HSCT confers a high risk of graft versus host disease (GVHD) and death. As a consequence of these treatment-related complications 5% of pediatric AML patients die during treatment, therefore a further intensification of this therapeutic strategy is not recommended.⁷

To ameliorate patient outcome there is an urgent need to discover new treatment approaches, those based on specific molecular alterations would create a targeted/personalized therapy toward leukemic blasts, that will help not only in preventing relapse, but also in reducing toxicity.

Recent advances in cancer genomics provide new insights into leukemogenesis and into AML drug resistance suggesting novel treatment strategies³³. By the way, even if a large number of molecular markers are taken into consideration for patient diagnosis, risk stratification and prognosis evaluation, still a very few number of targeted therapies have been translated into clinic for pediatric cancer.

This latter phenomenon is related to the fact that new drugs approved for adult AML treatment³³, cannot be easily translated into pediatric context because adult and childhood present different genetic background and different treatment tolerability³⁴. Moreover, the difficult translation from bench to bedside is strengthened by the low

number of pediatric AML cases, further subdivided accordingly to the sophisticated genetic characterization, that is not sufficient to start clinical trials.

Trying to overcome these limitations, national and international collaborative efforts has been put in the last years, by starting multicenter clinical trials for the screening of new therapies³⁵ in enlarged cohort of patients, where more robust results to identify therapies to be included in future protocols will be reached.

In this context a multi-stakeholder Paediatric Strategy Forum focused on AML in children and adolescents has been organized by the ACCELERATE group in collaboration with the European Medicines Agency (EMA) and Food and Drug Administration (FDA). The aim of this consortium is to enhance the development of innovative treatment for pediatric patients affected by AML and to finally include new drugs into the standard-of-care³⁴.

Thus, new drugs targeting key molecular pathways are under investigation for the management of pediatric AML, some relevant examples are kinase inhibitors (like Midostaurin, Quizartinib, Dasatinib, Trametinib) epigenetics regulators (like azacitidine, decitabine, BET inhibitor, vorinostat) as well as apoptosis regulators (an important example is Venetoclax). Besides, immunotherapy using CAR-T cells against CD123 and CD33, are promising cell based therapy for childhood leukemia (Table 4)³⁴⁻³⁶.

Pathway/mechanism of action	Target	Drug name
Kinase inhibition	JAK-STAT pathway	Ruxolitinib
	FLT3 inhibitor	Midostaurin, quizartinib, lestaurtinib
	MEK inhibitor	Trametinib, selumetinib
	Multi-kinase inhibitors	Imatinib, ponatinib, dasatinib, sorafenib
Epigenetic targeting	HDAC	Vorinostat, panobinostat
	DNMT	Azacitidine, decitabine
	DOT1L	Pinometostat
Apoptosis	TP53	APR-246
	MCL1	S64315
	BCL2	navitoclax, venetoclax
	survivin	EZN-3042, LY2181308
	Other approaches	IDH1
CDK4/6		Palbociclib, ribociclib
PARP		Olaparib, veliparib
mTOR		Everolimus, emsirolimus, sirolimus
Menin		MI-463, MI-503, MI-1481, MI-525
CBF β -SMMHC		AI-10-49
Proteasome/ubiquitin	Proteasome	Bortezomib, carfilzomib, ixazomib
	MDM2	Idasanutlin, milademetan, ALRN-6924
	NEDD8	Pevonedistat

Table 4. Targeted therapies approved for pediatric leukemia, with relative druggable pathways and targets ³⁶.

However, to date in pediatric AML context novel therapeutic strategies have not been included in trials yet.

2. AML PRECLINICAL MODELS

Low drugs predictivity after pre-clinical studies and of low number of eligible patients strongly reduced the successful introduction of new drugs into clinical trials. Nowadays, 90% of drugs that resulted promising from preclinical testing are ineffective in clinics³⁷ underlining the limited effectiveness of traditional preclinical models, such as cell lines culture or xenografts mice models generated with cell lines³⁸. Faithful tools to ameliorate pre-clinical validation of new drugs are needed to hit Achilles' heel in pediatric oncology drug development.

As a matter of fact, in AML context, most of *in vitro* and *in vivo* models used for drug screening has been revealed inadequate, and most of innovative drugs that underwent investigation showed a lower efficacy in clinical setting with respect to the preclinical testing. Main limitation is the inability to recapitulate physiological leukemia context, including inter- and intra-tumor genetic heterogeneity, cell-cell and cell-stroma interactions, as well as the BM microenvironment, all aspects playing fundamental roles in treatment response.

2.1 *In vitro* AML preclinical models

Historically, conventional *in vitro* models were represented by cell lines, that even if easy to use have important limitations: cell line generation process implies the complete loss of intra-tumoral heterogeneity, making impossible to take into consideration genetic and functional heterogeneity in studies using cell lines, moreover during long-term culture *in vitro* these cells may acquire major alterations affecting important biological process (such as genetic alterations, differences in growth and in invasion properties). At last, cell lines are usually established from adults most aggressive tumors, hence not being representative of patients inter-tumoral heterogeneity³⁹.

The use of primary cells is favorable but presents some other limitations: in addition to the difficulty in obtaining patients' samples, some troubles emerge in the set-up of optimal culture conditions for the maintenance of both, cells viability and intra-tumoral heterogeneity, without selective pressure on clones. Moreover, standard cell cultures are not able to mimic the physiological context, indeed cells grow within artificial

environments, on non-physiological substrates (glass or plastics) with non- physiological growth factors and without possibility to interact with different cell types³⁹.

In particular the equilibrium in the BM niche is not achieved by hematopoietic stem cell (HSCs) or progenitors autonomously, but rather it is due to fundamental communications with the surrounding hematopoietic microenvironment. During leukemogenesis blasts compete with healthy hematopoietic cells for niche resources, modifying the BM microenvironment and transforming it in a "leukemic BM niche"⁴⁰. Several studies documented signals deriving from different cellular components (mesenchymal stromal cells, osteoblasts, endothelial cells, nervous cells) able to regulate malignant cells dormancy and to enhance evasion from chemotherapy, suggesting the interaction between tumoral cells and microenvironment being responsible for drug resistance^{2,41-43}.

Accordingly, recently more predictive and robust *in vitro* AML models based on the use of three dimensional (3D) co-culture systems have been proposed. In this context different primary cells (tumoral and stromal) can be co-cultured on particular substrates that mimic tumor BM microenvironment. These culture systems better recapitulate the characteristics of BM niche, such as stiffness and tumor-stroma interaction. Different materials for scaffolds compositions have been exploited in order to mimic bone structure (such as ceramic-collagen-hydroxyapatite-functionalized hydrogel), and to be co-cultured with different cell combinations^{40,44-47}. 3D co-cultures, besides mimicking the BM niche in term of composition and cells interactions, have been reported to permit a longer primary blasts proliferation (up to 21 days), preserving the immunophenotypic profile of AML cells at diagnosis⁴⁰. In addition, 3D systems showed an increased cells resistance to treatments with respect to monolayer cultures^{43,47-49}, highlighting the importance of taking into consideration the complex BM microenvironment for further studies on therapy response. Overall, AML 3D co-cultures are models of BM niche, suitable for more predictive drug screenings.

Microenvironment plays a fundamental role in tumor growth both, at biochemical and biophysical levels, and the complexity of *in vitro* culture systems could be useful to mimic physiological context. In particular the vasculature presence, providing cells nutrients in the bulk of 3D system is a challenge to generate more realistic *in vitro* models thanks to microfluidic techniques, that recently implemented these culture

systems allowing a systematic perfusion of culture medium. Microfluidic platforms, mimicking interstitial fluid flow, ensure nutrients supply to all cells, moreover this innovative culture systems permit an accurate control on matrix mechanical properties and fluidic shear stress, other important parameters to be considered in the setup of optimal *in vitro* culture systems⁵⁰. In addition bioprinting strategies allowed the development of sophisticated constructs for *in vitro* modeling, based on the use of computer aided technology to assemble multiple biomaterials and cell types into different layers, providing controlled 3D structures^{51,52}; overall these systems can be defined as “organ-on-chip” and the optimization of these extremely complex but realistic culture systems represents a goal to be achieved in a near future.

2.2 *In vivo* AML preclinical models

A key goal in AML research is to provide advanced knowledge to select appropriate treatments. Despite the advent of innovative *in vitro* tools better mimicking AML disease, the predictive value of data resulting from the use of these models is limited by the lack of whole-organism systems complexity. Therefore, AML *in vivo* model are still used to improve tumor research, and historically mice models have been pursued by using different approaches⁵³ :

- A) AML mice model induced by chemicals (e.g., 3-methylcholantrene), viral infection (e.g. murine leukaemia virus, MuLV) or irradiation (e.g X-ray);
- B) Genetically engineer AML mouse models: transgenic mouse generated by DNA insertion into the genome, either randomly by pronuclear microinjections (MI) into fertilized Oocytes, or targeted by electroporation (EP) and homologous recombination in embryonic stem cells (ESC);
- C) Mouse models based on adaptive transfer of hematopoietic cells retrovirally (RV) expressing an AML-associated proto-oncogene or AML mouse models generated with genome-editing (GE) techniques;
- D) Modelling AML by transferring cells lines into immune-compromised mice.

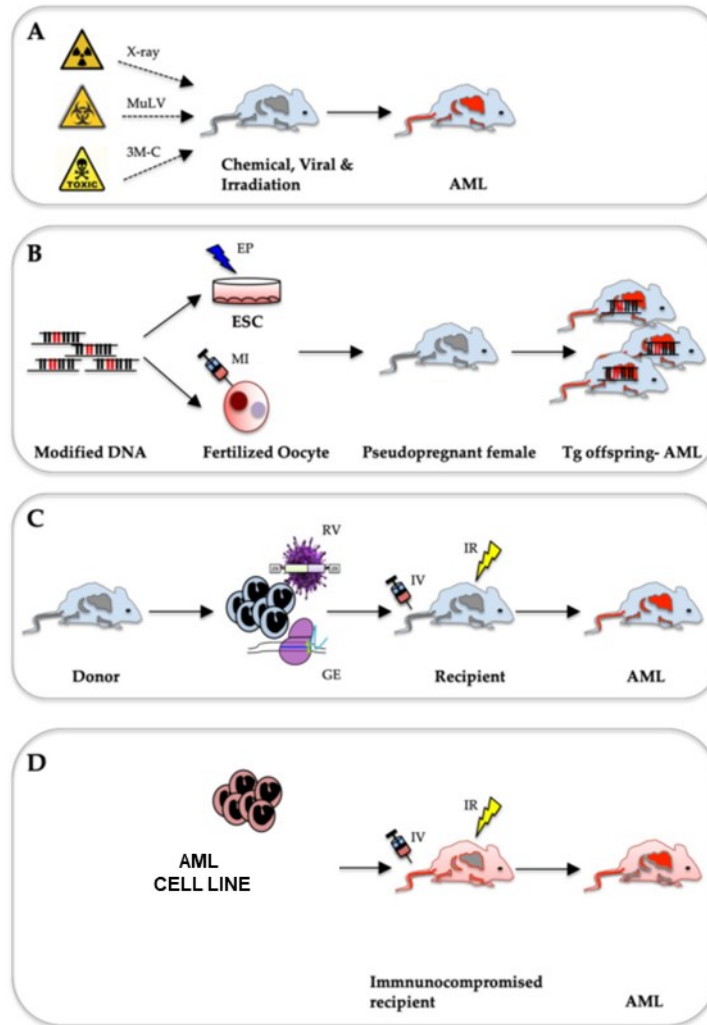


Figure 7. Approaches for AML mice model generation. (A) Spontaneous AML development upon exposure to carcinogens like chemicals, biologicals or radiation; (B) Conventional transgenic approach; (C) Adaptive transfer method of *in vitro* modified murine HSPC cells using either retroviral transduction or genome editing techniques followed by tail intravenous (IV) transplantation murine recipients; (D) xenotransplantation of AML cells lines into immunocompromised mice (adapted from ⁵³).

These models have been instrumental to decipher the underlying mechanisms of disease and advancing AML research. Historically, the chemical, irradiation and viral induced AML models were used to develop drugs. Transgenic mouse harboring AML associated genetic alterations enabled to link AML molecular features to disease initiation and progression ⁵³.

Nevertheless none of these models have been shown to faithfully recapitulate patients tumor heterogeneity and AML complex biology, the sophisticated genetic architecture of clonal evolution during tumor progression, nor therapy pressure and relapse occurrence^{9,14,15}.

More recently, patient derived xenografts (PDXs) models emerged as fundamental preclinical tool to substantially ameliorate drug testing process and to efficiently bridge bench and clinical data in translational research. PDXs generation consist of modelling tumor *in vivo* by directly transferring primary samples into immune-compromised mice, avoiding intermediate *in vitro* culture passages that may induce genetic transformations or clones selection. This methodology is based on sequential AML cells engraftment in different mice recipients. Briefly, once patient's tumor engrafts in mouse, denoted as PDX-P0, the harvested tumoral cells are subsequently inoculated in consecutive mice passage, in particular into two other recipients namely PDX-P1 and PDX-P2 (Figure 8). PDX-P2 is considered the stabilized model and subsequent mice expansion ensures a strong reproducibility of the original AML where reliable drug screening or biomarker evaluation studies can be performed^{38,54,55}.

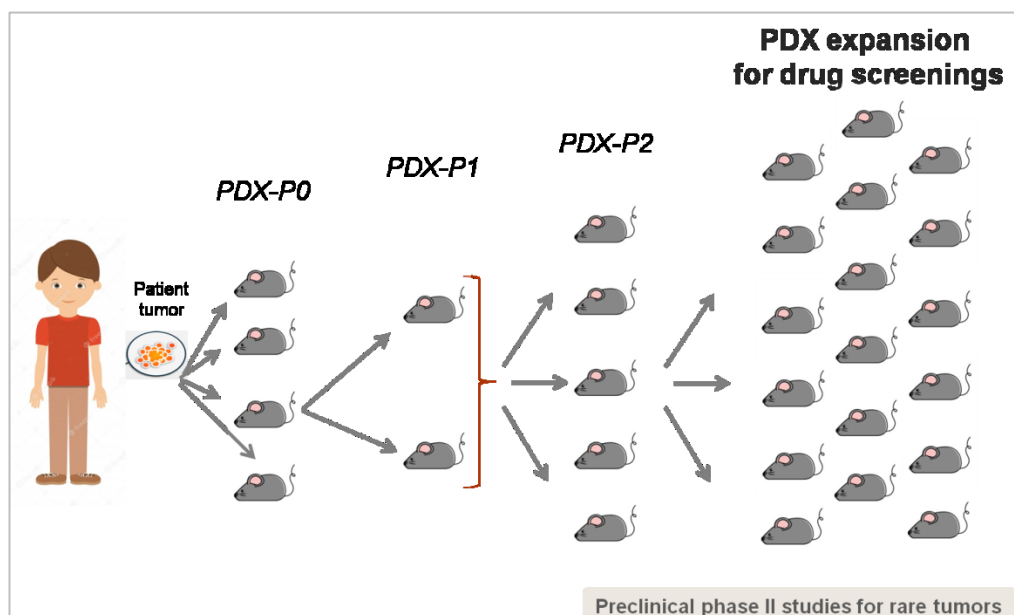


Figure 8. PDXs generation workflow: from primary patient's BM sample to subsequent transplantation passages in mice, up to stabilized PDX-P2 model.

The Pediatric Preclinical Testing Program (PPTP) is the first action in the field of pediatric oncology that aimed to generate PDXs and it is an initiative supported by the National Cancer Institute (NCI). PPTP would identify novel therapies by testing their activity in panels of PDX preclinical models, for their high potential for prioritizing agents that could advance in clinical trials for specific childhood cancers. Thanks to this initiative, panels of childhood cancer cell lines and *in vivo* xenografts models have been established. Tumors covered by these models were Wilms tumor, sarcomas (rhabdomyosarcoma, Ewing sarcoma, and osteosarcoma), neuroblastoma, brain tumors (glioblastoma, ependymoma, and medulloblastoma), rhabdoid tumors (CNS and renal), and acute lymphoblastic leukemia (ALL).⁵⁶

This initiative was successful, but several limitations concerning the use of PDXs as cancer models emerged, in particular:

- the low tumor engraftment rate renders the generation of these models time consuming, above all when designed for personalized treatment approaches;⁵⁷
- the murine context (tumor stromal cells and extracellular matrix) limits studies on tumor microenvironment;
- strong similarity between patient and PDX tumor has been largely reported, but fidelity and reliability of these models are still debated⁵⁸

The low engraftment rate remains one of the major limit in PDXs generation, and the introduction of highly immunocompromised mice (Table 5) is facilitating the use of PDXs as standard models for human cancer research.

Mouse Strain	Phenotype	Advantage	Disadvantage/Consideration	Success Rate of PDX
Nude	No thymus, no coat of hair	Well characterized, easy to detect s.c. tumor	Functional B and NK cells, increased T cell leakage with age	Low
SCID	No mature T and B cells	Better engraftment compared with nude	Functional NK cell, leakage of T cells, radiosensitive	Low
SCID/Beige	No mature T and B cells, impaired Mφ and NK function	Better engraftment compared with SCID	Leakage of T cells, radiosensitive	Moderate
NOD/SCID	No mature T and B cells Impaired NK function Impaired Mφ & DC	Better engraftment	Spontaneous lymphoma Short life span (av. 36wks) Radiosensitive	Moderate
NOG/NSG/NOJ	No mature T and B cells, no NK cells, impaired Mφ and DC	Excellent engraftment of PDX including hematopoietic malignancies	Need strict SPF conditions, breeding is not easy, expensive	High
BALB/c Rag2 ^{null} /IL2Rγ ^{null} (BRG) Rag-2 ^{null} /Jak3 ^{null} (BRJ)	No mature T and B cells, no NK cells	Excellent engraftment of PDX, resistant to stress, easy breeding, radio resistant		High

NK: natural killer cells, Mφ: macrophages, DCs: dendritic cells, NOG/NSG: NOD/SCID/IL2Rγ^{null}, NOJ: NOD/SCID/Jak3^{null}, s.c.: subcutaneous.

Table 5. Immunocompromised mice strain for PDXs generation (from ⁵⁴).

Nevertheless, AML engraftment in NSG mice is very difficult and positively correlates with patient dismal outcome, limiting the possibility to develop PDX models for less aggressive AML subtypes⁵⁹⁻⁶¹. To further enhance AML engraftment success in mice, different strategies have been used:

- 1) the ablation of mice hematopoietic cells (by irradiation) before human cell transplantation, in order to empty the mice BM for human blasts proliferation;
- 2) the use of humanized mice strains that are mice engineered to express human cytokines (such as IL-3, GM-CSF, SCF) facilitating human hematopoietic cell survival and spreadin⁵⁹;
- 3) intrahepatic injection of blasts in newborn mice to facilitate or speed the engraftment⁶¹, being the relation between mice age and engraftment efficiency previously reported⁶².

Recently, the creation of humanized BM niche by the use of biomimetic scaffolds that mimic human hematopoietic microenvironment, has been shown to favor AML cells survival and proliferation when implanted in mice.^{6,40,46,63,64} The creation of humanized BM niche may improve the study of tumor microenvironment role in therapy response or resistance. Indeed, scaffolds containing human MSC and blasts implanted in mice allowed to study stromal support and to test new drugs combinations disadvantaging these interactions and increasing tumor cells sensitivity to therapy^{40,43}. These studies would not be possible without the application of scaffolds permitting to recreate a human BM niche in murine host.

PDXs of different tumors have been described as faithful cancer models, showing similar histological and genetic characteristics of the original patient tumor and similar treatment susceptibility^{57,65-67}. Although PDX has been defined as “patient avatar useful for personalized medicine studies, some recent findings suggest that an accumulation of variability may arise during serial transplantation. This phenomenon can be attributed to intra-tumoral heterogeneity (ITH) and despite PDXs have been recognized to maintain ITH, little changes in tumor clonal composition might provide discrepancies between patients’ and AML-PDXs⁵⁸. Changes in ITH can be explained by both stochastic and deterministic evolution of the tumor in mice model as follow:

- sampling bias: primary tumor implanted in mice can hardly represent the whole heterogeneity of patient tumor cells (stochastic event);
- murine specific selective pressure: human tumor microenvironment and immune cells are not present in mice, and murine tissue microenvironment may induce a tumor adaptation/evolution resulting in an adapted xenograft tumor (deterministic event).

In particular, in leukemia context, recent works investigated tumor clonal dynamics from the original AML at diagnosis to PDXs thanks to barcoding and next generation sequencing (NGS) techniques. By barcoding techniques, PDXs presented a reduction in the number of original leukemic subclones (from 30% to 90%) after mice transplantations⁶⁸; differences in clonal composition between patients' samples and primary, secondary and tertiary recipients was shown, with less differences between secondary and tertiary recipients in which a more similar clonal distribution has been observed, confirming a model stabilization over serial transplantations (Figure 9)⁶⁸.

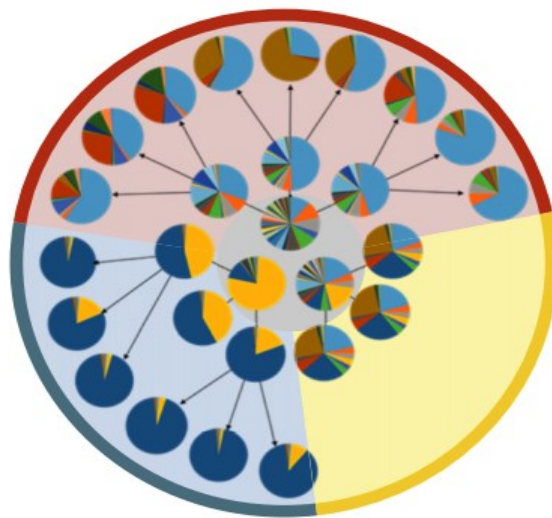


Figure 9. Representation of clonal selection during serial transplantations. Clonal composition in serial PDXs of an acute lymphoblastic leukemia, dissected by barcoding technique. Each circle represents a single mouse, and colors of pie chart indicate mice leukemic clones; primary xenografts (P0) are confined in the central gray circle, arrows connect each donor to its serial recipient mouse. The background colors of the bigger circle, mark descendants of the same primary PDX (adapted from ⁶⁸).

Clonal evolution during PDX transplantation passages with respect to initial AML sample is of great interest, and by whole-exome sequencing⁶⁹ changes in allelic frequency (AF) of selected genomic variants allowed to distinguish five patterns of clonal dynamics in PDX models: Monoclonal, Stable, Loss, Expansion and Burst (Figure 10). Monoclonal pattern is referred to AML characterized by a single clone perpetuated from P0 to P3; stable pattern has been defined by the presence of a major clone and minor subclones propagated at the same AF in mice; loss pattern is characterized by the loss of some subclones from original AML to PDX; expansion is referred to the presence of subclones that increase AF in PDX indicating a clonal expansion that permitted the detection of clones otherwise undetectable; burst pattern indicates subclones lost in one or more PDX passages but reappearing in a successive one⁶⁹.

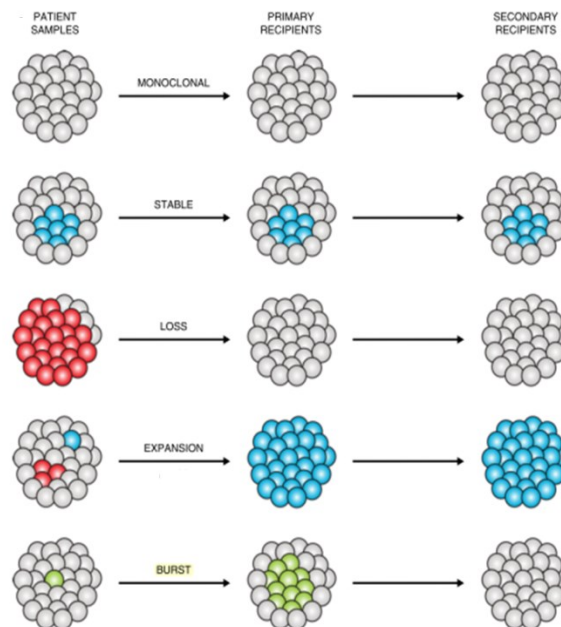


Figure 10. Patterns of AML clonal dynamics from primary AML to mice recipients (adapted from⁶⁹).

Overall, these data highlight that detailed studies on tumor dynamics in PDX are necessary to characterize the model and ensure robustness for PDXs application in precision medicine context (based on unique molecular/biological features of individual patients) since model infidelity should increase the risk of unreliable results⁶⁶. These warnings emphasize the importance of genomic profiling to study the concordance between patient' AML and PDXs before performing therapeutic studies.

3. PRECISION MEDICINE AND PERSONALIZED TREATMENT APPROACHES

The high heterogeneity of human cancer highlights the need to move toward personalized therapies to improve patients' outcome. Functional precision medicine (FPM) is an approach that considers individual tumor characteristics, dissected by genomic and transcriptomic analyses, to identify the best therapeutic intervention. FPM will provide information to guide personalized therapy⁷⁰ by preclinical studies where tumor cells are treated with specific drugs (Figure 11).

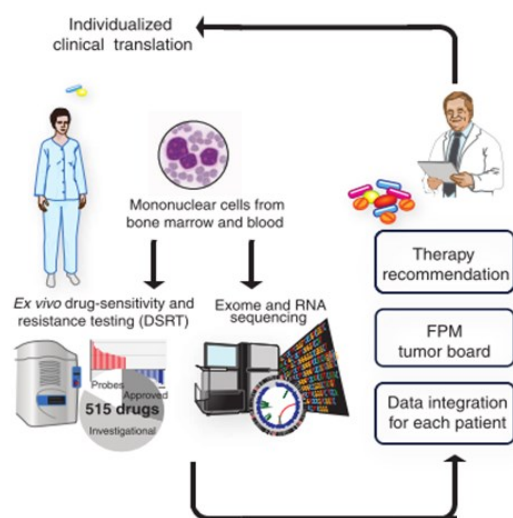


Figure 11. Scheme of a functional precision medicine study. The figure schematically illustrates data integration of drug response assay with molecular profiles specific for each AML patients, followed by clinical translation of results for individualized patients treatment assignment (adapted from ⁷¹).

The utility of FPM approaches is under evaluation in clinical trials,⁷⁰ such as:

- EXALT 2.0 (NCT04470947), a follow up study randomizing patients with hematological malignancies into different arms in which treatment are based according to functional *ex vivo* assays and genomic analysis;
- FORESEEE (NCT04450706), a study using FPM, testing drug response on organoids to predict therapy response in patients with metastatic breast cancer;

- PRISM (NTC03336931) PReCIStion Medicine for Children with Cancer, a multicenter prospective study for the feasibility and clinical value of a diagnostic service for identifying therapeutic targets to recommend personalized treatment for children and adolescents with high-risk cancer. Patient's cancer cells are tested for genetic abnormalities and undergo drug testing in laboratory (*in vitro* and *in vivo* on PDXs). Accordingly to screening results, recommendation on patient's management will be provided to clinicians.

Two additional important studies exploiting FPM for patients with refractory or relapsed hematological malignancies have also been reported. The first work by Allcyte company (Wien) used an approach called “pharmacoscopy” based on morphological changes in *ex-vivo* drug-treated cells, the authors were able to predicted the clinical response subdividing responders from non-responders patients and to successfully guide treatment decision, improving patients' outcome⁷². Another study has been recently conducted by Malani et al., and 347 emerging and 168 approved cancer drugs sensitivity/resistance have been tested on AML patient' cells. Integration of molecular and functional data for individual patients suggested that *ex vivo* drug responses, combined with molecular profiles, gave actionable data and recommended effective therapies for the treatment of refractory /relapsed AML (successful response reached in 59% of treated patients), thus providing clinically meaningful responses⁷¹.

Patients' derived *in vitro* and *in vivo* models available for FPM have advantages and disadvantages, and PDXs are the most suitable model to conduct these important preclinical studies, after testing of fidelity-to-human tumor validation, that is paramount prior to perform FPM studies (Figure 12).





PATIENT DERIVED MODEL	ADVANTAGES	DISADVANTAGES
2D culture 	<ul style="list-style-type: none"> • Rapid expansion • Low cost • High throughput • Amenable to rapid testing 	<ul style="list-style-type: none"> • Prolonged ex vivo culture; assay dependent • Missing many microenvironment components • Non-physiologic culture conditions
3D Organoids 	<ul style="list-style-type: none"> • Mimics the 3D tumor environment • Moderate cost • Moderate throughput • Amenable to rapid testing; assay dependent 	<ul style="list-style-type: none"> • Prolonged ex vivo culture; assay dependent • Missing some microenvironment components • Non-physiologic culture conditions
Microfluidics & Engineered Microenvironments 	<ul style="list-style-type: none"> • Engineered tumor microenvironment • Amenable to rapid testing; assay dependent 	<ul style="list-style-type: none"> • Prolonged ex vivo culture; assay dependent • Missing some microenvironment components • Generally low throughput
Patient Derived Xenografts 	<ul style="list-style-type: none"> • in vivo tumor environment • Incorporates drug pharmacokinetics • Clear toxicity readout 	<ul style="list-style-type: none"> • Slow expansion • High cost • Low scalability • Tumor-host species differences • Lacking immune system

Figure 12. *In vitro* and *in vivo* patient derived models applied to functional precision medicine: strengths and weaknesses (adapted from⁷⁰).

Noteworthy, deep genomic and transcriptomic characterization of tumor samples for FPM studies can be performed in matched patient' and PDX specimens⁷³, in order to identify most aggressive clones to be targeted with different drugs, opening for FPM preclinical trials⁶⁹. This studies are particularly important in AML context where clonal evolution is known to have a relevant role in tumor progression and relapse⁹. Moreover, the paired (patient-PDX) transcriptomic sequencing permits to identify altered pathways perpetuated from the original tumor to mice models, suggesting the recognition of fundamental traits implied in disease progression. Altogether these findings are essential for the identification of new personalized targeted therapy. In addition, the correlation of molecular characterization and therapeutic response could facilitate biomarker discovery as well as the identification of resistance mechanisms (Figure 13a). Another advantage in using PDX models in FPM approaches is the possibility to conduct co-clinical studies, consisting in simultaneous drug testing in mice and patients, helping to address a real-time therapeutic decision (Figure 13 b).

Finally, the possibility to molecularly profile all these models permits, thanks to integrative bioinformatics analysis, to identify a patient's best-matched PDX from an established *in vivo* model collection, with the final goal to choose the best clinical treatment options for patient according to previously conducted drug screening on these models, or according to results deriving from personalized drug testing using the best-matched PDX (Figure 13 c)⁵⁷.

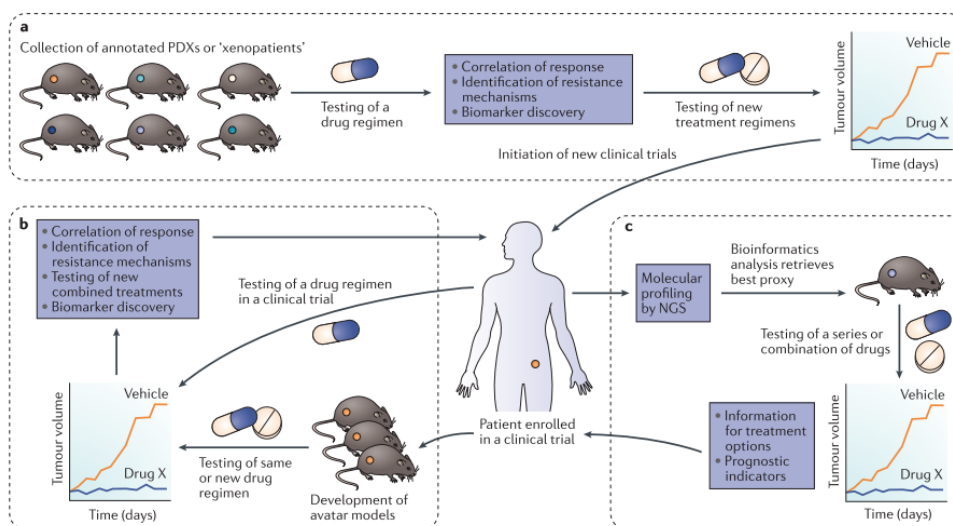


Figure 13. PDX preclinical study. a) PDX collections permit molecular characterization and correlation with therapeutic response, facilitating biomarker discovery as well as resistance mechanisms. Molecular characterization can lead to identification of druggable features and to new preclinical trials. b) PDX co-clinical studies for simultaneous drug testing in mice and patients for real-time therapeutic decisions. c) Integrative bioinformatics analysis permit to identify for each patient the best matched PDX from a collection of molecularly profiled models. PDX- associated information are then translated to take decision on clinical treatment options and to obtain prognostic indicators (from⁵⁷).

Accelerating cures for pediatric cancer remains an urgent challenge and PDXs, when associated to molecular characterization, represent a preclinical model with great potential for new agents prioritization, according to the identification of critical therapeutic targets, opening for a personalized treatment approach in the next future.

REFERENCES

1. Passegué, E., Jamieson, C. H. M., Ailles, L. E. & Weissman, I. L. Normal and leukemic hematopoiesis: Are leukemias a stem cell disorder or a reacquisition of stem cell characteristics? *Proc. Natl. Acad. Sci. U. S. A.* **100**, 11842–11849 (2003).
2. Hoggatt, J., Kfoury, Y. & Scadden, D. T. Hematopoietic Stem Cell Niche in Health and Disease. *Annu. Rev. Pathol. Mech. Dis.* **11**, 555–581 (2016).
3. Ugarte, F. & Forsberg, E. C. Haematopoietic stem cell niches: new insights inspire new questions. *EMBO J.* **32**, 2535–2547 (2013).
4. Morrison, S. J. & Scadden, D. T. The bone marrow niche for haematopoietic stem cells. *Nature* **505**, 327–334 (2014).
5. Méndez-Ferrer, S. *et al.* Mesenchymal and haematopoietic stem cells form a unique bone marrow niche. *Nature* **466**, 829–834 (2010).
6. Abarategi, A. *et al.* Modeling the human bone marrow niche in mice: From host bone marrow engraftment to bioengineering approaches. *J. Exp. Med.* **215**, jem.20172139 (2018).
7. de Rooij, J., Zwaan, C. & van den Heuvel-Eibrink, M. Pediatric AML: From Biology to Clinical Management. *J. Clin. Med.* **4**, 127–149 (2015).
8. Thiede, C. Mutant DNMT3A: Teaming up to transform. *Blood* **119**, 5615–5617 (2012).
9. Masetti, R. *et al.* Genomic complexity and dynamics of clonal evolution in childhood acute myeloid leukemia studied with whole-exome sequencing. *Oncotarget* **7**, 56746–56757 (2016).
10. Bertuccio, S. N. *et al.* Exploiting clonal evolution to improve the diagnosis and treatment efficacy prediction in pediatric aml. *Cancers (Basel)*. **13**, 1–10 (2021).
11. Duque-Afonso, J. & Cleary, M. L. The AML salad bowl. *Cancer Cell* **25**, 265–267 (2014).
12. Klco, J. M. *et al.* Functional heterogeneity of genetically defined subclones in acute myeloid leukemia. **25**, 379–392 (2015).
13. Farrar, J. E. *et al.* Genomic profiling of pediatric acute myeloid leukemia reveals a changing mutational landscape from disease diagnosis to relapse. *Cancer Res.* **76**, 2197–2205 (2016).
14. Morita, K. *et al.* Clonal evolution of acute myeloid leukemia revealed by high-throughput single-cell genomics. *Nat. Commun.* **11**, 1–17 (2020).
15. Petti, A. A. *et al.* Genetic and Transcriptional Contributions to Relapse in Normal Karyotype Acute Myeloid Leukemia. *Blood Cancer Discov.* **3**, 32–49 (2022).
16. Bennett, J. M. *et al.* Proposals for the classification of the acute leukaemias.

- French- American-British (FAB) co-operative group. *Br J Haematol* **33**, 451–458 (1976).
17. Vardiman, J. W., Harris, N. L. & Brunning, R. D. The World Health Organization (WHO) classification of the myeloid neoplasms. *Blood* **100**, 2292–2302 (2002).
 18. Vardiman, J. W. *et al.* The 2008 revision of the World Health Organization (WHO) classification of myeloid neoplasms and acute leukemia: Rationale and important changes. *Blood* **114**, 937–951 (2009).
 19. Arber, D. A. *et al.* The 2016 revision to the World Health Organization classification of myeloid neoplasms and acute leukemia. *Blood* **127**, 2391–2405 (2016).
 20. Pession, A. *et al.* Results of the AIEOP AML 2002/01 multicenter prospective trial for the treatment of children with acute myeloid leukemia. *Blood* **122**, 170–178 (2013).
 21. Bisio, V. *et al.* NUP98-fusion transcripts characterize different biological entities within acute myeloid leukemia: A report from the AIEOP-AML group. *Leukemia* **31**, 974–977 (2017).
 22. Masetti, R. *et al.* CBFA2T3-GLIS2 fusion transcript is a novel common feature in pediatric, cytogenetically normal AML, not restricted to FAB M7 subtype. *Blood* **121**, 3469–3472 (2013).
 23. Manara, E. *et al.* MLL-AF6 fusion oncogene sequesters AF6 into the nucleus to trigger RAS activation in myeloid leukemia. *Blood* **124**, 263–272 (2014).
 24. Pigazzi, M. *et al.* Screening of novel genetic aberrations in pediatric acute myeloid leukemia: A report from the AIEOP AML-2002 study group. *Blood* **120**, 3860–3862 (2012).
 25. Togni, M. *et al.* Identification of the NUP98-PHF23 fusion gene in pediatric cytogenetically normal acute myeloid leukemia by whole-transcriptome sequencing. *J. Hematol. Oncol.* **8**, (2015).
 26. Ommen, H. B. Monitoring minimal residual disease in acute myeloid leukaemia: a review of the current evolving strategies. *Ther. Adv. Hematol.* **7**, 3–16 (2016).
 27. Hourigan, C. S. & Karp, J. E. Minimal residual disease in acute myeloid leukaemia. *Nat. Publ. Gr.* **10**, (2013).
 28. Buldini, B. *et al.* Prognostic significance of flow-cytometry evaluation of minimal residual disease in children with acute myeloid leukaemia treated according to the AIEOP-AML 2002/01 study protocol. *Br. J. Haematol.* **177**, 116–126 (2017).
 29. Pession, A. *et al.* Treatment and long-term results in children with acute myeloid leukaemia treated according to the AIEOP AML protocols. *Leukemia* **19**, 2043–2053 (2005).
 30. Locatelli, F. *et al.* Outcome of children with high-risk acute myeloid leukemia

- given autologous or allogeneic hematopoietic cell transplantation in the aieop AML-2002/01 study. *Bone Marrow Transplant.* **50**, 181–188 (2015).
31. Elgarten, C. W. & Aplenc, R. Pediatric acute myeloid leukemia: Updates on biology, risk stratification, and therapy. *Curr. Opin. Pediatr.* **32**, 57–66 (2020).
 32. Conneely, S. E. & Stevens, A. M. Acute Myeloid Leukemia in Children: Emerging Paradigms in Genetics and New Approaches to Therapy. *Curr. Oncol. Rep.* **23**, 16 (2021).
 33. Fiorentini, A. *et al.* The Time Has Come for Targeted Therapies for AML: Lights and Shadows. *Oncol. Ther.* **8**, 13–32 (2020).
 34. Pearson, A. D. J. *et al.* Paediatric Strategy Forum for medicinal product development for acute myeloid leukaemia in children and adolescents: ACCELERATE in collaboration with the European Medicines Agency with participation of the Food and Drug Administration. *Eur. J. Cancer* **136**, 116–129 (2020).
 35. Zwaan, C. M. *et al.* Collaborative efforts driving progress in pediatric acute myeloid leukemia. *Journal of Clinical Oncology* **33**, 2949–2962 (2015).
 36. Kuhlen, M., Klusmann, J. H. & Hoell, J. I. Molecular Approaches to Treating Pediatric Leukemias. *Front. Pediatr.* **7**, 1–12 (2019).
 37. Johnson, J. I. *et al.* Relationships between drug activity in NCI preclinical in vitro and in vivo models and early clinical trials. *Br. J. Cancer* **84**, 1424–1431 (2001).
 38. Collins, A. T. & Lang, S. H. A systematic review of the validity of patient derived xenograft (PDX) models: The implications for translational research and personalised medicine. *PeerJ* **2018**, 1–22 (2018).
 39. Horvath, P. *et al.* Screening out irrelevant cell-based models of disease. *Nat. Rev. Drug Discov.* **15**, 751–769 (2016).
 40. Borella, G. *et al.* Targeting the plasticity of mesenchymal stromal cells to reroute the course of acute myeloid leukemia. *Blood* **138**, 557–570 (2021).
 41. Zhang, B. *et al.* Altered microenvironmental regulation of leukemic and normal stem cells in chronic myelogenous leukemia. *Cancer Cell* **21**, 577–92 (2012).
 42. Wong, R. S. Y. & Cheong, S. K. Role of mesenchymal stem cells in leukaemia: Dr. Jekyll or Mr. Hyde? *Clin. Exp. Med.* **14**, 235–248 (2014).
 43. Ma, C. *et al.* Leukemia-on-a-chip: Dissecting the chemoresistance mechanisms in B cell acute lymphoblastic leukemia bone marrow niche. *Sci. Adv.* **6**, (2020).
 44. Menon, K. *et al.* Development and molecular characterization of polymeric micro-nanofibrous scaffold of a defined 3-D niche for in vitro chemosensitivity analysis against acute myeloid leukemia cells. *Int. J. Nanomedicine* 3603 (2015). doi:10.2147/IJN.S80397

45. Leisten, I. *et al.* 3D co-culture of hematopoietic stem and progenitor cells and mesenchymal stem cells in collagen scaffolds as a model of the hematopoietic niche. *Biomaterials* **33**, 1736–1747 (2012).
46. Abarrategi, A. *et al.* Versatile humanized niche model enables study of normal and malignant human hematopoiesis. *J. Clin. Invest.* **127**, 543–548 (2017).
47. Bray, L. J. *et al.* A three-dimensional ex vivo tri-culture model mimics cell-cell interactions between acute myeloid leukemia and the vascular niche. *Haematologica* **102**, 1215–1226 (2017).
48. Aljitawi, O. S. *et al.* A novel three-dimensional stromal-based model for in vitro chemotherapy sensitivity testing of leukemia cells. *Leuk. Lymphoma* **55**, 378–391 (2014).
49. Houshmand, M. *et al.* Mimicking the Acute Myeloid Leukemia Niche for Molecular Study and Drug Screening. *Tissue Eng. Part C Methods* **23**, 72–85 (2017).
50. Bruce, A. *et al.* Three-dimensional microfluidic tri-culture model of the bone marrow microenvironment for study of acute lymphoblastic leukemia. *PLoS One* **10**, 1–16 (2015).
51. Fetah, K. *et al.* The emergence of 3D bioprinting in organ-on-chip systems. *Prog. Biomed. Eng.* **1**, (2019).
52. Bova, L., Billi, F. & Cimetta, E. Mini-review: advances in 3D bioprinting of vascularized constructs. *Biol. Direct* **15**, 1–5 (2020).
53. Almosailleakh, M. & Schwaller, J. Murine models of acute Myeloid Leukaemia. *Int. J. Mol. Sci.* **20**, (2019).
54. Okada, Vaeteewoottacharn & Kariya. Application of Highly Immunocompromised Mice for the Establishment of Patient-Derived Xenograft (PDX) Models. *Cells* **8**, 889 (2019).
55. Fujii, E., Kato, A. & Suzuki, M. Patient-derived xenograft (PDX) models: Characteristics and points to consider for the process of establishment. *J. Toxicol. Pathol.* **33**, 153–160 (2020).
56. Houghton, P. J. *et al.* The pediatric preclinical testing program: description of models and early testing results. *Pediatr. Blood Cancer* **49**, 928–40 (2007).
57. Byrne, A. T. *et al.* Interrogating open issues in cancer precision medicine with patient-derived xenografts. *Nat. Rev. Cancer* **17**, 254–268 (2017).
58. Shi, J., Li, Y., Jia, R. & Fan, X. The fidelity of cancer cells in PDX models: Characteristics, mechanism and clinical significance. *Int. J. Cancer* **146**, 2078–2088 (2020).
59. Wunderlich, M. *et al.* AML xenograft efficiency is significantly improved in NOD/SCID-IL2RG mice constitutively expressing human SCF, GM-CSF and IL-3. *Leukemia* **24**, 1785–1788 (2010).

60. Pearce, D. J. *et al.* AML engraftment in the NOD / SCID assay reflects the outcome of AML : implications for our understanding of the heterogeneity of AML. *Blood* **107**, 1166–73 (2006).
61. Her, Z. *et al.* An improved pre-clinical patient-derived liquid xenograft mouse model for acute myeloid leukemia. 1–14 (2017). doi:10.1186/s13045-017-0532-x
62. Ishikawa, F. *et al.* Chemotherapy-resistant human AML stem cells home to and engraft within the bone-marrow endosteal region. *Nat. Biotechnol.* **25**, 1315–1321 (2007).
63. Reinisch, A. *et al.* A humanized bone marrow ossicle xenotransplantation model enables improved engraftment of healthy and leukemic human hematopoietic cells. *Nat. Med.* **22**, 812–821 (2016).
64. Antonelli, A. *et al.* Establishing human leukemia xenograft mouse models by implanting human bone marrow-like scaffold-based niches. *Blood* **128**, 2949–2959 (2016).
65. Yoshida, G. J. Applications of patient-derived tumor xenograft models and tumor organoids. *J. Hematol. Oncol.* **13**, 1–16 (2020).
66. Wang, K. *et al.* Patient-derived xenotransplants can recapitulate the genetic driver landscape of acute leukemias. *Leukemia* **31**, 151–158 (2017).
67. Kunz, J. B. *et al.* PDX models recapitulate the genetic and epigenetic landscape of pediatric T-cell leukemia. 1–13 (2018). doi:10.15252/emmm.201809443
68. Belderbos, M. E. *et al.* Clonal selection and asymmetric distribution of human leukemia in murine xenografts revealed by cellular barcoding. *Blood* **129**, 3210–3220 (2017).
69. Sandén, C. *et al.* Clonal competition within complex evolutionary hierarchies shapes AML over time. *Nat. Commun.* **11**, 1–10 (2020).
70. Letai, A., Bholra, P. & Welm, A. L. Functional precision oncology: Testing tumors with drugs to identify vulnerabilities and novel combinations. *Cancer Cell* **40**, 26–35 (2022).
71. Malani, D. *et al.* Implementing a Functional Precision Medicine Tumor Board for Acute Myeloid Leukemia. *Cancer Discov.* **12**, 388–401 (2022).
72. Snijder, B. *et al.* Image-based ex-vivo drug screening for patients with aggressive haematological malignancies: interim results from a single-arm, open-label, pilot study. *Lancet Haematol.* **4**, e595–e606 (2017).
73. Rokita, J. L. *et al.* Genomic Profiling of Childhood Tumor Patient-Derived Xenograft Models to Enable Rational Clinical Trial Design. *Cell Rep.* **29**, 1675–1689.e9 (2019).

CHAPTER 2

“DEVELOPMENT AND CHARACTERIZATION OF *IN VIVO* PRECLINICAL MODELS FOR AN EFFECTIVE THERAPEUTIC STRATEGY IN PEDIATRIC ACUTE MYELOID LEUKEMIA”

1. INTRODUCTION

Acute leukemia is the most common type of cancer in childhood, accounting for 25–30% of all pediatric cancers¹. Acute myeloid leukemia (AML) accounts for 15-20% of pediatric leukemic cases and, to date, the overall survival for children with AML does not exceed 70%^{1,2}. Chemotherapy and hematopoietic stem cell transplantation (HSCT) still represent the standard of care with more than 25% of patients still experiencing relapse and a dismal prognosis below 50%^{2,3}. To ameliorate AML patients' outcome there is an urgent need to identify new therapeutic strategies. Recent advances in cancer genomics provide new insights into leukemogenesis and into AML drug resistance, suggesting novel treatment strategies^{1,4,5}. Nevertheless, pediatric drug development is extremely limited and most of new drugs are approved for adult AML treatment⁴, but cannot be easily translated into pediatric context because of their different genetic background and treatment tolerability⁶. Moreover, the reduced number of pediatric AML patients that can be included in clinical trials⁶ increases the difficulties in identifying novel effective drugs. A lot of efforts has been spent in last years to identify new molecularly targeted therapies for pediatric leukemia,^{1,5} but less than 10% of candidate drugs have been authorized for market^{7,8} despite promising preclinical data. This latter phenomenon can be explained by the fact that drug efficacy in patients poorly correlated with the activity found in preclinical studies suggesting that they were not predictive. Traditional preclinical models, such as cell lines culture or xenografts mice generated with cell lines, are nowadays considered to reduce success rate of oncology drug development⁹. Indeed, these models are unable to recapitulate disease

heterogeneity, thus being rarely predictive of patients' therapeutic response^{9,10}. Thus, the successful identification of novel drugs may depend on the availability of robust pre-clinical models that need to be more informative. Patient derived xenografts (PDXs) have been suggested as the more realistic preclinical models¹¹⁻¹⁵. The potential advantage of PDXs to recapitulate the *in vivo* drug response and the tumor genetic heterogeneity is considered fundamental for preclinical testing of new drugs, specifically for the targeting of molecular alterations. PDXs are anticipated to reliably bridge non-clinical and clinical results in translational research. However, the ability of these models to faithfully recapitulate patients' disease still remains unclear¹⁶⁻¹⁹. These warnings emphasize the necessity of genomic and transcriptomic profiling to study the concordance between patients' and PDXs tumor features before performing therapeutic studies^{14,15,18}. AML clonal heterogeneity and clonal evolution are well known²⁰⁻²⁵, and clonal dynamics in mice modelling by genome sequencing and barcoding techniques in leukemia PDXs is under investigation^{17,18,26,27}.

2. AIM

In this study we establish pediatric AML-PDXs and characterize them by flow cytometric immunophenotyping, whole exome and RNA sequencing. The advent of high-throughput sequencing techniques will generate dataset of genomic and transcriptomic data that may provide new insights into leukemogenesis and novel therapeutic targets. We want to unravel new druggable variants and pathways by the dissection of next generation sequencing data, and perform personalized drug testing in AML-PDXs. We aim to accelerate the identification and the efficacy evaluation of innovative medicines for AML, and to facilitate their clinical translation to improve patients' outcome.

3. MATERIALS AND METHODS

Patients' samples

Bone marrow (BM) or peripheral blood (PB) samples of a total of 61 pediatric patients affected by de novo AML were provided by the pediatric OncoHematology Lab of the Padova Hospital, being the Associazione Italiana Emato Oncologia Pediatrica (AIEOP) reference centre for the pediatric AML diagnosis. Samples were obtained at diagnosis (n=56) or at relapse (n=6) of AML disease, established according to standard criteria based on immune-histochemical staining, immune-phenotyping, cytogenetic studies and molecular genetics, as detailed in the AIEOP AML 2002/01 treatment protocol (ref Pession 2013).

Cell lines and primary cells culture

The leukemic cell lines NOMO, HL-60 and ML-2 (DMSZ, Braunschweig, DE) were cultured in RPMI 1640 (Thermo Fisher Scientific, Waltham, MA, USA), while SHI-1 (DMSZ) were maintained in culture with DMEM (Thermo Fisher Scientific). All the media were enriched with 10% FBS (Thermo Fisher Scientific), 2mM glutamine (Gibco, Life Technologies, CA, USA) and 100U/mL streptomycin/penicillin (Gibco, Life Technologies). Primary cells were cultured at 37°C in RPMI Medium 1640 with 10% FBS, 2mM glutamine (Gibco, Life Technologies), 100U/mL streptomycin/penicillin (Gibco, Life Technologies), and supplemented with 50 ng/mL thrombopoietin (TPO), 50 ng/mL stem cell factor (SCF), 50 ng/mL FMS-like tyrosine kinase 3 ligand (Flt3L), 20 ng/mL interleukin-3 (IL 3) and 20 ng/mL interleukin-6 (IL 6), all these cytokines purchased from Miltenyi Biotec (Miltenyi Biotec, Bergisch Gladbach, DE). Table 1 report main characteristics of AML patients from whom AML cells have been obtained.

Patient ID	Genetic marker	Gender	Age
#1	t(8;21) RUNX1- RUNX1T1 +CKIT*mut	F	11
#2	FLT3ITD	M	17
#3	FLT3ITD	F	15
#4	FLT3ITD	M	16
#5	FLT3ITD	M	4
#6	FLT3ITD+NPM*mut	M	16
#7	FLT3ITD+NPM*mut	M	13
#8	FLT3ITD+NPM*mut	F	5
#9	NPM1*mut	M	16
#10	inv16 (CBFB-MYH11)	F	15
#11	inv16 (CBFB-MYH11)	M	18
#12	inv16 (CBFB-MYH11)	F	18
#13	inv16 (CBFB-MYH11) +CKIT*mut	F	8
#14	inv16 (CBFB-MYH11) +CKIT*mut	F	4
#15	t(16;16) CBFA2T3-GLIS2	F	2
#16	t(16;16) CBFA2T3-GLIS2	M	3
#17(REL)	t(16;16) CBFA2T3-GLIS2	F	2
#18	t(16;21) FUS-ERG	F	3
#19	t(16;21) FUS-ERG	M	11
#20	t(3;5) NPM1-MLF1 +FLT3ITD	M	8
#21	t(5;11)NUP98-NSD1	M	17
#22 (REL)	t(5;11)NUP98-NSD1 + FLT3ITD	F	15
#23	t(5;11)NUP98-NSD1 + FLT3ITD	M	4
#24 (REL)	t(5;11)NUP98-NSD1 + FLT3ITD	M	7
#25	t(5;11)NUP98-NSD1 +FLT3ITD	F	12
#26	KMT2A_PTD+FLT3ITD	F	13
#27	t(6;11)KMT2A-AFDN	M	16
#28	t(6;11)KMT2A-AFDN	M	12

#29	t(6;11)KMT2A-AFDN	M	14
#30	t(6;11)KMT2A-AFDN	M	6
#31	t(6;11)KMT2A-AFDN	M	7
#32	t(4;11) KMT2A-AFF1	M	10
#33	t(10;11) KMT2A-MLLT10	F	
#34	t(10;11) KMT2A-MLLT10	M	7
#35	t(10;11) KMT2A-MLLT10	F	14
#36	t(10;11) KMT2A-MLLT10	F	0
#37(REL)	t(10;11) KMT2A-MLLT10	M	1
#38	t(10;11) KMT2A-MLLT10	M	9
#39	t(11,19) KMT2A-ENL	F	10
#40	t(11;19)KMT2A-ENL	M	8
#41	t(9;11)KMT2A-MLLT3	M	2
#42	t(9;11)KMT2A-MLLT3	F	12
#43	t(9;11)KMT2A-MLLT3	F	18
#44	t(9;11)KMT2A-MLLT3	M	1
#45	t(9;11)KMT2A-MLLT3	M	1
#46	t(8;21) RUNX1- RUNX1T1	F	17
#47	t(8;21) RUNX1- RUNX1T1	M	23
#48	t(8;21) RUNX1- RUNX1T1	M	7
#49	t(8;21) RUNX1- RUNX1T1 +CKIT* ^{mut}	F	6
#50	NEG	M	18
#51	NEG	M	10
#52	NEG	F	15
#53	NEG	M	6
#54	NEG	M	13
#55	NEG	F	1
#56(REL)	NEG	M	0
#57	NEG	F	2

#58	NEG	F	7
#59	NEG	M	3
#60	NEG	F	9
#61	NEG	M	2

Table1. Main characteristics of AML patients, whose blasts have been used in this study. NEG=No mutations detected by the current diagnostic screening; REL= AML samples obtained at patients' relapse.

Isolation and culture of Mesenchymal Stromal Cells

MSCs of AML patients (AML-MSCs) were derived from BM mononuclear cells. Briefly, cells were plated at 100.000 cells/cm² in StemMACS MSC Expansion Media (Miltenyi Biotec) supplemented with 100 U/mL penicillin/streptomycin (Gibco, Life Technologies) and 2mM glutamine (Gibco, Life Technologies), and incubated at 37°C. After one day of culture, the non-adherent cells were removed and fresh medium was added to the adherent ones. The resulting adherent cells were expanded until 90% confluence, then split by trypsin (Trypsin/EDTA Solution, Biochrom GmbH) at 37°C for 5 min, harvested in medium with FBS to inactivate trypsin, centrifuged and plated at 5.000 cells/cm² in fresh medium. AML-MSCs were used within 5th passage.

Flow cytometry

For the detection of the surface markers, the following anti-human antibodies conjugated with proper fluorophores were used: CD45 (Beckman Coulter, Brea, CA), CD11b (Beckman Coulter), CD34 (BD Biosciences, Franklin Lakes, NJ), CD38 (BD Biosciences), CD33 (BD Biosciences), HLADR (BD Biosciences), NG2 (Beckman Coulter), CD56 (Beckman Coulter), CD7 (Beckman Coulter), CD11a (BD Biosciences), CD38 (BD Biosciences). Briefly, cells obtained after haemolysis of PB or BM samples, were stained with the conjugated primary antibody for 30', rinsed in PBS1x and then fluorescence was detected with Cytometer FC 500 Instrument (Beckman Coulter) or FACSCanto (BD Biosciences).

Cell treatments

Cell lines were treated at a concentration of 0.5×10^6 /ml, whereas primary cells at 0.75×10^6 /ml, with the following drugs: Cytarabine (Ara-C), Venetoclax, Rotenone, Oligomycin, Asparaginase (all purchased from Sigma Aldrich-Merck Millipore, Darmstadt, DE), Gallein and YM-254890 (Bio-Techne, Minneapolis, MN, USA), Thapsigargin, IACS-010759 and Disulfiram (Selleckchem, Houston, TX, USA).

Cell viability assay

Cell viability of AML cells was evaluated using PrestoBlu Cell Viability (Invitrogen, Thermo Fisher Scientific) following the manufacturer's guidelines. Briefly, 0.75×10^5 cells in 100 μ L of proper medium were cultured in sterile flat-bottom 96-well plates and incubated at 37°C. Cell viability was measured at the indicated time points by adding 10 μ L of PrestoBlu reagent, after 2 hours of incubation at 37°C, recording the absorbance with the Spark® multimode microplate reader (TECAN, Männedorf, Switzerland). Cell viability was compared to the cells treated with dimethyl sulfoxide (DMSO) as control.

3D *in vitro* model

The 3D model consists of a scaffold composed by 70% hydroxyapatite/30% collagen type I with 2% 1,4-butanediol diglycidyl ether (BDDGE), of 2 mm in height and diameter, synthesized by Prof. Tampieri laboratory at 'Istituto di Scienza e Tecnologia dei Materiali Ceramici' (ISTEC-Consiglio Nazionale delle Ricerche' CNR, Faenza Italy). Briefly, scaffolds were soaked in DMEM medium overnight prior to cell seeding. After medium removal, scaffolds were equally split in 4 parts, each part was transferred into a well of 48-well plate, where 1×10^5 AML-MSCs in 10 μ L of StemMACS were slowly seeded on the upper surface of the scaffold. Scaffolds seeded with AML-MSCs were incubated for 4 hours at 37°C, in order to facilitate cell spreading, then 0.5 mL of StemMACS was gently added to each well. After 7 days of culture at 37°C, the medium was removed and 2×10^5 AML primary cells in 10 μ L of proper medium (see "Cell lines and primary cells cultures") were slowly seeded on the upper surface of the AML-MSCs coated-scaffold. Seeded scaffolds were incubated for 15' at 37°C, prior to gently add 0.5 mL of primary cells medium, with

or without selected drugs, then incubated at 37°C for 72 hours prior to cell viability assay.

3D cell viability assay

Cell viability was measured using CellTiter-Glo® 3D reagent (Promega, Fitchburg, WI) according to the manufacturer's instructions. Briefly, scaffolds were individually transferred into wells of flat-bottom white-opaque 96-well plates (Corning, Sigma-Aldrich-Meck Millipore) with 100 µL of RPMI, then 100 µL of CellTiter-Glo® 3D reagent were added into each well. Plates were shaken for 5' to induce scaffold and cells lysis. Samples were then incubated for additional 20' in the dark, at RT, to stabilize the bioluminescent signal, which was then recorded using the Spark® multimode microplate reader (TECAN). Cell viability was compared to the control sample, the scaffold seeded with the same cells but treated with dimethyl sulfoxide (DMSO).

Immunohistochemistry

Harvested scaffolds were fixed overnight in Paraformaldehyde 4% in PBS1x. Fixed samples were then paraffin embedded and sectioned (6 µm of thickness) for histological studies. Slides were incubated with human CD45 (Dako-Agilent Technologies, Santa Clara, Ca, USA), mouse CD31 (BD Bioscience) and human Osteopontin (R&D) overnight, and then developed with the DAKO Envision Detection Kit (Dako-Agilent Technologies). Hematoxylin/eosin was performed to confirm the quality of the section.

3D-AML *in vivo* model

To establish the 3D-AML *in vivo* model, scaffolds were previously seeded *in vitro* with $0,4 \times 10^6$ AML-MSCs, and with 1×10^6 CD3-depleted primary AML cells 24 hours later. After additional 24 hours, the seeded scaffolds were implanted in a subcutaneous pocket in the back of irradiated (1.5 Gy) mice.

***In vivo* PDXs models**

All the *in vivo* experimental procedures were performed in accordance with the Institutional Animal Care and Use Committee and with international laws (authorization n. 512/19PR and 622/17PR). For PDX generation, NOD.Cg-Prkdc^{scid} Il2rg^{tm1Wjl}/SzJ

(NSG) mice (4-8 weeks old) were used; mice were conditioned by irradiation at 1.5 Gy 24 hours prior to leukemic cell transplantations. Briefly, 1×10^6 primary AML cells preemptively depleted of CD3+ T cells by immune-magnetic cell separation (Miltenyi Biotec) using CD3 MicroBead Kit (Miltenyi Biotec) to avoid the graft-versus host disease (GVHD), were injected into first mice recipients (P0), using different techniques: intravenous injection (i.v.), intrafemoral (i.f) injection or intrahepatic (i.h) injection in newborn mice (3days). Cells were resuspended in different volumes of medium according to different injection techniques: 100 μ l for i.v., 30 μ l for i.f. and i.h. To monitor engraftment, tumor burden was assessed every two week starting from 1 month after AML cell injection by flow cytometric measurement of hCD45 positive cells in PB (see “flow cytometry” section). The detection of hCD45>20% in PB defined AML engraftment. At that point, mice were sacrificed, and organs (femur and spleen) were recovered; femurs were flushed and spleens were mechanically dissociated to harvest cells to analyze for engraftment analysis by flow cytometry. After PDX establishment, for successive PDX passages, 1×10^6 human CD45 (hCD45) cells harvested from BM or spleen of previous mice recipients were intravenously injected into not previously conditioned recipient mice, generating P1 and P2-PDXs.

PDXs treatment

At leukemia onset, when hCD45 positive cells in PB reached >20%, mice were randomized into 2 groups namely treated and controls. Mice of the treated group were treated with Cytarabine (50 mg/kg) plus Doxorubicin (1.5 mg/kg) intravenously for 3 days, then treated with intraperitoneal (i.p.) Cytarabine (50 mg/kg) injection for the next 2 days. Treatment efficacy was assessed by flow cytometric measurement of hCD45 positive cells, and remission was defined when blasts in PB were <5%. Doxorubicin (Selleckchem) and Cytarabine (Sigma Adrich- Merck Millipore) powder were dissolved in DMSO for stock solutions, then freshly diluted in sterile saline solution at appropriate concentration for daily injection. Mice weight was monitored in order to adjust the dose of drugs. Appropriate vehicle was used for control group.

After treatment discontinuation mice were monitored every 10 days, and relapse was defined when hCD45 in PB>20%. At relapse, mice were randomized into 3 groups: Venetoclax+Disulfiram, Venetoclax+Asparaginase and controls. Drugs were administered

at day 1-3-5 for two weeks. At the following concentrations: Venetoclax (Merck Millipore) at 50 mg/kg, dissolved in 60% Phosal-50PG (Lipoid), 30% polyethylene glycol-400 (Sigma Adrich- Merck Millipore), and 10% ethanol, by oral gavage; Disulfiram (Sigma) at 50mg/kg, dissolved in peanuts oil, by i.p. injection; Asparaginase (ProSpec, Rehovot, Israel) at 10.0000 U/kg, dissolved in water, by i.p. injection. Mice weight was monitored in order to adjust the dose of drugs. Appropriate vehicle was used for control group. After treatment discontinuation mice were monitored every 7 days for hCD45 detection in PB by flow cytometry.

RNA extraction

Total RNA was isolated using Trizol (Invitrogen) according to manufacturer's protocol and nucleic acid were quantified by using Qbit RNA BR Assay Kit on a Qbit fluorometer (Thermo Scientific). Quality of RNA samples has been analysed using The 2100 Bioanalyzer instrument (Agilent).

DNA extraction

DNA was isolated using QIAamp DNA Mini Kit (Qiagen) according to manufacturer's protocol and nucleic acid were quantified by using Qbit dsDNA BR Assay Kit on a Qbit fluorometer (Thermo Scientific). Quality of DNA samples has been analysed by gel electrophoresis.

Next Generation Sequencing

RNA sequencing: library were prepared using NEB Next Ultra II with RiboZero Plus kit following the manufacturer protocol, then sequenced 150x2 bp (paired-end mode) on the NovaSeq 6000 System -S4 (Illumina). Whole exome sequencing (WES): library were prepared using SureSelect V6+UTR kit (Agilent) following the manufacturer protocol, then sequenced 150x2 bp (paired-end mode) on the NovaSeq 6000 System-S4 (Illumina). Data analysis workflow was build and performed on CentOS7 Linux server, adopting an open source customized bioinformatic pipeline. Paired-end short reads were trimmed to clean the sequencing adapters, and to filter or trim the reads for sequence quality (Phred quality > 10 and minimum length of trimmed sequence of 30nt). These two steps were performed with AdapterRemoval v.2.1.7 tool [1]. Cleaned reads were then aligned

on human reference genome hg38 with Burrows–Wheeler Aligner *mem* (BWA v0.7.17) [2] for WES data, and with the STAR v2.6.1 [3] pipeline for RNA-seq data. An additional processing step was adopted in the case of PDX samples, for both WES and RNA-seq datasets, aimed to remove the host genome. This procedure was performed with the tool *disambiguate* [4] using the mm39 as murine reference genome. Samtools v1.9 [5] was used to remove the sequencing duplicates (optical and PCR related) and to index the alignment files.

Then, the RNA-seq data was analyzed with STAR-fusion v1.10.0 algorithm [6] with the aim to detect and confirm the presence of chromosomal rearrangements leading to gene fusions previously detected by RT-PCR. Gene expression profiles and differential expression of AML was evaluated comparing AML molecular subgroups in three steps: 1) the function *htseq-count* (Python package HTseq) [7] was adopted to count the number of reads mapped on known genes, included in the Ensembl release 95 annotation features (<http://www.ensembl.org>); 2) the differential expressed genes were evaluated using the R-Bioconductor packages *edgeR* and *limma*; 3) Principal component analysis (PCA) was applied with the aim to assess the transcriptome similarities and differences in unsupervised way adopting the R package *stats* (function *prcomp*). The pathway enrichment analysis was performed with WEB-based GENE SeT AnaLYsis Toolkit (www.webgestalt.org) adopting the Reactome functional database (<https://reactome.org/>) as reference and the default settings of the tool and using the pre-ranked gene list as input. Heatmap showing the gene expression levels was built with the R package *pheatmap*.

WES data were analyzed with the aim to discover point mutations in the coding region of the genome. As first step, the alignments were processed with Genome Analysis Toolkit v4.2.1.0 (GATK) [8] to realign around insertions and deletions (InDels) and to perform the base quality recalibration. Then, the function Mutect2 (implemented within GATK4) was used to call the single nucleotide variants (SNVs) and InDels, adopting the default parameters. Among the whole set of called variants, we selected those with total depth > 10, present within coding exons and having a non-silent effect on protein sequence (non-synonymous and nonsense SNVs, frameshift and non-frameshift InDels). The alterations were filtered on databases of human variability (1000Genomes: <http://www.internationalgenome.org/>; ExAC: <http://exac.broadinstitute.org/>) in order

to discard polymorphism and keep novel or very rare variants (allele frequency on population < 0.01). Each variant were annotated with a gene name, and a cDNA/protein coordinate with the tool Annovar [9], moreover the presence on Catalogue of Somatic Mutations in Cancer (COSMIC: <https://cancer.sanger.ac.uk>) was reported. In order to additionally refine the set of interesting variants we also applied several filtering criteria aimed to keep: 1) variants detected in patients samples and reported on COSMIC; 2) variants detected in patients and showing an increased frequency of at least 25% in P2-PDX; 3) variants detected in all mouse passages and not detected in the corresponding patient. The correlation analysis of allelic frequencies was performed by Pearson Correlation method implemented on Prism-GraphPAD (<https://www.graphpad.com>).

Statistical analyses

The *t*-test was adopted for significance between differences in means when two groups were evaluated. ANOVA test was performed when comparing more than two groups. Graphs and associated statistical analyses were generated using GraphPad Prism 9 (GraphPad, La Jolla, CA). Graphs and associated statistical analyses were generated using GraphPad Prism 9. All data are presented as mean \pm standard error of the mean (SEM). Differences were considered to be statistically significant at p-value of <0.05(*), <0.01(**), <0.001(***), <0.0001(****).

Material and method: references

1. Lindgreen S. AdapterRemoval: Easy cleaning of next-generation sequencing reads. *BMC Res. Notes.* 2012;5:337. doi: 10.1186/1756-0500-5-337.
2. Li H., Durbin R. Fast and accurate short read alignment with Burrows-Wheeler Transform. *Bioinformatics.* 2009;25:1754–1760. doi: 10.1093/bioinformatics/btp324.
3. Trapnell C., Pachter L., Salzberg S.L. TopHat: Discovering splice junctions with RNA-Seq. *Bioinformatics.* 2009;25:1105–1111. doi: 10.1093/bioinformatics/btp120.
4. Ahdesmäki MJ, Gray SR, Johnson JH, Lai Z. Disambiguate: An open-source application for disambiguating two species in next generation sequencing data from grafted samples. *F1000Res.* 2016 Nov 22;5:2741.
5. Li H., Handsaker B., Wysoker A., Fennell T., Ruan J., Homer N., Marth G., Abecasis G., Durbin R. The Sequence alignment/map (SAM) format and SAMtools. *Bioinformatics.* 2009;25:2078–2079. doi: 10.1093/bioinformatics/btp352.
6. Brian J. Haas, Alex Dobin, Nicolas Stransky, Bo Li, Xiao Yang, Timothy Tickle, Asma Bankapur, Carrie Ganote, Thomas G. Doak, Nathalie Pochet, Jing Sun, Catherine J.

- Wu, Thomas R. Gingeras, Aviv Regev STAR-Fusion: Fast and Accurate Fusion Transcript Detection from RNA-Seq. bioRxiv 120295.
7. Anders S, Pyl T P , Huber W. *HTSeq — A Python framework to work with high-throughput sequencing data*. bioRxiv 2014.
 8. McKenna A., Hanna M., Banks E., Sivachenko A., Cibulskis K., Kernytsky A., Garimella K., Altshuler D., Gabriel S., Daly M., et al. The Genome Analysis Toolkit: A MapReduce framework for analyzing next-generation DNA sequencing data. *Genome Res.* 2010;20:1297–1303. doi: 10.1101/gr.107524.110. [PMC free article] [PubMed] [CrossRef] [Google Scholar]
 9. ANNOVAR: Functional annotation of genetic variants from high-throughput sequencing data. *Nucleic Acids Res.* 2010;38:e164. doi: 10.1093/nar/gkq603. [PMC free article] [PubMed] [CrossRef] [Google Scholar]

4.RESULTS

4.1 AML patient derived xenograft (PDX) establishment

To generate AML-PDXs we transplanted bone marrow samples obtained from pediatric patients affected by *de novo* AML at diagnosis or relapse into NOD.Cg-*Prkdcscid Il2rgtm1Wjl/SzJ* (NSG) mice. These samples (n=61) were different from immunophenotype and genetics, thus representing almost all the heterogeneity of the disease and the AML different subgroups (as described in Table 1 of Material and Method “Primary cell culture” section).

Each AML sample have been injected in 3 recipients and after one month, engraftment has been evaluated routinely for a median time of one year (see Material and Method “Mice engraftment monitoring” section) by monitoring the percentage of hCD45 positive cells in mice peripheral blood (PB)(Figure1).

This approach allowed the engraftment of 22/61 AML samples (36%) in a total number of 67/265 (25.3%) mice engrafted at first passage, namely P0-PDX generation.

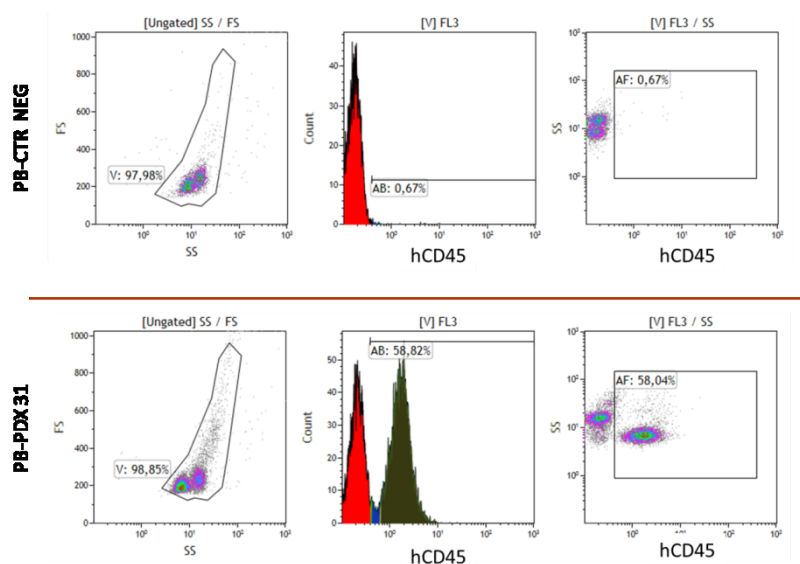


Figure 1. Representative image of mice engraftment monitoring: hCD45 positive cells in PB were measured by flow cytometry. A control PB (CTR-negative) and a model that showed AML engraftment (PB-PDX3) are shown.

Since this approach was not satisfying in terms of timing (one year for generating a model) and in the engraftment percentage we injected mice with classical intravenous (i.v.) and intrafemoral (i.f.) injection, or we inoculated blasts directly in the liver of newborn mice (intrahepatic injection, i.h.). In addition, we took advantages of biomimetic scaffolds pre-seeded *in vitro* with mesenchymal stromal cells isolated from the AML sample (AML-MSCs) and AML blasts, implanted subcutaneously in the back of the mice 24 hours (see Material and Method section “3D AML *in vivo* models” and Table 1).

INOCULATION METHODS	INOCULATED AML SAMPLES (n)	ENGRAFTED AML SAMPLES (n)	ENGRAFTMENT RATE (%)	INOCULATED P0 MICE (n)
SCAFFOLD	14	1	7,1%	48
I.F.	15	2	13,3%	67
I.V.	27	15	55,6%	71
I.H.	24	6	25,0%	79

Table 1. Number of AML samples transplanted and engrafted in mice and percentage of engraftment by different inoculation methods.

We observed that major engraftment rate was reached by intravenous injected samples (55,6%) and by intrahepatic injection in newborn mice (25%). Note of worthy, the three-dimensional scaffolds were well tolerated in the NSG hosts, without generating infection nor ulceration, but were ineffective for the PDXs generation, mediating engraftment only in one case. This latter result prompted us to trying to understand why the humanized niche was unable to improve blasts proliferation and dissemination, and for this reason harvested 3D scaffolds from mice were used for immunohistochemistry analysis that revealed the presence of human CD45 positive cells (Figure 2), as well as of mouse vascularization (by mCD31 staining) shown to pervade the whole exogenous structure after 3 weeks from inoculation. Moreover, osteoblasts (hOsteopontin and

Alizarin Red staining) were also evidenced, suggesting that human MSCs were able to differentiate creating an ectopic human bone marrow microenvironment (Figure 2).

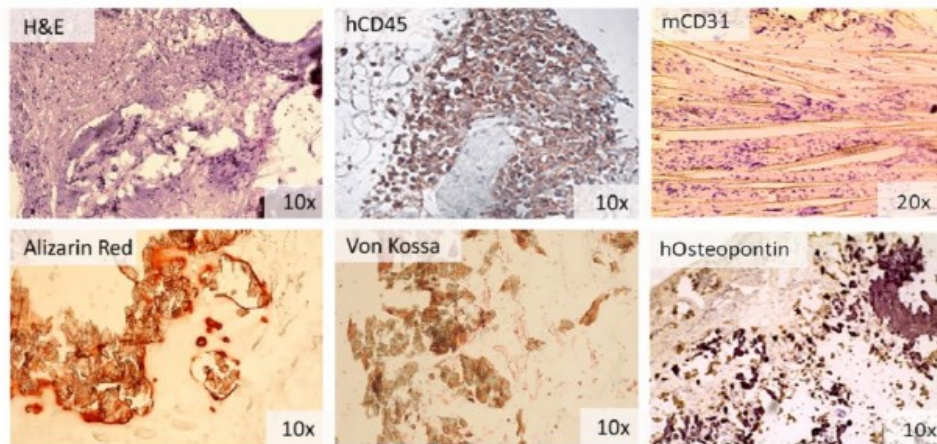


Figure 2. Histochemical staining of 3D scaffold slices after 3 weeks post-implantation in mice: representative image of H&E stain, DAB peroxidase stain for human CD45 and for murine CD31, Alizarin Red stain, Von Kossa stain and DAB peroxidase and human Osteopontin.

In light of these results, we used intravenous or intrahepatic injections obtaining a total of 22 different PDX models encompassing a wide spectrum of AML genetic lesions, being representative of 13 different AML subtypes (Table 2).

We collected AML cells from BM or spleen from engrafted mice, and these blasts have been transplanted into subsequent mice recipients, denoted as P1 and P2-PDXs (Figure 3 and Material and Methods section “PDX establishment”). At P2, these models are considered as stable and can be used in experimental settings. Ten are complete PDX models at P2, whereas 12 are still under development waiting for AML engraftment in P1 or P2 recipients (see Table 2). Notably, we observed an engraftment rate of 92% in P2 mice (46/51 mice engrafted at P2 generation).

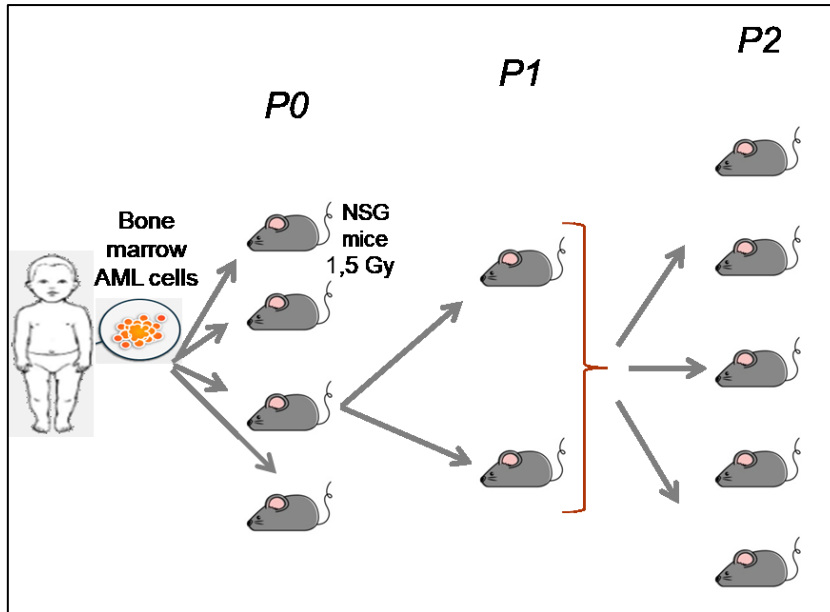


Figure 3. PDXs generation workflow starting from 1×10^6 primary cells implanted in first recipient (from patient's BM sample at AML diagnosis), to subsequent transplantation passages in other two mouse recipients, up to P2- that represent the generation of a stable model.

<u>Genetic marker</u>	<u>PDX ID</u>	<u>PDX development (mice passage)</u>
<i>FLT3ITD+NPM*^{mut}</i>	PDX#6	P1
<i>inv(16) (CBFB-MYH11)</i>	PDX#11	P2
	PDX#12	Established
<i>Inv(16) (CBFB-MYH11) +CKIT*^{mut}</i>	PDX#13	P1
	PDX#14	P1
<i>t(16;16) CBFA2T3-GLIS2</i>	PDX#17	P1
<i>t(16;21) FUS-ERG</i>	PDX#18	Established
<i>t(3;5) NPM1-MLF1 +FLT3ITD</i>	PDX#20	Established
<i>t(5;11)NUP98-NSD1 + FLT3ITD</i>	PDX#22(REL)	Established

t(5;11)NUP98-NSD1 +FLT3ITD	PDX#25	P1
t(6;11)KMT2A-AFDN	PDX#30	Established
	PDX#31	Established
t(4;11) KMT2A-AFF1	PDX#32	Established
t(10;11) KMT2A-MLLT10	PDX#34	Established
	PDX#36	P1
	PDX#37(REL)	P1
t(11;19)KMT2A-ENL	PDX#40	P1
t(9;11)KMT2A-MLLT3	PDX#41	Established
	PDX#42	P2
	PDX#43	P2
	PDX#44	P1
	PDX#45	Established

Table 2. AML-PDX models generated (established) or under generation with detail of genetics.

4.1.1 AML-PDX generation timing

We defined the disease latency as the time from AML cell inoculation to engraftment in mice. Primary AML cells engrafted in P0 in an average time of 148 days (5 months, Figure 4) with a high heterogeneity according to different models, reaching one year for some P0-PDXs. Briefly, from Table 3 we observed that latency exceeded 6 months for 9/22 models, 6/22 presented an engraftment latency between 3 and 6 months, and 7/22 engrafted in less than 3 months. By the way, disease latency from P0 to P2 was extremely reduced to an average of 74 days (Figure 5).

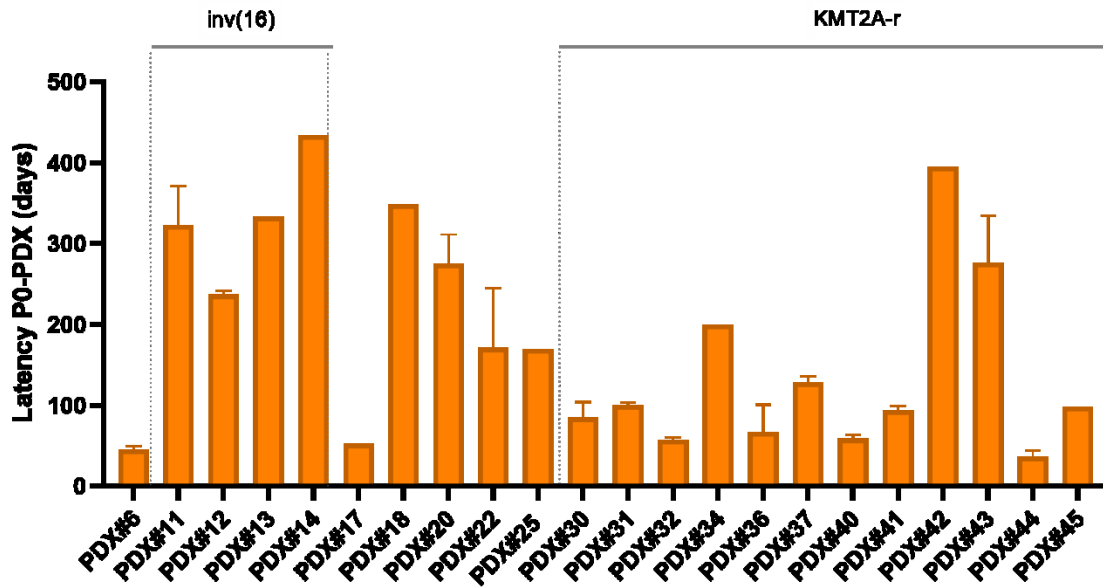


Figure 4. Disease latency from primary AML cells to P0-PDXs.

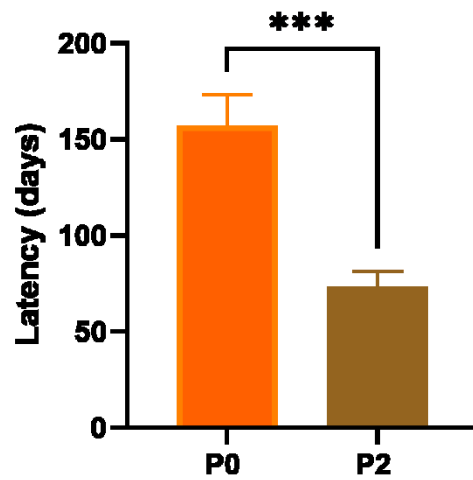


Figure 5. Average disease latency in P0 (orange, n=51) and P2 mice (brown, n=26)

p-value <0.001(**).

We observed a correlation between AML genetic and disease latency: a faster engraftment of *KMT2A*-rearranged leukemia (*KMT2A-r*) with respect to other AML subtypes, in particular with respect *inv(16)*-r P0, was observed (Figure 6).

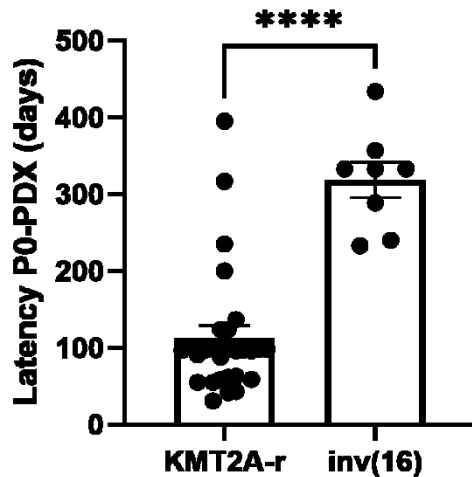


Figure 6. Average disease latency in P0-PDXs according to different genetic: *KMT2A-r* PDXs (n=28) compared to *inv(16)-r* PDXs (n=8). p-value <0.0001(****).

To assess the ability of primary leukemic cells to infiltrate mice organs, we evaluated the percentage of hCD45 positive cells in PDXs at sacrifice. We analysed mice bone marrow (BM) and spleen^{18,28}. Mice showed splenomegaly, and cells derived from both spleen and BM resulted positive for hCD45 by flow cytometry analysis (representative samples are reported in Figure 7A-B-C). We highlighted that PDXs harbouring *inv(16)-r* AML engrafted in longer time (average of 331 days) and presented lower blasts percentage in BM (average of 19%, by hCD45 positive cells), with respect to other genetic subtype such as *KMT2A-r* AML, where a median latency of 132 days with an average percentage of blasts of 60% was observed.

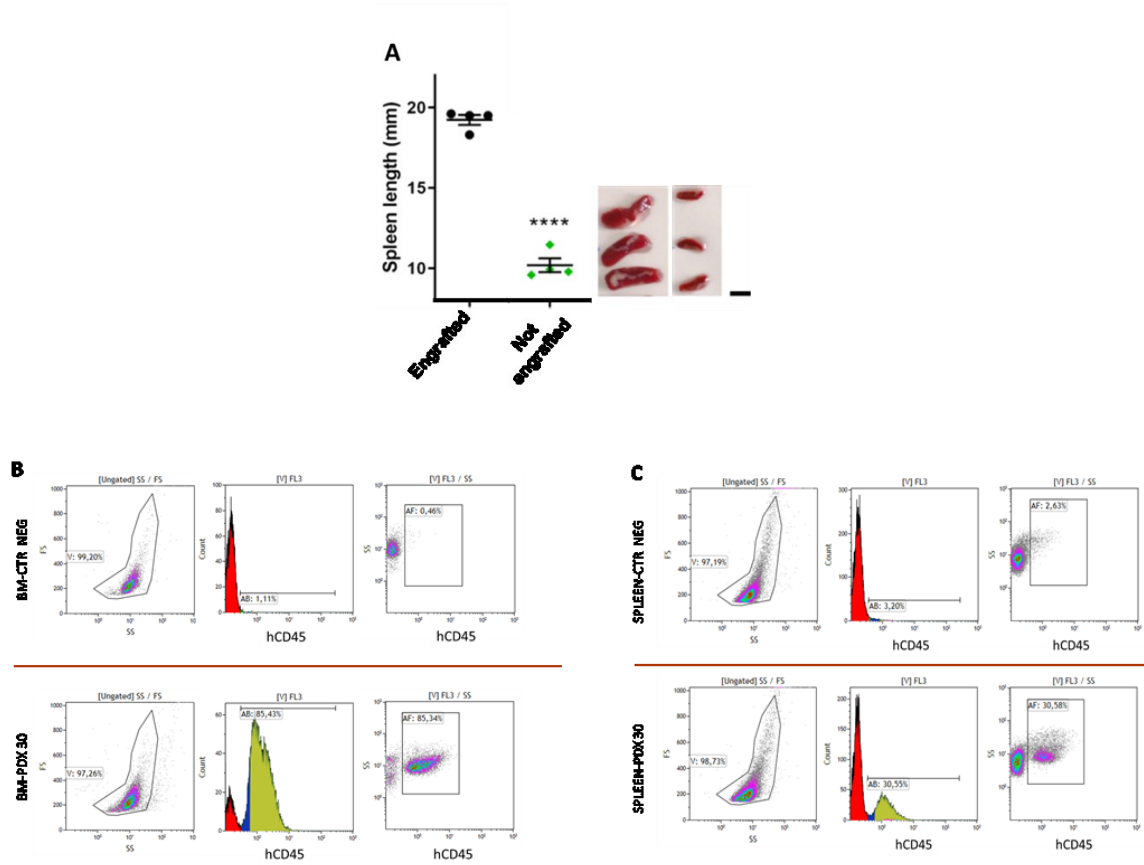


Figure 7. AML infiltration in PDX organs. A) Spleen length measure and representative images of 3 spleens/group (scale bar =10mm). B-C) Representative image of PDX organs invasion by flow cytometry monitoring of hCD45 in cells harvested from mouse BM (B) and spleen (C).

<u>Genetic marker</u>	<u>PDX ID</u>	<u>Latency</u> <u>P0-PDX</u> <u>(average days)</u>	<u>BM engraftment</u> <u>P0-PDX</u> <u>(average hCD45%)</u>
<i>FLT3ITD+NPM*mut</i>	PDX#6	45 (n=3)	70% (n=1)
<i>Inv(16) (CBFB-MYH11)</i>	PDX#11	323 (n=2)	15% (n=2)
	PDX#12	236 (n=2)	13% (n=2)
<i>Inv(16) (CBFB-MYH11) +CKIT*mut</i>	PDX#13	333 (n=3)	nv
	PDX#14	434 (n=1)	30% (n=3)

t(16;16) CBFA2T3-GLIS2	PDX#17	52 (n=3)	60% (n=3)
t(16;21) FUS-ERG	PDX#18	348 (n=2)	60% (n=2)
t(3;5) NPM1-MLF1 +FLT3ITD	PDX#20	275 (n=3)	90% (n=3)
t(5;11)NUP98-NSD1 +FLT3ITD	PDX#22(REL)	171 (n=3)	13% (n=3)
t(5;11)NUP98-NSD1 +FLT3ITD	PDX#25	170 (n=1)	89% (n=1)
t(6;11)KMT2A-AFDN	PDX#30	85 (n=3)	61% (n=2)
	PDX#31	100 (n=3)	88% (n=2)
t(4;11) KMT2A-AFF1	PDX#32	57 (n=3)	48% (n=3)
t(10;11) KMT2A-MLLT10	PDX#34	200 (n=1)	nv
	PDX#36	67 (n=2)	54% (n=2)
	PDX#37(REL)	128 (n=3)	60% (n=2)
t(11;19)KMT2A-ENL	PDX#40	58 (n=2)	4% (n=2)
t(9;11)KMT2A-MLLT3	PDX#41	94 (n=3)	56% (n=3)
	PDX#42	395 (n=1)	90% (n=1)
	PDX#43	276 (n=2)	64% (n=2)
	PDX#44	36 (n=2)	66% (n=2)
	PDX#45	98 (n=3)	73% (n=3)

Table 3. Established AML-PDXs grouped according to genetic markers with details of average P0 engraftment latency (days) and mean BM engraftment percentage; (n= number of P0 mice analyzed; nv= not evaluable).

4.1.2 Variables associated with AML engraftment success

We explored which variables were associated with the engraftment success observing that AML expressing particular genetic alterations involving KTM2A-rearrangements (2 cases t(6;11), 5 cases t(9;11), 3 cases t(10;11), 1 case with t(4;11) and 1 with t(11;19) rearrangements) were particularly represented in our models. On the contrary, we observed a low engraftment rate of AML harbouring t(5;11) NUP98-NSD1, t(16;16)CBFA2T3-GLIS2 , t(8;21)RUNX1-RUNX1T1, FLT3ITD mutation or of samples that resulted negative for the molecular markers screened at diagnosis (Figure 8).

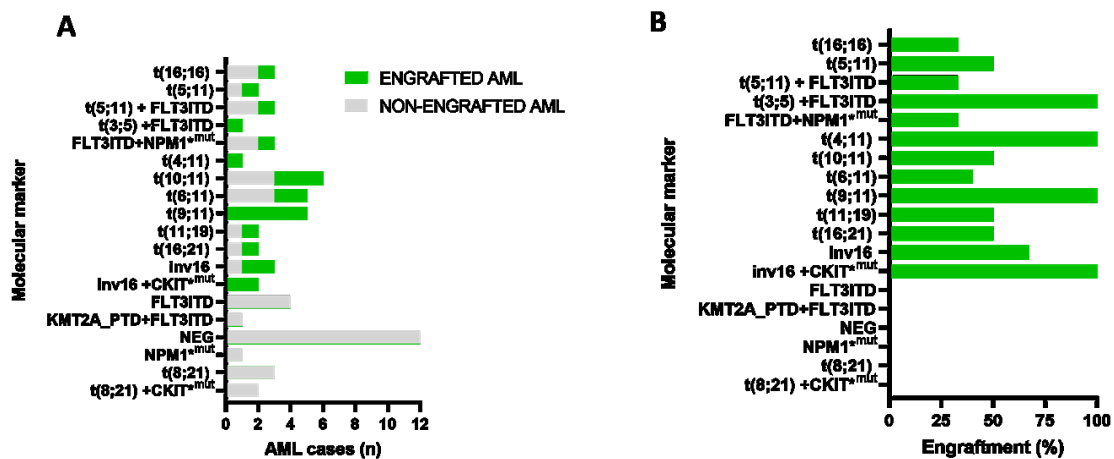


Figure 8. Bars represent the (A) number of AML cases implanted mice according to genetic rearrangement, and (B) engraftment rate (%).

Furthermore, Overall Survival(OS) and Event Free Survival (EFS) analysis of patient's whose AML was implanted in mice was performed showing a significant correlation between patient' outcome and mice engraftment success (Figure 9).

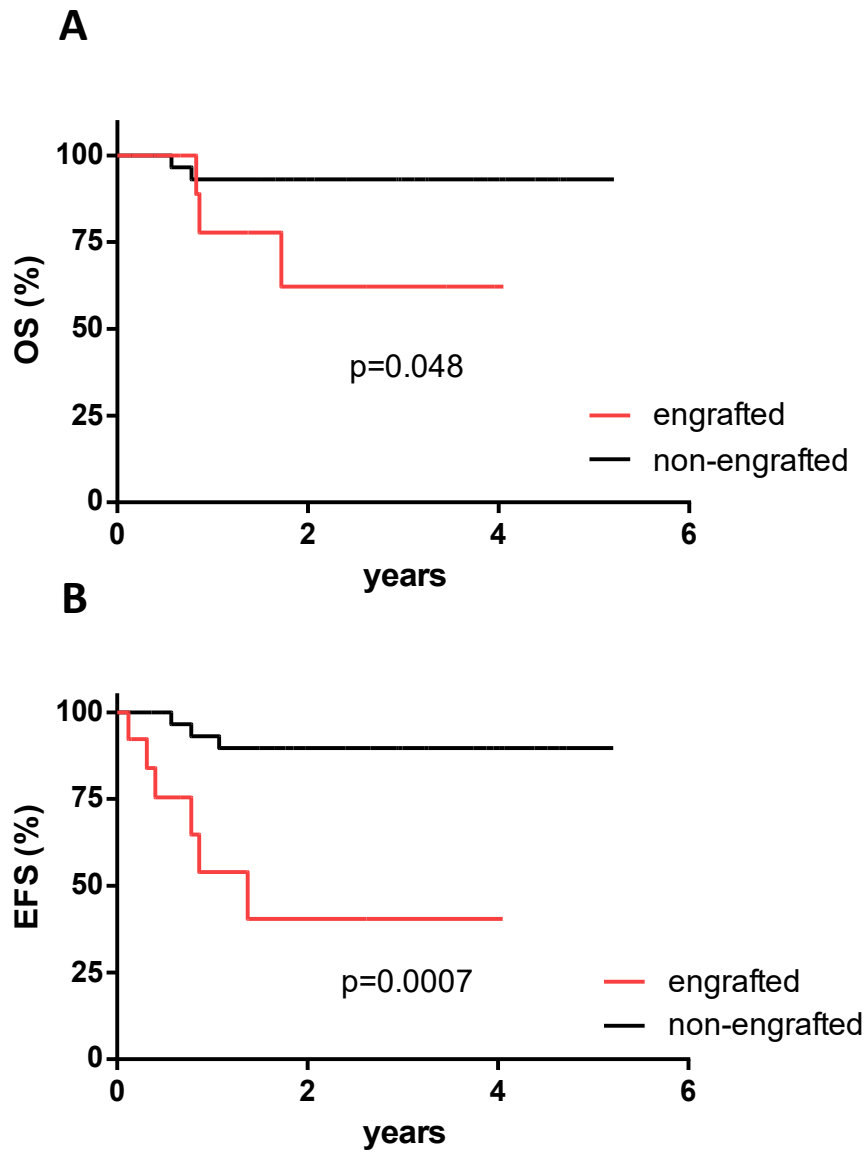


Figure 9. A) Kaplan-Meier curve showing 3-year OS and EFS (B) for the patient' AML (n=13) which engrafted in mice with respect to non-engrafted cases (n=31) (OS= 62.2% vs 93.1% $p=0.048$; EFS=40.5% vs 89.7%, $p=0.0007$ respectively).

4.2 AML-PDXs characterization

We characterized the established AML-PDX models (Table 4) from genetic, immunophenotypic and genomic point of view.

<u>Genetic marker</u>	<u>PDX ID</u>	<u>WES</u>	<u>RNA seq</u>	<u>Immunophenotype</u>
<i>FLT3ITD+NPM*^{mut}</i>	PDX#6			
Inv(16)	PDX#11			YES, ongoing
<i>CBFB-MYH11</i>	PDX#12			
Inv(16)	PDX#13			
<i>CBFB-MYH11 +CKIT*^{mut}</i>	PDX#14			
t(16;16)	PDX#17			
<i>CBFA2T3-GLIS2</i>				
t(16;21) <i>FUS-ERG</i>	PDX#18			
t(3;5) <i>NPM1-MLF1 +FLT3ITD</i>	PDX#20	YES		YES (ongoing)
t(5;11)<i>NUP98-NSD1 +FLT3ITD</i>	PDX#22 (REL)			YES
t(5;11)<i>NUP98-NSD1 +FLT3ITD</i>	PDX#25			
t(6;11)<i>KMT2A-AFDN</i>	PDX#30	YES	YES	YES
	PDX#31	PT no material	YES	YES
t(4;11) <i>KMT2A-AFF1</i>	PDX#32		YES (ongoing)	YES
t(10;11) <i>KMT2A-MLLT10</i>	PDX#34	YES-PT and P2 only	YES –P2 only(ongoing)	YES
	PDX#36			

	PDX#37 (REL)			
t(11;19)KMT2A-ENL	PDX#40			
t(9;11)KMT2A-MLLT3	PDX#41	YES	YES	YES
	PDX#42			
	PDX#43			
	PDX#44			
	PDX#45	YES	YES	YES

Table 4. Established AML-PDXs grouped according to genetic markers, with indications of models characterized by Whole exome sequencing (WES), RNA sequencing and immunophenotype.

4.2.1 PDXs genetic markers and immunophenotypic features

We explored the PDX models for their ability to preserve the characteristics of the original patient' AML. We screened the genetic markers detected in AML at diagnosis in *ex vivo* PDX-derived AML blasts by performing RT-PCR showing that all PDXs preserved the genetic lesions.

We explore also immunophenotype in 8 complete PDX models. In particular, we investigated immunophenotypic features of PDXs representative of different genetics subgroups: 1 AML model harbouring t(4;11) *KMT2A-AFF1* (AML#32), 2 model with t(9;11)*KMT2A-MLLT3* rearrangement (AML#41 and AML#45), 2 model of t(6;11)*KMT2A-AFDN* (AML#30 and AML#31), one model presenting t(10;11) *KMT2A-MLLT10* rearrangement (AML#34), 1 model t(3;5) *NPM1-MLF1 +FLT3ITD* mutated (AML#20) and 1 model t(5;11)*NUP98-NSD1+FLT3ITD* rearranged (AML#22). Moreover immunophenotypic profiles of two models, that are still under development, have been analysed up to P0 mice passage (AML#11 and AML#25, harbouring inv(16) and t(5;11)*NUP98-NSD1+FLT3ITD* respectively). Antigens expression according to AIEOP-BFM consensus guidelines²⁹ was interrogated revealing PDXs maintenance of the surface

markers pattern found in patient' AML. Slight expression variations were observed for CD34, CD117, CD11A/B in PDX samples; in particular CD34 and CD117 decreased during passages in mice, whereas CD11A/B and CD15 slightly increased in PDXs with respect to original AML. In Figure 10 we reported a representative immunophenotypic profiles comparison between AML#31 and respective P0-P1, P2 and P3-PDX generation.

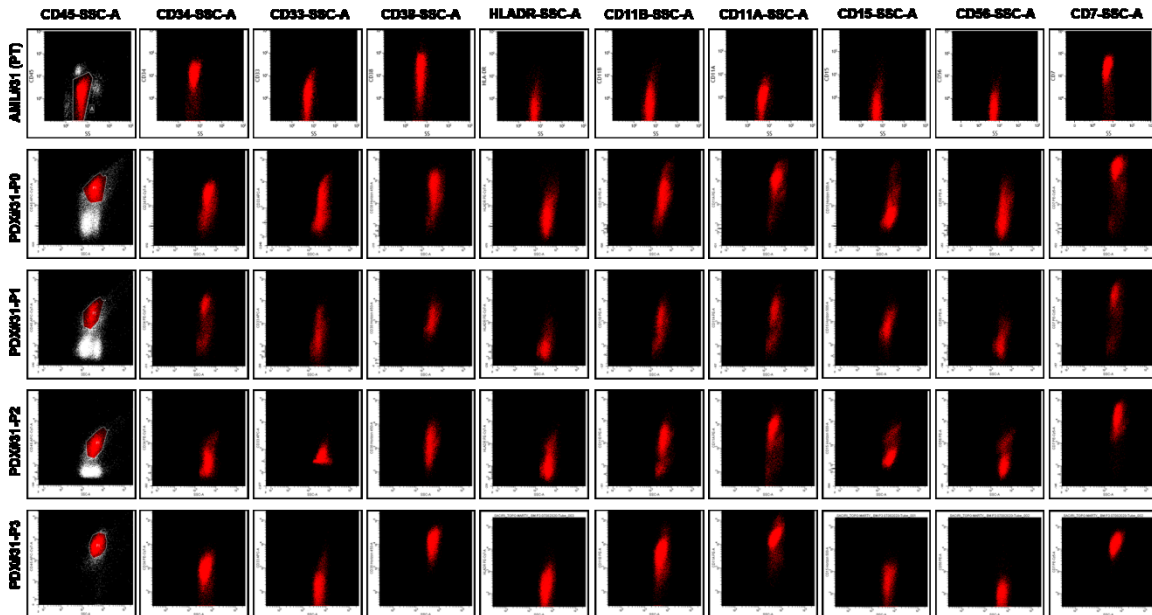


Figure 10. Immunophenotypic analysis of AML cells derived from patient (PT) at diagnosis (AML#31) and from matched PDX#31 passages by flow cytometry.

Since most of AML disseminate in mice spleen, we compared immunophenotypic profile of AML cells derived from BM or spleen at P1 (PDX#41 and PDX#34, Figure 11); moreover we compared cells derived from two different P0 mice of PDX#32 (Figure 12). Data showed a similar markers expression profile in both tissues indicating that during AML expansion we can use cells harvested from different mice organs since we did not observe substantial differences. We also confirmed that AML grew in different mice are equivalent (PDX#32, Figure 12).

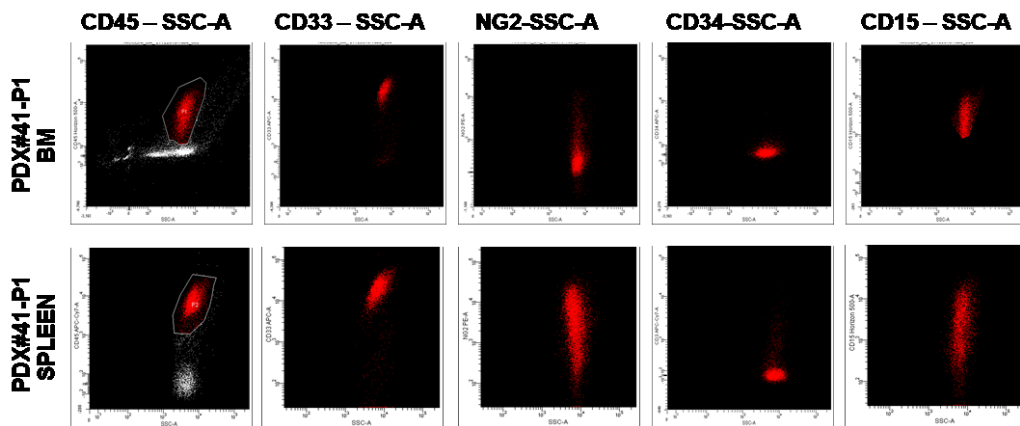
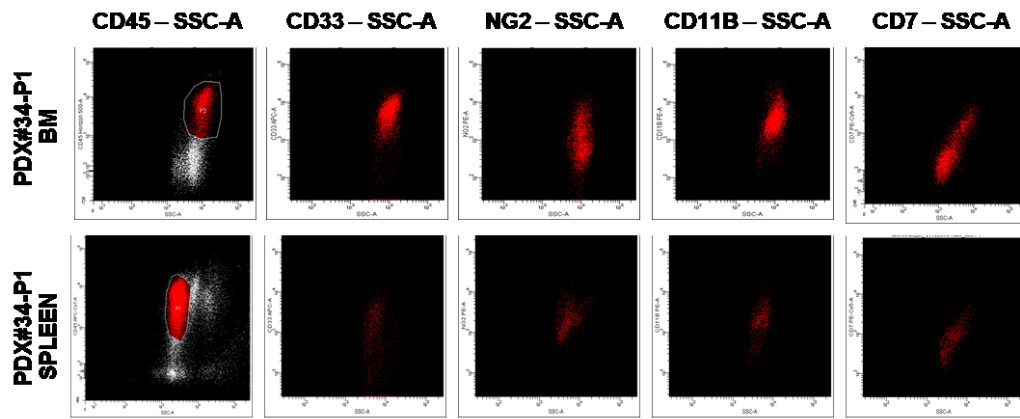


Figure 11. Immunophenotypic profile of AML cells derived from BM or spleen of PDXs#34 and PDX#41 by flow cytometry.

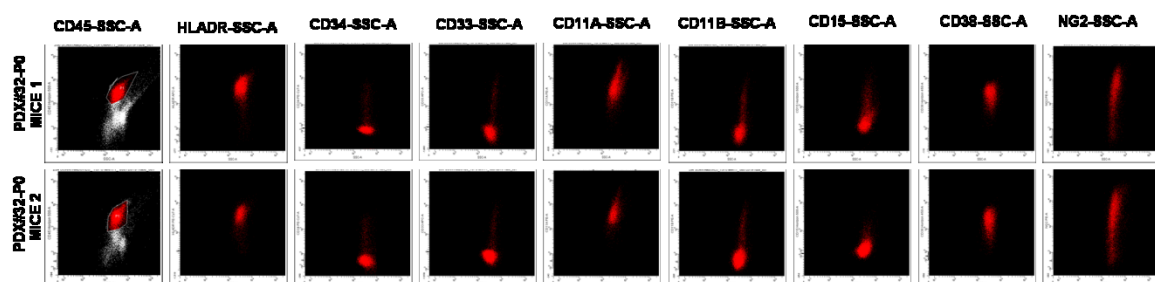


Figure 12. Immunophenotypic analysis of AML cells derived from two P0 mice derived from PT32 AML by flow cytometry.

PDXs characterization confirmed these models perpetuating leukemia with the maintenance of the genetic and immunophenotypic original tumor characteristics.

4.2.2 WHOLE EXOME SEQUENCING

The maintenance of the molecular marker detected at diagnosis is not sufficient to ensure PDX similarity to the original AML. Therefore, Whole Exome Sequencing (WES-300X) have been performed on patient and matched PDX samples (Table 4).

AML variants, AML clonal composition and AML clonal dynamics *in vivo*

Serial transplantations of AML cells in consequent mouse passages should mimic the AML clonal and hierarchical structure observed in patient' AML. In this context, WES of patient' AML and respective PDX passages enable to investigate AML clonal evolution *in vivo* trying to unmask the complexity and heterogeneity of AML. For each AML sample, single nucleotide variants (SNVs) or Insertion/Deletion (InDels) detected by WES have been critically analyzed applying filtering steps to obtain lists of selected variants. Then according to variant allelic frequency (AF) we delineated the AML clonal composition in patient' AML(PT) and in PDXs. In detail, starting from the initial list of thousand genetic alterations detected by WES in each AML samples, we performed a variants refinement process, based on the application of exclusion and inclusion criteria workflow, (reported in Figure 13, and in Material and Method "Next generation sequencing" section) that identifies variants most likely to be pathogenic.

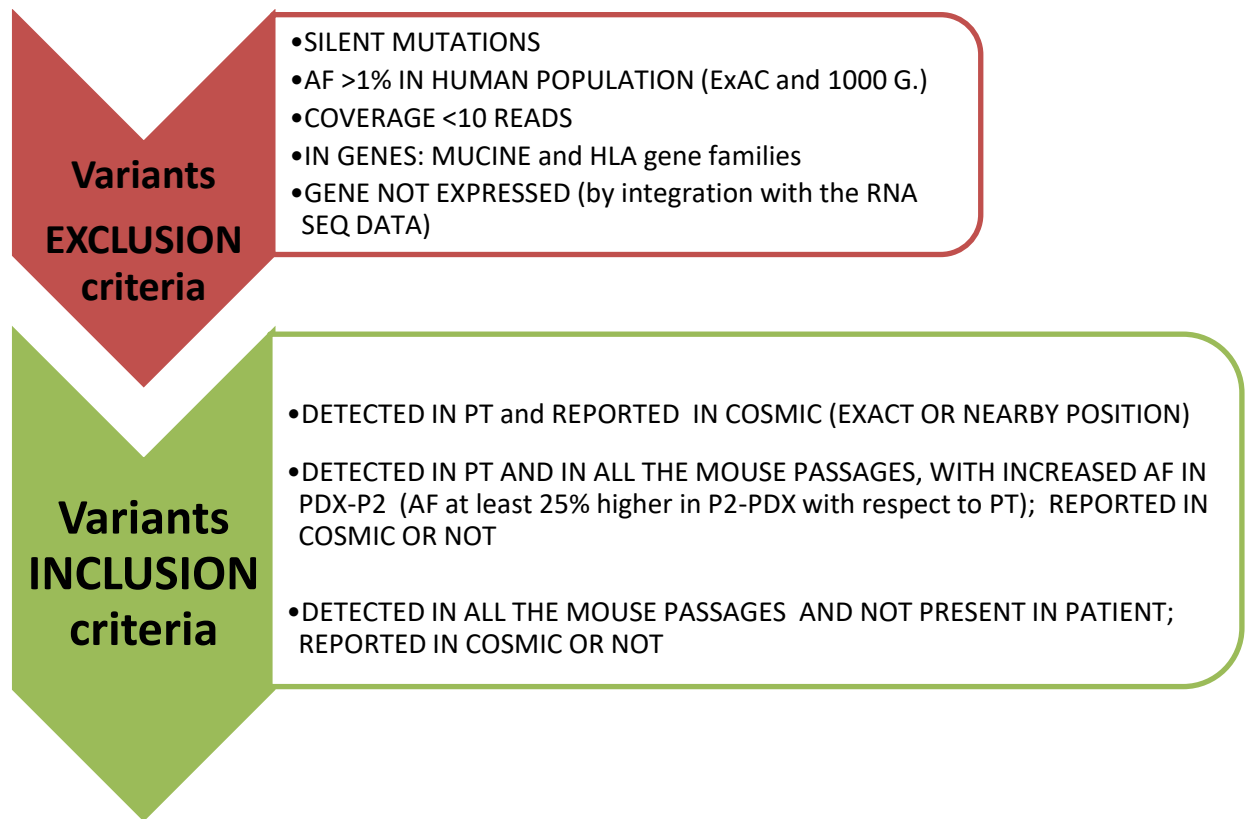


Figure 13. Workflow for WES variants refinement process.

After applying variants refinement workflow, we obtained a list of genetic alterations specific for each AML model.

Taking into consideration all analyzed models (n=5), 95.7% (181/189) of variants detected in patient' sample have been maintained in the corresponding P2-PDX. Overall, matched PT and P2-PDX samples showed a high genomic stability (Figure 14, $R^2=0.975$). In 4 out of 5 patient' samples we detected 30 variants on average, for AML#30 we detected 69 genetic variants.

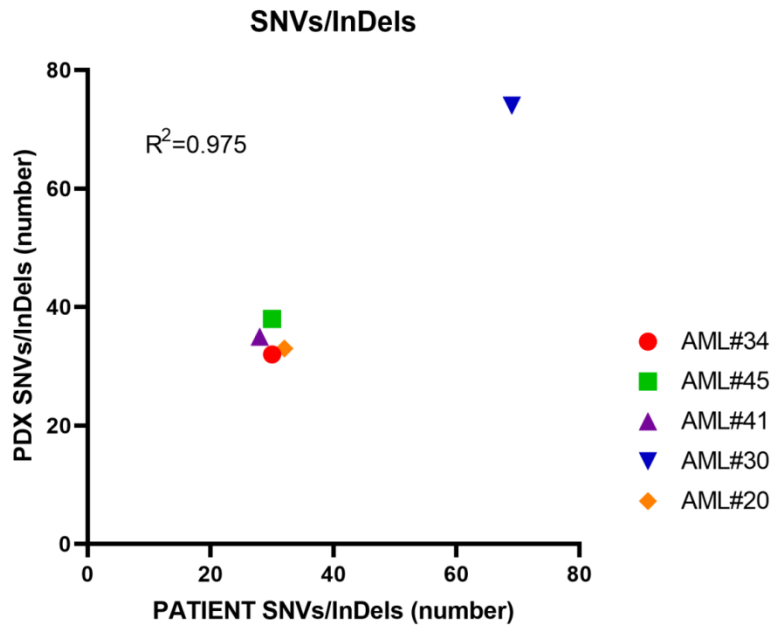


Figure 14. Total number of SNVs/InDels detected in patient' AML (x-axis) and in the corresponding P2-PDX (y-axis). R^2 : coefficient of determination.

In addition, we investigated variant AF correlation between PT and the PDX in order to dissect the clonal composition of AML at diagnosis with relative changes occurred in mice. In Figure 15 we reported AF of all variants found in AML patient' samples, compared to the AF of the same mutations found in P2-PDX: we observed a partial preservation of clonal hierarchy with a Person correlation coefficient=0.52, confirming a proportion of cells carrying articular variants maintained from PT-AML to P2-PDX, as expected³⁰. This result suggest the importance of these model in highlighting relevant leukemia clones preserved in PDXs.

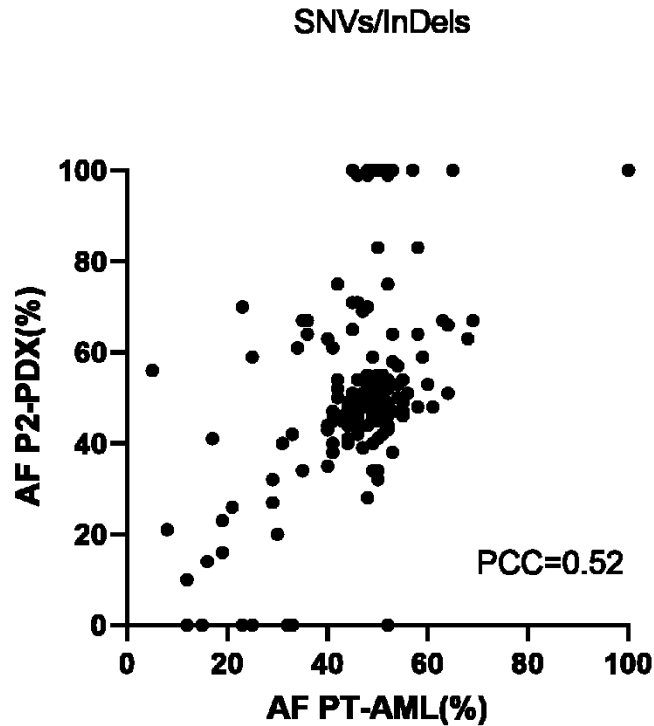


Figure 15. Variants AF in PT-AML (x-axis) and in P2-PDX (y-axis). PCC: Pearson's correlation coefficient.

We then considered variants detected in each AML model (AML#20, AML#30, AML#34, AML#41 and AML#45). After variants refinement, we subdivided SNVs/InDels as follow:

- Variant detected in PT, reported in COSMIC
- Variant with AF increase in PDX-P2 of at least 25% with respect to PT, suggesting a clonal expansion
- Variants detected in PDXs only

In the following tables we reported the name of mutated genes, the chromosome in which the gene is located, variant cDNA position with information on the alteration type (SNVs/InDels), association with COSMIC with details on the variant at the exact genomic position or nearby (± 10 nt); variant allelic frequency (AF) observed in patient's sample and in respective PDX samples (P0-P1 and P2). In blue we reported genes associated to driver mutations (following Papaemmanuil et al. ³¹) and in particular variants with AF between 40 and 60%, are considered typical of the AML founder clone.

AML#20

AML#20, harboring t(3;5)+*FLT3*ITD, is characterized by 27 variants: 15/27 variants are reported in COSMIC in the exact position, whereas 12/27 mutations are not reported but a nearby genetic alteration has been reported in COSMIC. Driver genes mutated in AML#20 are *FLT3* (*FLT3*ITD screened at diagnosis confirmed BY WES in patient and PDXs), *WT1*, *NUP98*, *TET1*, *TET2* and *GNAS*. 2/26 driver gene variants, on *WT1* and *NUP98* genes, were lost in all PDXs passages (red dots, Figure 16). Six variants increased AF from PT to mice passages (in particular a *WT1* variant, present in COSMIC). PDXs had 3 mutations (green dots, Figure 16) that were not previously identified in patient's sample (one nearby variant was reported in COSMIC).

AML#20							
Variants detected in PT, reported in COSMIC							
Chr	Gene	cDNA variant	COSMIC	AF PT	AF PDX-P0	AF PDX-P1	AF PDX-P2
1	<i>PDE4DIP</i>	c.C4672T	NEAR	30	19	32	20
1	<i>PDE4DIP</i>	c.G243T	EXACT_POS	19	14	21	16
1	<i>TPR</i>	c.C6502T	NEAR	50	45	48	41
2	<i>MSH6</i>	c.T1727C	EXACT_POS	52	41	42	44
3	<i>PIK3CA</i>	c.A1544G	EXACT_POS	53	48	54	64
3	<i>CACNA1D</i>	c.C3952T	EXACT_POS	41	51	48	40
4	<i>TET2</i>	c.C5167T	EXACT_POS	64	67	64	66
4	<i>TET2</i>	c.T2599C	EXACT_POS	69	72	67	67
5	<i>MAP3K1</i>	c.C824T	EXACT_POS	42	54	43	52
6	<i>EZR</i>	c.G1577A	NEAR	51	52	45	46
8	<i>RECQL4</i>	c.C2377T	NEAR	68	66	65	63
10	<i>TET1</i>	c.A4261G	EXACT_POS	41	36	46	45
11	<i>CARS</i>	c.C1709T	NEAR	53	100	100	100
11	<i>WT1</i>	c.1093_1106del	EXACT_POS	48	100	100	100
11	<i>WT1</i>	c.G101C	NEAR	52	0	0	0
11	<i>NUP98</i>	c.C2029T	NEAR	52	0	0	0
12	<i>STAT6</i>	c.G1400A	EXACT_POS	54	51	48	57
12	<i>NACA</i>	c.G1201A	EXACT_POS	40	43	41	43

12	MDM2	c.G519C	NEAR	49	45	55	45
14	GOLGA5	c.G1120A	NEAR	50	43	48	50
13	FLT3	c.1837-ITD	NEAR	41	57	61	66
16	LOC100129697	c.894_1094del	NEAR	45	43	45	44
16	LOC100129697	c.C641G	EXACT_POS	33	35	31	42
17	SUZ12	c.G211A	EXACT_POS	50	52	60	52
17	ERBB2	c.G3044A	EXACT_POS	44	49	45	47
20	GNAS	c.1189_1190ins	EXACT_POS	47	33	48	39
22	CLTCL1	c.4550_4559del	NEAR	52	42	38	47
Variants with AF increase in PDXs							
Chr	Gene	cDNA variant	COSMIC	AF PT	AF PDX-P0	AF PDX-P1	AF PDX-P2
5	EPB41L4A	c.G887A		5	41	45	56
11	CARS	c.C1709T	NEAR	53	100	100	100
11	DENND5A	c.G81T		52	100	100	99
11	WT1	c.1093_1106del	EXACT_POS	48	100	100	100
11	DNHD1	c.G1160A		48	100	100	100
22	MAPK12	c.101dupG		34	68	74	61
Variants detected in PDX only							
Chr	Gene	cDNA variant	COSMIC	AF PT	AF PDX-P0	AF PDX-P1	AF PDX-P2
6	CCND3	c.A587G	NEAR	0	49	60	42
21	TIAM1	c.C1217T		0	52	51	48
19	KXD1	c.G37A		0	7	6	27

Table 5. Variants detected in AML#20 and matched PDXs.

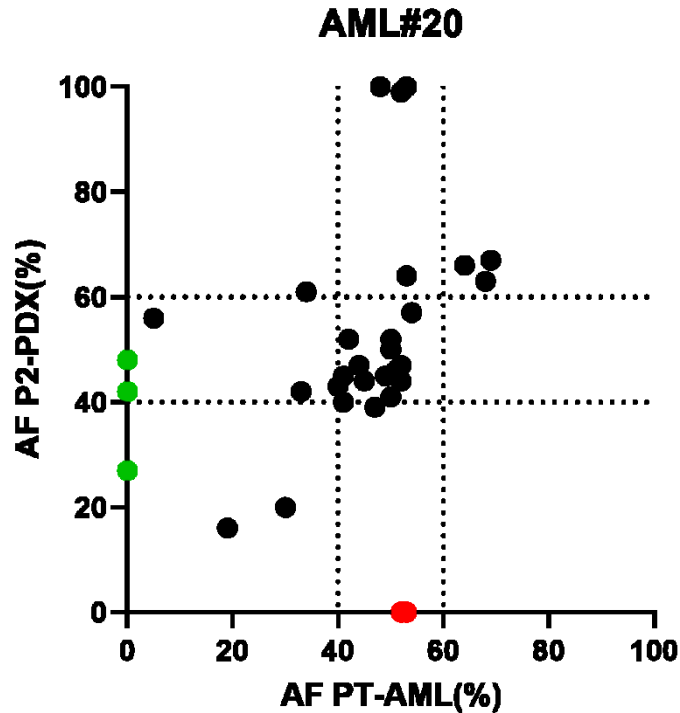


Figure16. Variants AF in PT-AML#20 (x-axis) and in matched P2-PDX#20 (y-axis). In green genetic alterations absent in PT, in red mutations lost in PDX, in black preserved mutation in the model.

AML#30

AML#30 is a $t(6;11)KMT2A-AFDN$ rearranged AML and had 50 variants: 26/50 genetic alterations are reported in COSMIC in the exact position, whereas for 24/50 a nearby variants is described in COSMIC. AML#30 has one driver gene, *NRAS*; 19 variants increased AF from PT to PDXs (none reported in COSMIC). PDXs showed 5 mutations (green dots, Figure 17) that were not detected in patient's sample (one nearby variant was reported in COSMIC).

AML#30

Variants detected in PT, reported in COSMIC

Chr	Gene	cDNA variant	COSMIC	AF PT	AF PDX-P0	AF PDX-P1	AF PDX-P2
1	NRAS	c.A182G	EXACT_POS	45	35	46	45
1	<i>PDE4DIP</i>	c.G2026A	NEAR	51	50	49	46
1	<i>SPEN</i>	c.T4910C	NEAR	48	35	40	52
1	<i>PTPRC</i>	c.A1085T	NEAR	52	67	54	54
1	<i>PDE4DIP</i>	c.A749G	NEAR	51	57	51	42
1	<i>PDE4DIP</i>	c.G2838A	NEAR	44	54	59	49
1	<i>SPEN</i>	c.A7657G	EXACT_POS	45	42	44	46
1	<i>BCL9</i>	c.G4096C	EXACT_POS	51	47	47	48
1	<i>PDE4DIP</i>	c.C4300T	EXACT_POS	21	25	22	26
2	<i>PMS1</i>	c.T653C	EXACT_POS	100	100	99	100
2	<i>PMS1</i>	c.G973A	EXACT_POS	100	100	100	100
2	<i>PMS1</i>	c.A1115G	EXACT_POS	49	34	53	59
2	<i>PMS1</i>	c.T1849C	EXACT_POS	100	100	100	100
2	<i>MSH2</i>	c.A380G	EXACT_POS	48	53	48	48
3	<i>BCL6</i>	c.C1375T	EXACT_POS	44	57	44	41
3	<i>LPP</i>	c.T775C	NEAR	46	47	50	49
3	<i>LPP</i>	c.T775C	NEAR	46	47	50	49
4	<i>FAT1</i>	c.A7141G	NEAR	50	43	46	46
4	<i>FAT1</i>	c.C13042A	NEAR	49	48	43	46
4	<i>FAT1</i>	c.G2035A	EXACT_POS	100	100	100	100
5	<i>NSD1</i>	c.750_752del	NEAR	45	44	46	45
6	<i>HSP90AB1</i>	c.G1617C	NEAR	53	34	46	58
6	<i>FOXO3</i>	c.237_242del	NEAR	64	52	48	51
6	<i>FOXO3</i>	c.1141dupG	NEAR	12	9	14	10
6	<i>ECT2L</i>	c.G1024A	NEAR	50	35	46	46
7	<i>AKAP9</i>	c.G8485A	NEAR	100	100	100	100
7	<i>KIAA1549</i>	c.G2770A	EXACT_POS	50	51	49	51
8	<i>COX6C</i>	c.A62G	NEAR	45	45	46	45
8	<i>RECQL4</i>	c.C1772T	EXACT_POS	49	48	46	50
10	<i>TCF7L2</i>	c.C1484G	EXACT_POS	58	62	62	64
11	<i>FANCF</i>	c.G373A	EXACT_POS	50	43	48	54
11	<i>NUMA1</i>	c.G5431A	NEAR	40	45	44	44

12	ARID2	c.G4945C	EXACT_POS	61	45	52	48
12	KDM5A	c.G761A	EXACT_POS	41	43	48	38
13	BRCA2	c.G7017C	EXACT_POS	44	60	46	40
13	BRCA2	c.G9730A	EXACT_POS	55	54	56	47
13	BRCA2	c.G1564C	NEAR	48	56	52	51
13	BRCA2	c.A7319G	EXACT_POS	50	51	51	55
14	NIN	c.G5075A	NEAR	48	40	49	50
16	TSC2	c.A2968G	NEAR	51	48	50	47
16	ZFH3	c.C2392T	NEAR	51	52	44	50
16	AXIN1	c.G1672A	EXACT_POS	47	44	48	54
16	CREBBP	c.G2974A	EXACT_POS	47	50	44	48
16	ZFH3	c.A2354G	EXACT_POS	54	44	53	50
17	BRCA1	c.A3418G	EXACT_POS	51	47	50	55
17	CANT1	c.G967A	EXACT_POS	48	39	29	28
17	RNF213	c.G103A	NEAR	49	23	36	34
19	ELL	c.C704T	EXACT_POS	48	51	54	53
19	CRTC1	c.G919A	NEAR	42	43	48	54
20	CRNKL1	c.G1675A	NEAR	50	52	46	48

Variants with AF increase in PDX

Chr	Gene	cDNA variant	COSMIC	AF PT	AF PDX-P0	AF PDX-P1	AF PDX-P2
1	NBPF10	c.G2056T		45	61	54	65
2	SPAG16	c.C970A		45	79	100	100
2	HTR2B	c.A1135G		46	71	99	99
2	BOLL	c.C40G		48	69	100	99
2	SP110	c.C1100T		49	82	97	100
2	C2orf54	c.C305T		51	85	100	100
2	SPAG16	c.A1885G		52	80	100	100
2	FAM124B	c.A1210G		53	76	100	100
2	ANKZF1	c.A185G		53	94	99	100
2	LANCL1	c.T414G		57	100	100	100
2	CROCC2	c.G3449A		65	100	100	100
3	TRAK1	c.2063_2064ins		50	100	92	100
5	ZBED3	c.99_100ins		17	21	44	41
5	NSUN2	c.C22T		40	27	46	63
8	TIGD5	c.G688C		42	60	72	75
10	DCLRE1C	c.A939C		48	37	60	70

11	<i>OSBP</i>	c.G184T		52	50	38	75
17	<i>MYO15B</i>	c.C5656A		47	65	68	69
20	<i>CENPB</i>	c.1283_1284ins		36	54	48	67
Variants detected in PDX only							
Chr	Gene	cDNA variant	COSMIC	AF PT	AF PDX-P0	AF PDX-P1	AF PDX-P2
1	<i>ARID1A</i>	c.113_114ins	NEAR	0	43	48	50
2	<i>USP34</i>	c.T8266C		0	12	1	6
3	<i>SCHIP1</i>	c.103_104ins		0	51	45	42
4	<i>CRIPAK</i>	c.489_490ins		0	55	45	50
21	<i>PLAC4</i>	c.122_123ins		0	23	59	43

Table 6. Variants detected in AML#30 and matched PDXs.

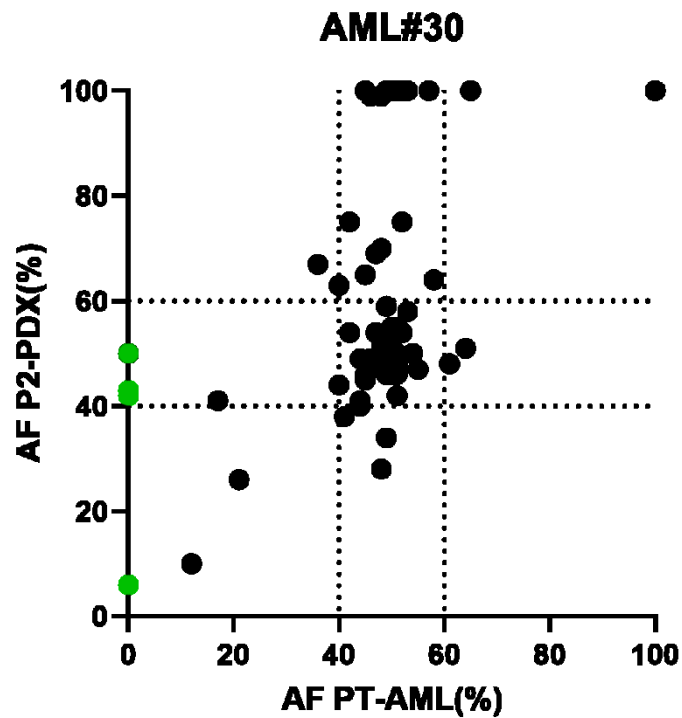


Figure 17. Variants AF in PT-AML#30 (x-axis) and in matched P2-PDX#20 (y-axis). In green genetic alterations absent in PT, in red mutations lost in PDX, in black preserved mutation in the model.

AML#34

AML#34 a t(10;11) *KMT2A-MLLT10* rearranged AML, is characterized by 28 variants: 17/28 variants are reported in COSMIC in the exact position, whereas for 11/28 a nearby variant is reported in COSMIC. Driver genes found mutated in AML#34 are *TET2*, *PTEN*, *KRAS* and *FLT3*; 3/28 variants were lost in all PDXs (red dots, Figure 18). Two variants increased AF from PT to PDX (in particular a SNV in *FLT3* reported in the exact position in COSMIC). Five mutations were not identified in patient's sample (green dots, Figure 18) and not reported in COSMIC.

AML#34					
Variants detected in PT, reported in COSMIC					
Chr	Gene	cDNA variant	COSMIC	AF PT	AF PDX-P2
1	<i>BCL9</i>	c.C337T	NEAR	35	34
1	<i>TAL1</i>	c.C287T	NEAR	50	32
2	<i>STRN</i>	c.G100A	NEAR	63	67
2	<i>AFF3</i>	c.G2857A	EXACT_POS	54	53
3	<i>ROBO2</i>	c.C1388T	EXACT_POS	48	44
3	<i>FBLN2</i>	c.C2246T	NEAR	56	51
3	<i>FANCD2</i>	c.T2692C	NEAR	56	51
3	<i>CBLB</i>	c.G1865C	NEAR	50	45
4	<i>TET2</i>	c.G5103A	EXACT_POS	53	47
5	<i>APC</i>	c.G7460A	EXACT_POS	44	48
7	<i>AKAP9</i>	c.A10840G	EXACT_POS	49	49
10	<i>PTEN</i>	c.C511G	EXACT_POS	44	44
10	<i>KIF5B</i>	c.C73G	NEAR	51	42
11	<i>DDX10</i>	c.T1340G	NEAR	46	46
12	<i>KRAS</i>	c.G38A	EXACT_POS	15	0
12	<i>SETD1B</i>	c.A1478G	NEAR	43	46
12	<i>SH2B3</i>	c.T17C	EXACT_POS	48	49
12	<i>KDM5A</i>	c.G4831A	NEAR	55	46
13	<i>FLT3</i>	c.A2027C	EXACT_POS	23	70
14	<i>NIN</i>	c.G3647A	EXACT_POS	52	52
16	<i>LOC100129697</i>	c.C1094G	EXACT_POS	32	0

16	LOC100129697	c.G1091C	EXACT_POS	33	0
16	LOC100129697	c.C641G	EXACT_POS	31	40
16	MYH11	c.C1913T	EXACT_POS	47	50
17	NCOR1	c.G5744A	EXACT_POS	43	45
20	NFATC2	c.G91C	EXACT_POS	46	50
22	BCR	c.G3184A	EXACT_POS	16	14
22	BCR	c.3142_3143ins	NEAR	29	27
Variants with AF increase in PDXs					
Chr	Gene	cDNA variant	COSMIC	AF PT	AF PDX-P2
8	MTUS1	c.A473C		45	71
13	<i>FLT3</i>	c.A2027C	EXACT_POS	23	70
Variants detected in PDX only					
Chr	Gene	cDNA variant	COSMIC	AF PT	AF PDX-P2
9	TRPM6	c.G1526T		0	48
13	DGKH	c.G2174A		0	64
14	NOP9	c.483_484ins		0	0
16	DPEP2	c.G203A		0	13
X	DMD	c.G271A		0	15

Table 7. Variants detected in AML#34 and matched PDXs.

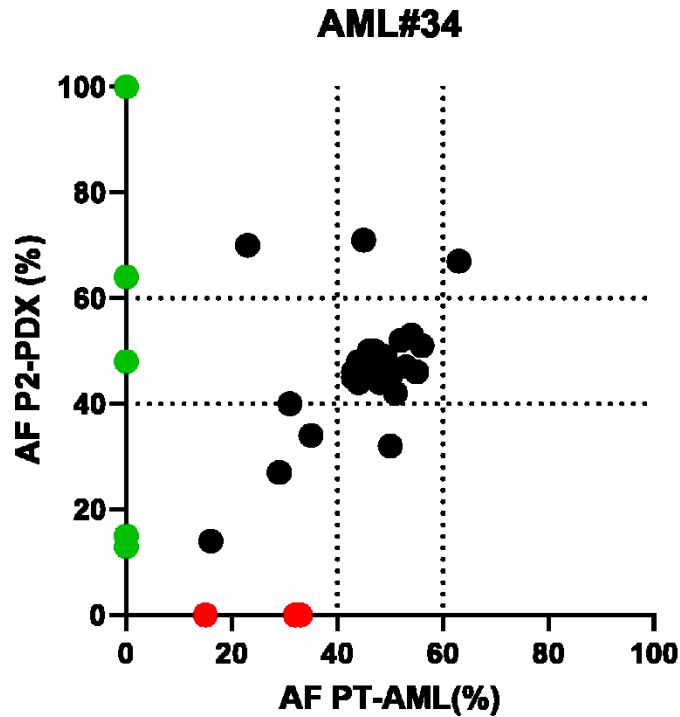


Figure 18. Variants AF in PT-AML#34 (x-axis) and in matched P2-PDX#34 (y-axis). In green genetic alterations absent in PT, in red mutations lost in PDX, in black preserved mutation in the model.

AML #41

AML#41 was $t(9;11)KMT2A-MLLT3$ rearranged and showed 24 variants: 14/24 are reported in COSMIC in the exact position; 10/24 mutations were reported nearby in COSMIC; *TET1*, *NOTCH1* and *KRAS* were the driver genes; 4 variants increased AF from PT to PDXs; 7 mutations were present in PDXs but absent patient's sample (green dots, Figure 19) and one of them on *ARID1A* gene was reported in the exact position in COSMIC.

AML#41

Variants detected in PT, reported in COSMIC

Chr	Gene	cDNA variant	COSMIC	AF PT	AF PDX-P0	AF PDX-P1	AF PDX-P2
1	ARID1A	c.A4790G	NEAR	47	47	48	39
1	CFAP126	c.G233A	EXACT_POS	47	46	51	51
2	LRP1B	c.A12161C	EXACT_POS	46	49	44	50
3	MITF	c.C326T	EXACT_POS	49	46	52	47
3	TP63	c.C1459T	EXACT_POS	51	48	46	47
5	DROSHA	c.C248T	EXACT_POS	59	56	65	59
6	LATS1	c.C286T	EXACT_POS	50	54	46	51
7	SMO	c.47_48insGCT	NEAR	50	54	57	47
7	HIP1	c.C1843T	NEAR	49	49	42	45
9	NOTCH1	c.C2734T	EXACT_POS	50	51	56	48
9	KLF4	c.716_766del	NEAR	29	28	32	32
9	BRD3	c.A1964G	EXACT_POS	46	47	48	48
10	TET1	c.A4534T	NEAR	42	48	46	50
11	FAT3	c.G10552A	EXACT_POS	46	55	43	42
11	DDX10	c.C811G	NEAR	41	48	52	61
12	KRAS	c.A183C	EXACT_POS	45	55	40	51
12	POLE	c.G776A	EXACT_POS	50	40	48	49
12	USP44	c.A367C	NEAR	44	43	47	46
13	LPAR6	c.460_461insA	NEAR	49	46	52	40
13	LPAR6	c.G460T	NEAR	49	46	52	40
14	TRIP11	c.G5298T	EXACT_POS	48	48	53	55
15	BLM	c.G1223A	NEAR	53	47	40	38
17	SUZ12	c.G211A	EXACT_POS	42	60	39	52
22	APOBEC3B	c.C631T	EXACT_POS	50	54	51	55

Variants with AF increase in PDXs

Chr	Gene	cDNA variant	COSMIC	AF PT	AF PDX-P0	AF PDX-P1	AF PDX-P2
5	ZSWIM6	c.55_60del		46	55	71	71
7	FASTK	c.G172A		48	100	100	100
12	ATN1	c.1462_1485del		35	36	67	67
19	RASAL3	c.1221_1234del		58	52	71	83

Variants detected in PDX only							
Chr	Gene	cDNA variant	COSMIC	AF PT	AF PDX-P0	AF PDX-P1	AF PDX-P2
1	ARID1A	c.6773_6777del	EXACT_POS	0	48	43	48
3	ACTL6A	c.C586T		0	54	44	44
5	SYNPO	c.2367_2368ins		0	60	40	50
12	NOC4L	c.897_901del		0	98	96	95
13	SLAIN1	c.219_220ins		0	100	100	100
19	DMKN	c.860_861ins		0	58	44	55
19	CAPNS1	c.112_114del		0	2	12	6

Table 8. Variants detected in AML#41 and matched PDXs.

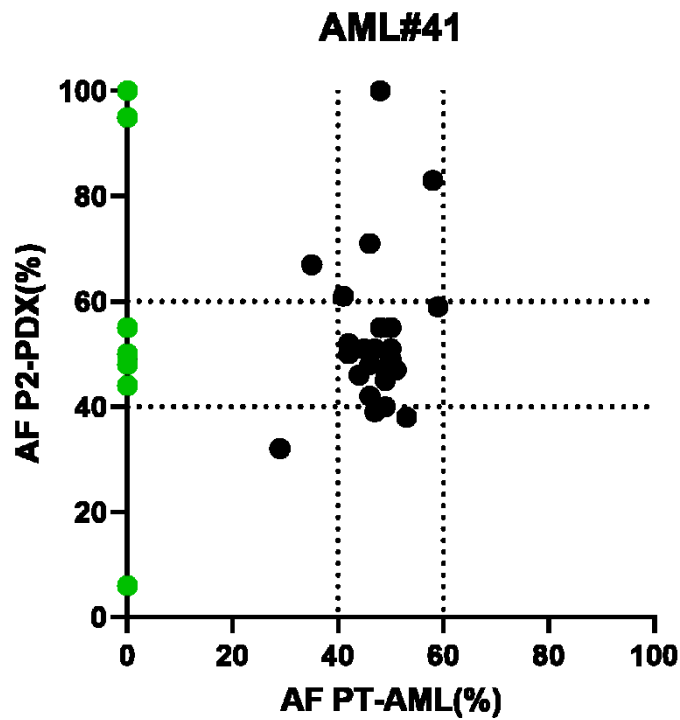


Figure 19. Variants AF in PT-AML#41 (x-axis) and in matched P2-PDX#41 (y-axis). In green genetic alterations absent in PT, in red mutations lost in PDX, in black preserved mutation in the model.

AML#45

AML#45 harbor *t(9;11)KMT2A-MLLT3* rearrangement and had 27 variants: 16/27 variants are reported in COSMIC in the exact position, whereas 11/27 were reported nearby in COSMIC. Drivers genes were *TET2* and *CBL*. 3/27 variants were lost in all PDXs (red dots, Figure 20). Three variants increased AF from PT to PDXs (one on *BCL6* gene was reported in the exact position in COSMIC). Eleven mutations were detected in PDXs but have not been identified in patient's sample (green dots, Figure 20): one mutation in *RB1* gene, suggested as a driver gene³¹, was associated to a nearby alteration in COSMIC; another variant detected in PDXs but not in the PT, occurred in *POT1* gene and has been reported in COSMIC in the exact chromosomal location.

AML#45							
Variants detected in PT, reported in COSMIC							
Chr	Gene	cDNA variant	COSMIC	AF PT	AF PDX-P0	AF PDX-P1	AF PDX-P2
1	<i>MUTYH</i>	c.G1106A	EXACT_POS	52	43	52	49
1	<i>ANGPTL7</i>	c.G934A	NEAR	46	44	50	49
2	<i>MSH2</i>	c.C382G	NEAR	52	41	46	46
2	<i>MYCN</i>	c.100_101del	NEAR	12	0	0	0
2	<i>BIRC6</i>	c.A1679C	NEAR	46	48	53	54
3	<i>SETD2</i>	c.7306dupC	NEAR	23	0	0	0
3	<i>TP63</i>	c.G1127A	EXACT_POS	50	44	48	34
3	<i>BCL6</i>	c.C1375T	EXACT_POS	36	53	47	64
4	<i>TET2</i>	c.A3251C	EXACT_POS	52	46	49	49
6	<i>ARID1B</i>	c.G736A	EXACT_POS	60	46	52	53
6	<i>TNFAIP3</i>	c.G1316C	EXACT_POS	55	59	57	49
6	<i>ARID1B</i>	c.919_927del	EXACT_POS	52	41	45	43
7	<i>ELN</i>	c.2137_2151del	EXACT_POS	50	54	43	49
8	<i>WRN</i>	c.A970G	EXACT_POS	46	55	48	45
9	<i>TNC</i>	c.C2701T	NEAR	25	0	0	0
9	<i>KLF4</i>	c.G651T	NEAR	51	52	51	45
11	<i>FAT3</i>	c.G11057A	NEAR	50	50	50	50

11	CBL	c.C1027G	EXACT_POS	46	48	44	50
11	SDHD	c.G34A	EXACT_POS	52	50	46	46
11	ARHGEF1 2	c.G1469A	EXACT_POS	50	44	46	49
14	TSHR	c.C1538T	EXACT_POS	46	47	47	48
14	GPHN	c.A800G	NEAR	55	50	54	54
16	RFWD3	c.C1241T	NEAR	40	46	58	35
17	RNF213	c.G13195A	EXACT_POS	41	49	51	47
17	RNF213	c.A6551G	EXACT_POS	58	50	53	48
22	BCR	c.3142_3143ins	NEAR	19	31	8	23
22	BCR	c.G3184A	EXACT_POS	8	21	0	21
Variants with AF increase in PDX							
Chr	Gene	cDNA variant	COSMIC	AF PT	AF PDX -P0	AF PDX- P1	AF PDX- P2
1	NBPF26	c.G2017C		50	63	78	83
3	BCL6	c.C1375T	EXACT_POS	36	53	47	64
4	RUFY3	c.A116C		25	43	34	59
Variants detected in PDX only							
Chr	Gene	cDNA variant	COSMIC	AF PT	AF PDX -P0	AF PDX- P1	AF PDX- P2
1	SLAMF8	c.G170A		0	33	4	39
5	PPP2R2B	c.55_57del		0	4	3	5
6	HIVEP2	c.C4655T		0	38	5	40
7	POT1	c.A281G	EXACT_POS	0	45	48	52
8	TEX15	c.A7203T		0	49	51	36
10	STK32C	c.315dupG		0	53	43	47
12	MMP17	c.64_65ins		0	68	50	67
13	RB1	c.A397G	NEAR	0	54	45	53
13	SLAIN1	c.229dupC		0	100	100	100
18	MBD2	c.345_346insGGC		0	28	56	28
19	APC2	c.C2131T		0	46	44	45

Table 9. Variants detected in AML#45 and matched PDXs.

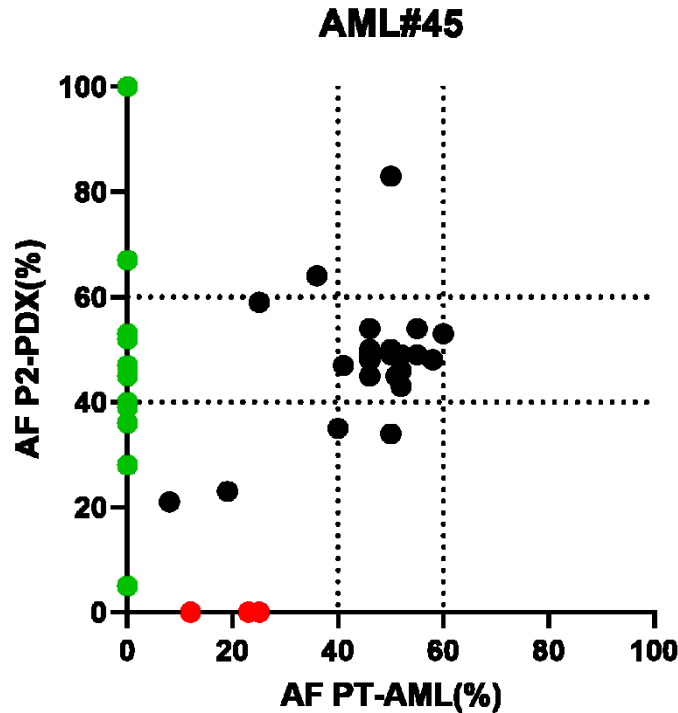


Figure 20. Variants AF in PT-AML#45 (x-axis) and in matched P2-PDX#45 (y-axis). In green genetic alterations absent in PT, in red mutations lost in PDX, in black preserved mutation in the model.

Overall, these data showed that AML models preserved the founder clone, characterized by mutations with AF around 50%, that contained the majority of detected variants; PT-AML had at least one secondary clone characterized by variants with an AF < 30%, or >60% supporting a hierarchical genomic landscape. Regarding variants, two models preserved all patients' AML variants (AML#30 and AML#41), whereas 3 models (AML#45, AML#34 and AML#20) lost part of the original AML genetic alterations. Noteworthy, all PDXs carried variants that were not found in the original AML at diagnosis. Briefly, considering PDXs of all models we observed 21 variants not detected in PTs: 2 of these mutations were previously reported in COSMIC in the exact position, whereas 3 variants were associated to nearby variants reported in COSMIC, suggesting a putative role for them to be further investigated.

Interestingly, a strong similarity among PDXs (P0-P1-P2 passages) was evident in particular for the likely pathogenic variants, suggesting that models are quite stabilized since P0. To confirm this hypothesis, we performed an AF correlation analysis among the

PDXs (Figure 21) indicating a Pearson correlation of 0.90. Indeed, we did not observe variants acquired or lost among *in vivo* passages.

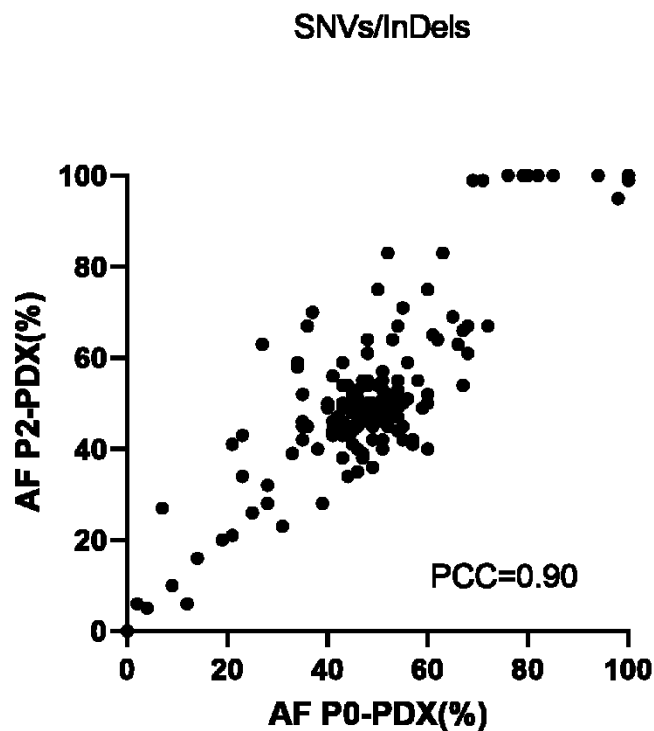


Figure 21. AF of variants detected in P0-PDXs (x-axis) and matched P2-PDXs (y-axis). PCC= Pearson's correlation coefficient.

4.2.3 RNA SEQUENCING

RNA sequencing of AML-models have been performed, including the primary AML and the four consecutive mice passages (P0,P1,P2, and P3-PDXs). Up to now, we obtained the gene expression profile of *KMT2A*-rearranged models: AML#30 and AML#31 harboring the *t(6;11)KMT2A-AFDN*, and AML#41 and AML#45 harboring *t(9;11)KMT2A-MLL3* (Table 2).

PDXs' transcriptome analysis

We interrogated the transcriptomic profiles of the original AML and that of the PDXs. Unsupervised principal component analysis (PCA) showed PT-AML and the

corresponding PDXs clustering together (Figure 22), indicating that PDXs display a strong similarity with the original AML.

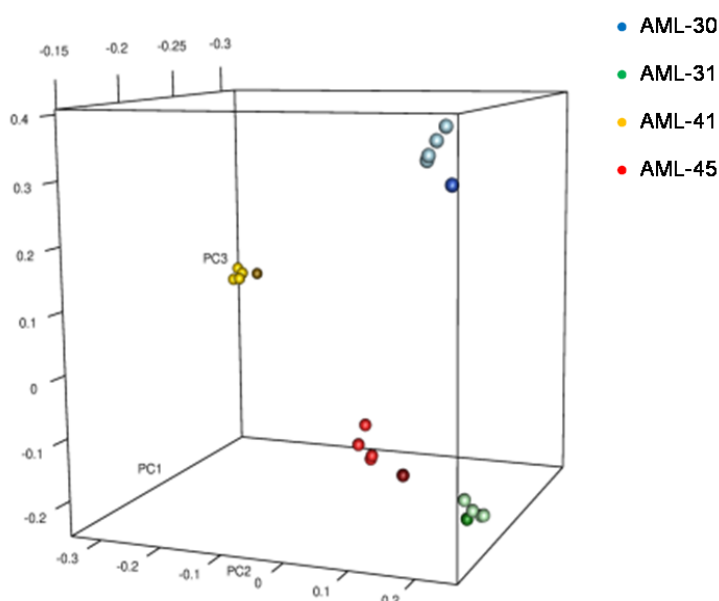


Figure 22. Unsupervised PCA of 4 models generated from AML#30-AML#31 t(6;11) rearranged, and AML#41-AML#45 t(9;11) rearranged. PT sample are represented by the darker circle and the correspondent PDX circles are represented using the same lighter colors.

Differential gene expression analysis

We performed a differential gene expression analysis by comparing samples with different genetic aberrancy, the t(6;11)*KMT2A-AFDN* or t(9;11)*KMT2A-MLLT3*. Since P0-P1 and P2-PDX samples showed a strong similarity by PCA, we proceeded to analyze the PT-AML and P2-PDX samples. RNA-seq revealed 1266 significantly differentially expressed genes in t(6;11) models with respect to t(9;11) (p-value<0.01). Then, by gene set enrichment analysis gene classes of solute carrier (SLC) membrane transporters, G proteins, G protein-coupled receptors (GPCR), GPCR ligands binding, as well as pathways of calcium homeostasis and respiratory electron transport were found differentially enriched in t(6;11) *KMT2A-AFDN* AML, with respect to the t(9;11) *KMT2A-MLLT3* AML (Figure 23).

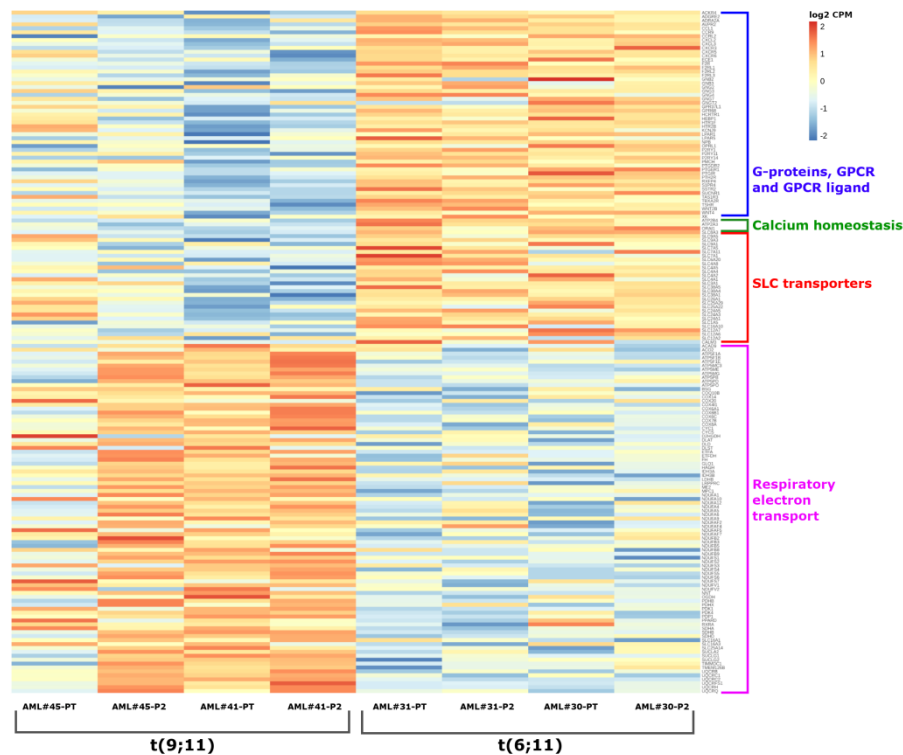


Figure 23. Heatmap of differentially expressed genes, grouped by gene classes, in t(9;11) rearranged samples (AML#31-PT and P2, and AML#30-PT and P2) versus t(6;11) (AML#45-PT and P2, and AML#41- PT and P2).

4.3 New targeted drugs identification and testing

Omics data allowed the identification of AML vulnerabilities that might be targeted with selected drugs. We focused on RNA-seq analysis uncovering deregulated pathways to be explored for their contribution in sustaining AML, by selecting genes and pathways reported to be targeted by specific drugs.

The *ATP2A3*, a SERCA Ca^{++} ATPase involved in calcium homeostasis, was targeted either by Thapsigargin, a specific SERCA inhibitor³² or by Disulfiram, a drug that stimulate SERCA Ca^{++} ATPase activity³³.

We interfered with *SLC38A1*, a glutamine transporter, by using Asparaginase, an approved anticancer drug known to reduce the amount of asparagine and glutamine in the cells through its asparaginase and glutaminase activity³⁴.

To target mitochondrial respiratory electron transport we used Rotenone and IACS-010759, both mitochondrial respiratory complex I inhibitors, and Oligomycin which inhibits ATP synthase.

For targeting G proteins, we selected Gallein inhibiting G $\beta\gamma$ subunits and YM-254890 targeting G α subunit.

4.3.1 Drug testing in AML cell lines

Selected compounds were initially tested using AML cell lines, in particular SHI-1 and ML-2 as representative of t(6;11) rearranged AML, and NOMO-1 and THP-1 being t(9;11) rearranged. The targeting of SERCA Ca⁺⁺ATPase by Thapsigargin resulted highly effective in reducing cell viability of treated cell lines, with t(6;11) rearranged cells being more sensitive with respect to t(9;11) cell lines (Figure 24), indicating SERCA as a good target. However considering that Thapsigargin has been reported to have high toxicity,³² we tested Disulfiram, impacting on the same target but being more suitable for clinical translation. We observed efficacy in reducing cell viability in SHI-1 cell line (Figure 25).

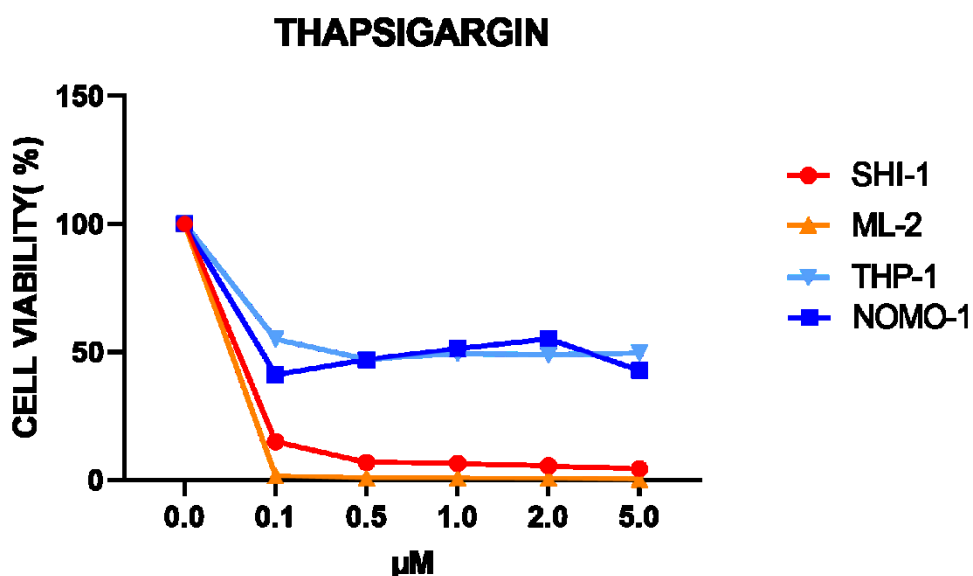


Figure 24. Cell viability of t(6;11) SHI-1 and ML-2 and t (9; 11) THP-1 and NOMO-1 cell lines, after 72 h of Thapsigargin treatment.

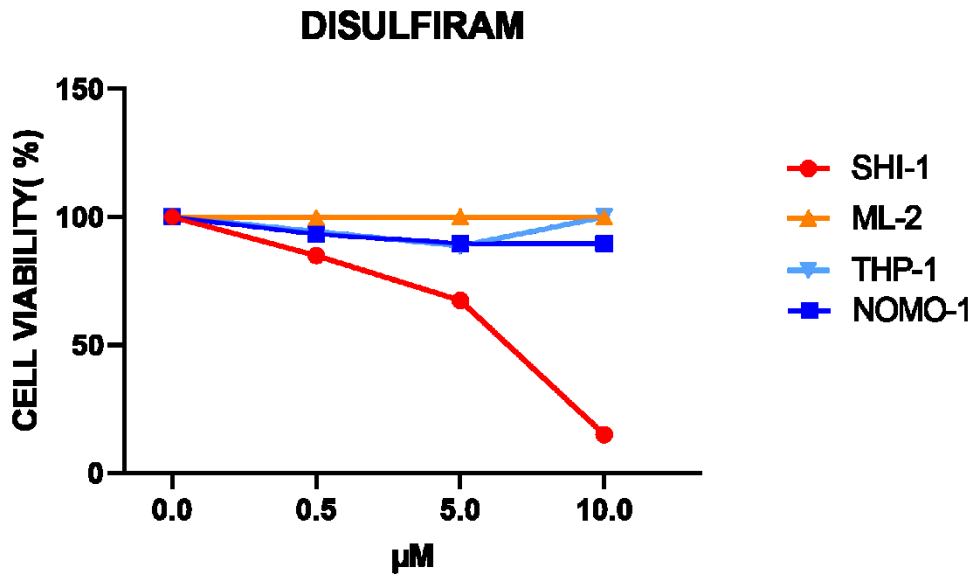


Figure 25. Cell viability of t(6; 11) SHI-1 and ML-2 and t(9; 11) THP-1 and NOMO-1, after 72 h of Disulfiram treatment.

Asparaginase resulted effective in all cell lines, with high potency in SHI-1, ML-2 and THP-1 (Figure 26), confirming SLC38A1 involvement in AML.

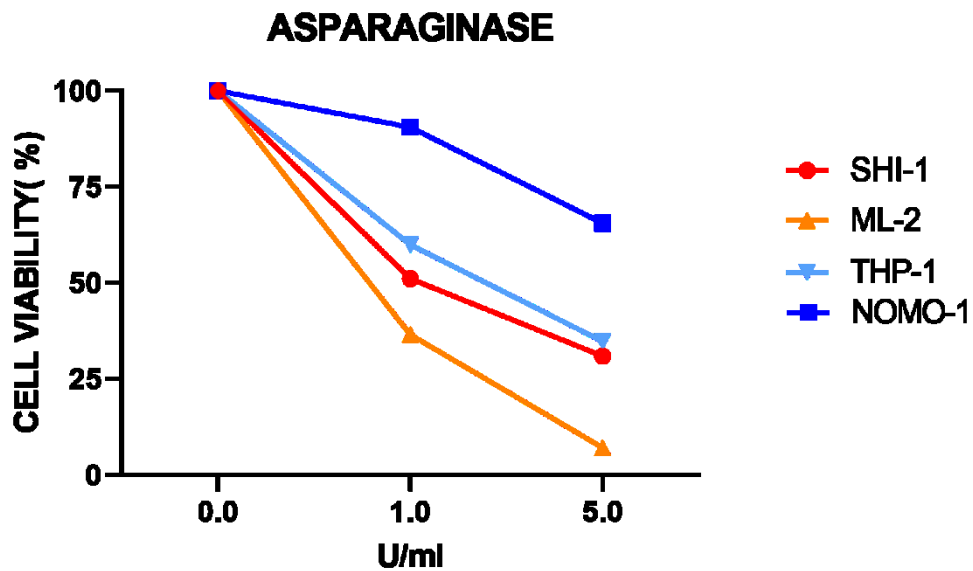


Figure 26. Cell viability of t(6; 11) SHI-1 and ML-2 and t(9; 11) THP-1 and NOMO-1, after 72 h of Asparaginase treatment.

Rotenone (Figure 27) and Oligomycin (Figure 28), were both efficacious with high potency in THP-1, suggesting the targeting of mitochondrial respiratory electron transport as a promising therapeutic strategy. Being Rotenone and Oligomycin previously reported to be toxic³⁵, we tested also IACS-010759, an innovative compound targeting OXPHOS, confirming a major sensitivity of THP-1 cells (Figure 29).

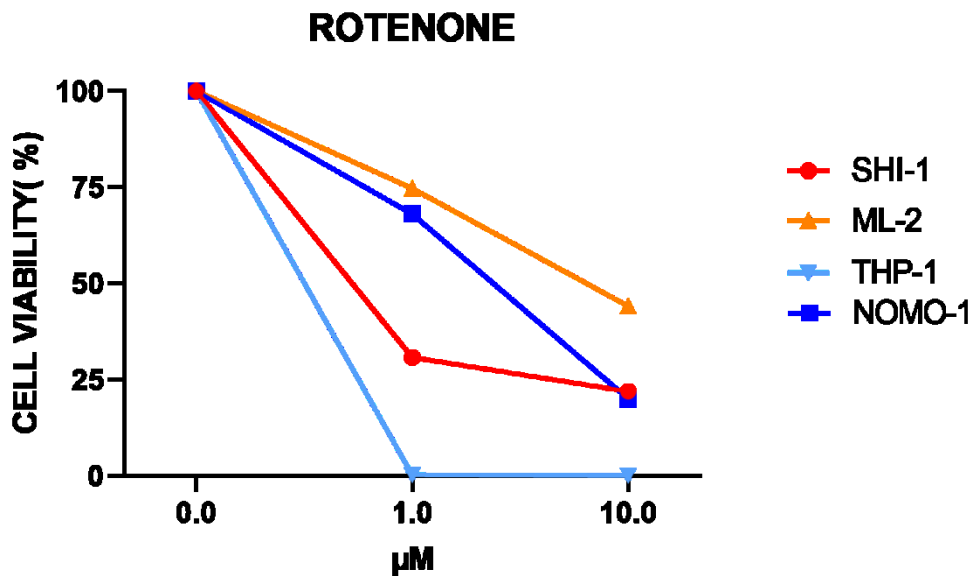


Figure 27. Cell viability of t(6; 11) SHI-1 and ML-2 and t(9; 11) THP-1 and NOMO-1, after 48h of Rotenone treatment.

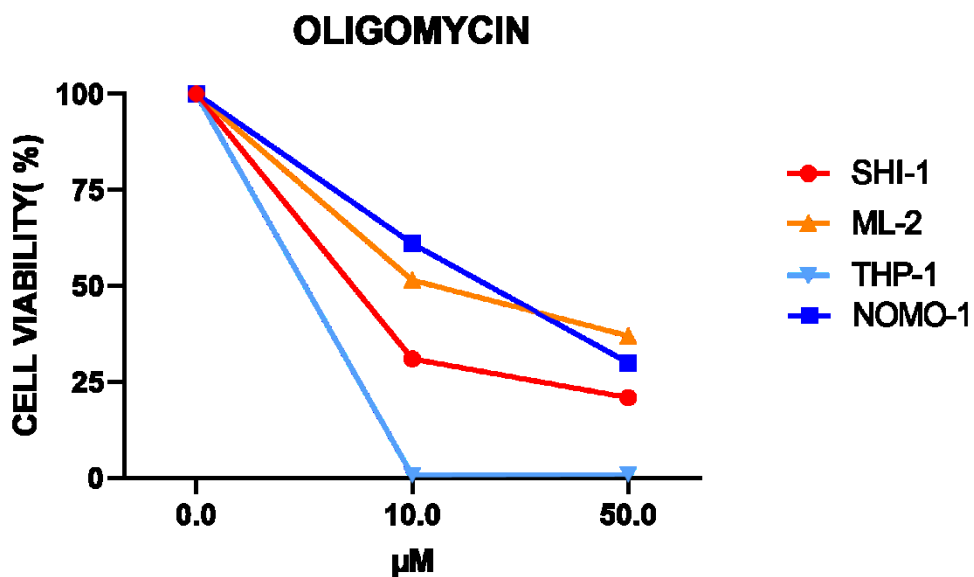


Figure 28. Cell viability of t(6; 11) SHI-1 and ML-2 and t(9; 11) THP-1 and NOMO-1, after 48 h of Oligomycin treatment.

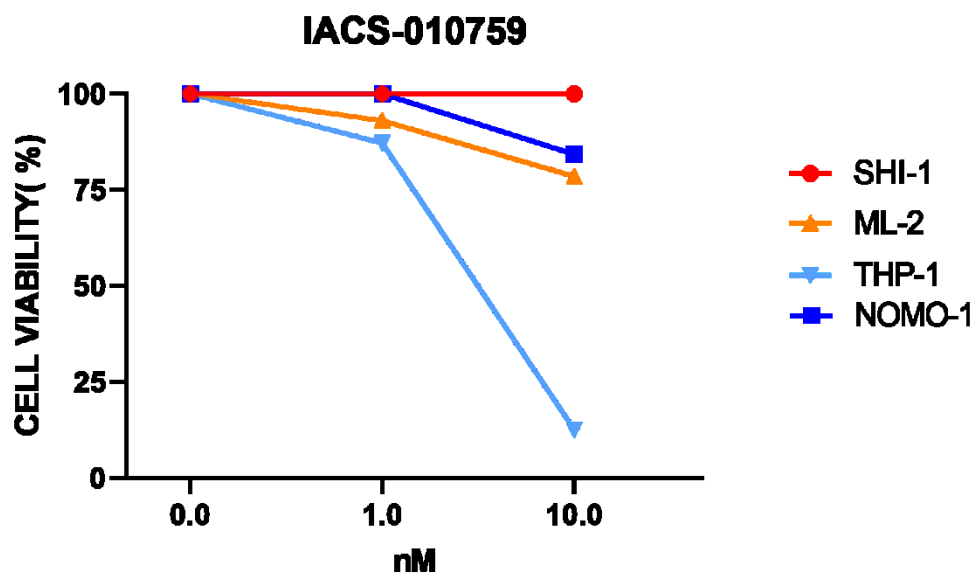


Figure 29. Cell viability of t(6; 11) SHI-1 and ML-2 and t(9; 11) THP-1 and NOMO-1, after 48 h of IACS-010759 treatment.

The targeting of G proteins by YM-254890 resulted ineffective in reducing AML cell viability (Figure 30), whereas Gallein showed a substantial inhibition of cell proliferation in all cell lines, suggesting the targeting of G $\beta\gamma$ subunit more effective than G α (Figure 31).

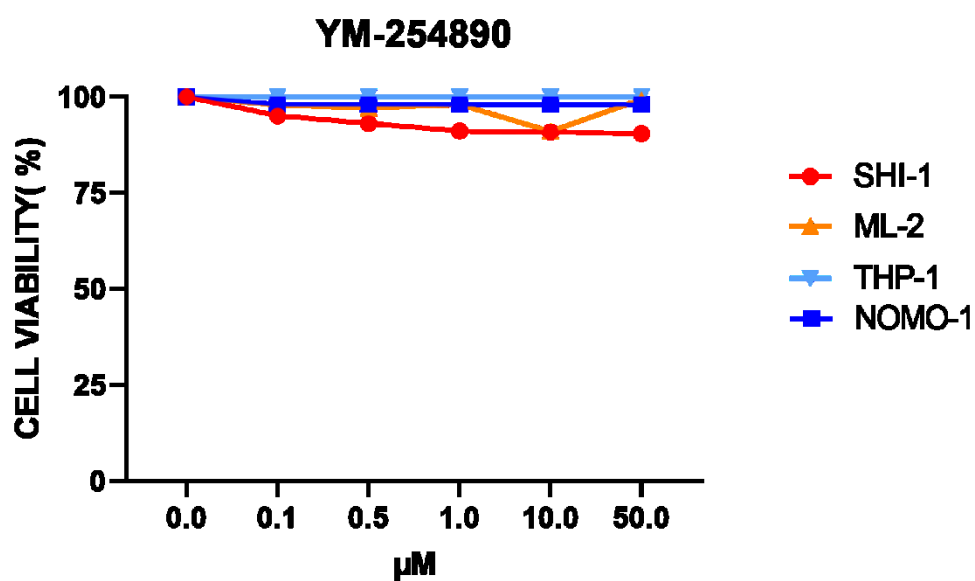


Figure 30. Cell viability of t(6; 11) SHI-1 and ML-2 and t(9; 11) THP-1 and NOMO-1, after 72 h of YM-254890 treatment.

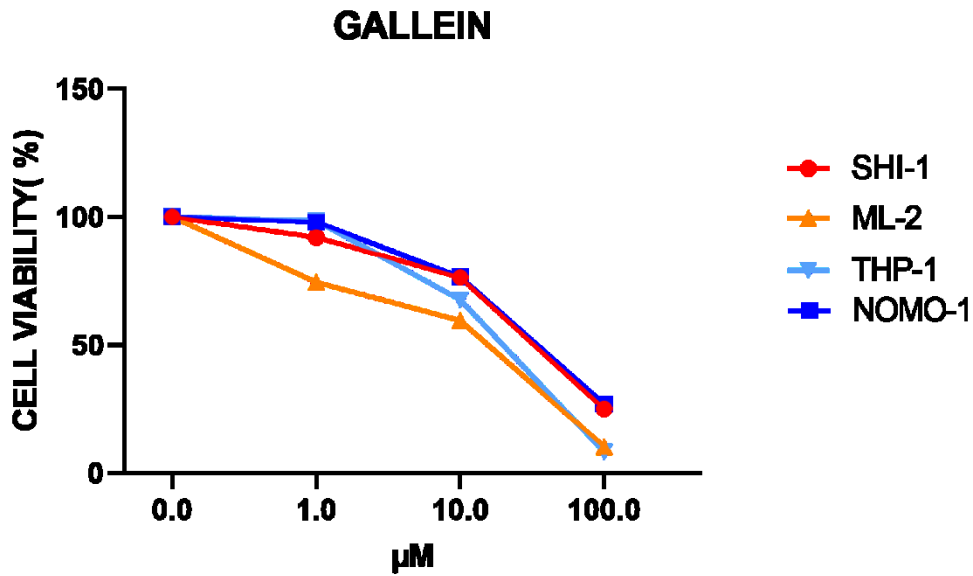


Figure 31. Cell viability of t(6; 11) SHI-1 and ML-2 and t (9; 11) THP-1 and NOMO-1, after 72 h of Gallein treatment.

4.3.2 Testing of selected drugs on primary *ex vivo* cells

To date all drugs, were found to be efficacious in AML cell lines. Thus, to refine their potential use *in vivo*, we tested their efficacy on our PDX-*ex vivo* cells, representing different primary samples with different genetic background.

To identify drugs IC50 we tested different doses that allowed to reveal a great heterogeneous sensitivity of the tested compounds depending on the cells (Table 10), with EC50 ranging from 8.6 to 37.7 μM for Disulfiram, from 0.53 to >15 U/ml for Asparaginase, and from 57.4 to 167 μM for Gallein (Figure 32-33-34) . Conversely, IACS-10759 treatment resulted effective only in one t(9;11) rearranged AML showing an EC50 of 59nM (Figure 35).

PDX	Genetic marker	Disulfiram (μM)	Asparaginase (U/ml)	Gallein (μM)	IACS-010759 (nM)
AML#31	t(6;11)	8,61	4,34	139,50	>2000
AML#30	t(6;11)	37,72	2,66	125,93	>2000
AML#41	t(9;11)	35,99	12,86	125,50	57,54
AML#45	t(9;11)	29,04	2,53	133,12	>2000
AML#34	t(10;11)	37,59	2,53	133,12	>2000
AML#37	t(10;11)	21,97	0,63	100,45	>2000
AML#20	t(3;5)+FLT3ITD	17,40	1,07	57,44	>2000
AML#22	t(5;11)+FLT3ITD	10,32	0,53	109,31	>2000
AML#17	t(16;16)	36,93	>15	167,09	>2000

Table 10. EC50 dose, specific for different *ex vivo* AML cells.

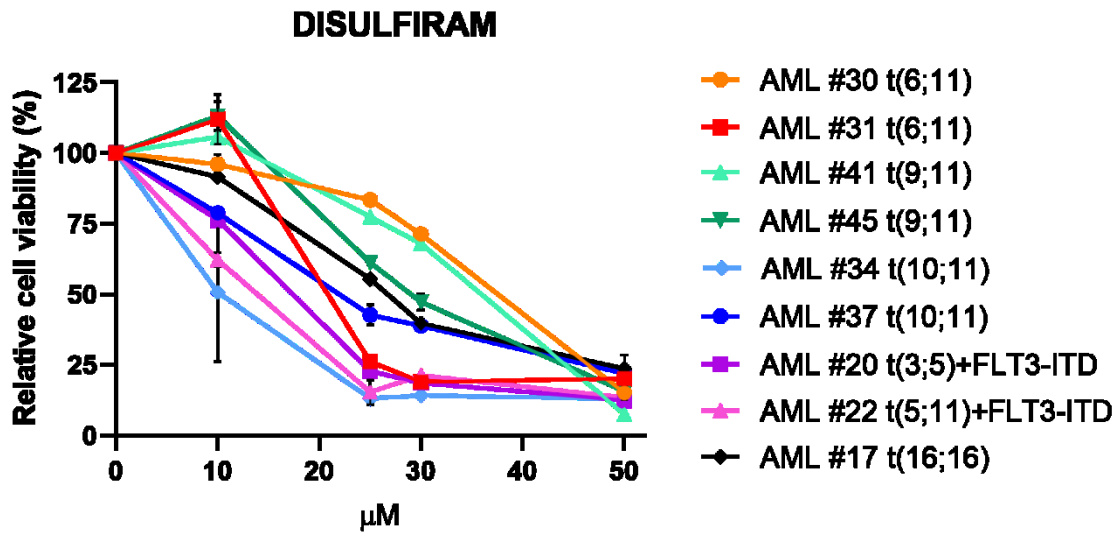


Figure 32. Cell viability of different *ex vivo* AML cells, after 72h of Disulfiram treatment.

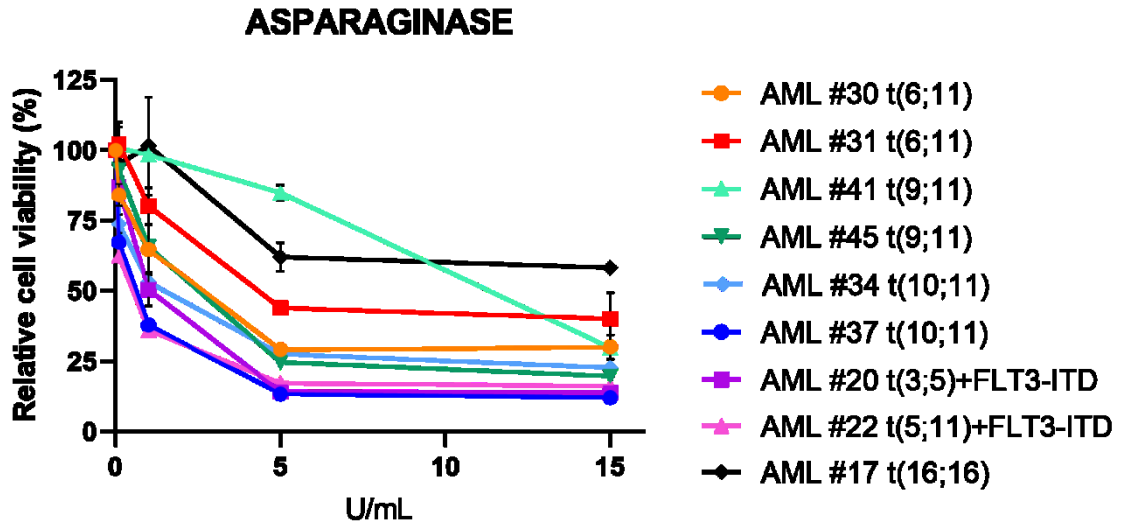


Figure 33. Cell viability of different *ex vivo* AML cells, after 72h of Asparaginase treatment.

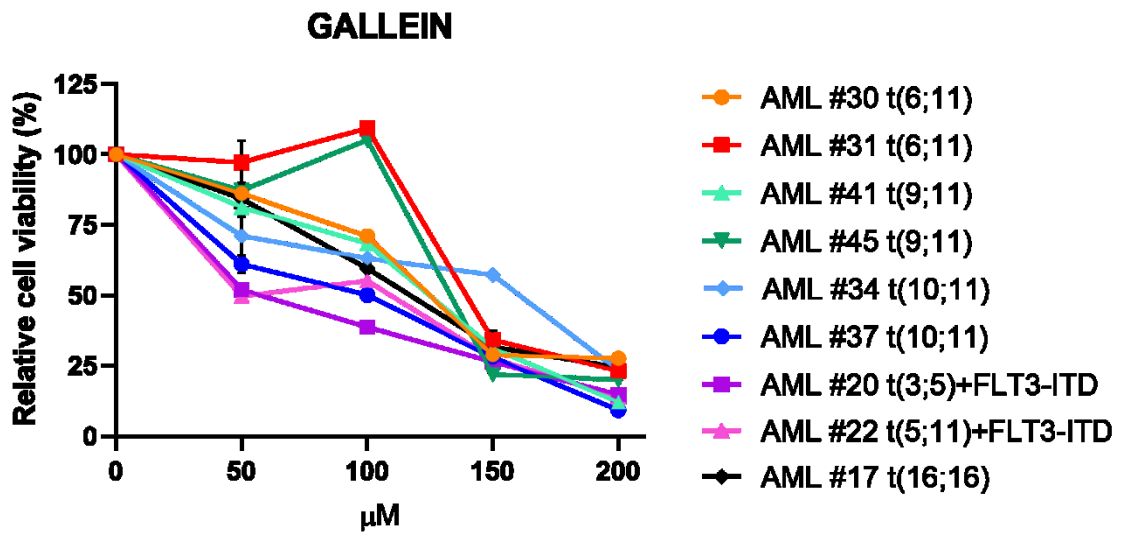


Figure 34. Cell viability of different *ex vivo* AML cells, after 72h of Gallein treatment.

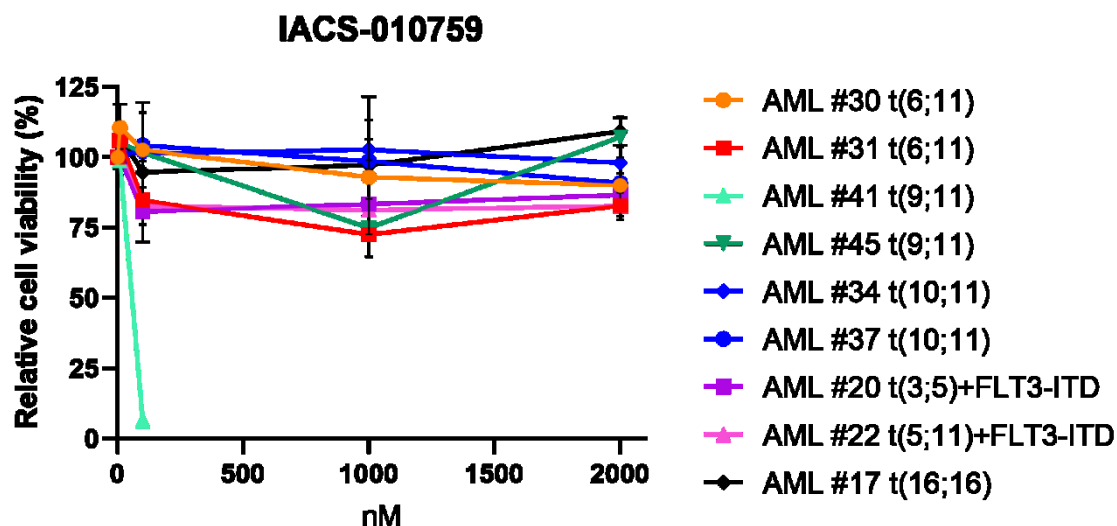


Figure 35. Cell viability of different *ex vivo* AML cells, after 72h of IACS-010759 treatment.

We decided to combine these compounds, representing targeted therapies, with Venetoclax, one of the most promising agents recently proposed for AML. This latter is a B-cell lymphoma-2 (BCL-2) inhibitor that can restore activation of caspase-dependent apoptosis in malignancies, but showing limited activity as a single agent. The synergy of these compounds has been tested in an innovative three-dimensional (3D) culture model that we recently developed, that consists of a 3D biomimetic scaffold made of Hydroxyapatite/Collagen (70/30%) that allowed long-term AML co-culture with mesenchymal stromal cells (MSCs) derived from BM of leukemia patients at diagnosis of *de novo* AML (namely AML-MSCs), recapitulating crucial physiological aspects of leukemia niche³⁶. This 3D system was demonstrated to be a *bona fide* model where performing robust and reliable drug screening due to the recapitulation of the BM microenvironment. At this point, combo strategies will be tested in 3D models by using AML-PDX *ex vivo* cells. Here we presented the drug testing by using t(6;11) *ex vivo* cells (AML#31), seeded in the 3D system together with AML-MSCs, following a sequential cell seeding schema of long term AML cultures in 3D (Figure 36).

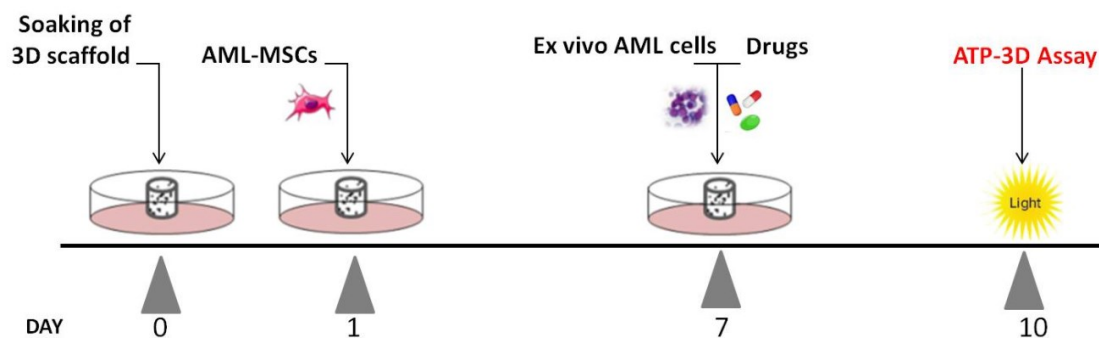


Figure 36 .Workflow of 3D culture and drug testing setup.

The 3D treatment has been performed using patient (AML#31) specific-EC50 dose of all drugs, previously determined in 2D culture setting (Figure 32-34, Figure 37). Even if IACS-010759 did not show efficacy in AML#31 (Figure 35) we decided to test its synergy with Venetoclax, using the EC50 of the *ex vivo* AML resulting sensitive to this compound.

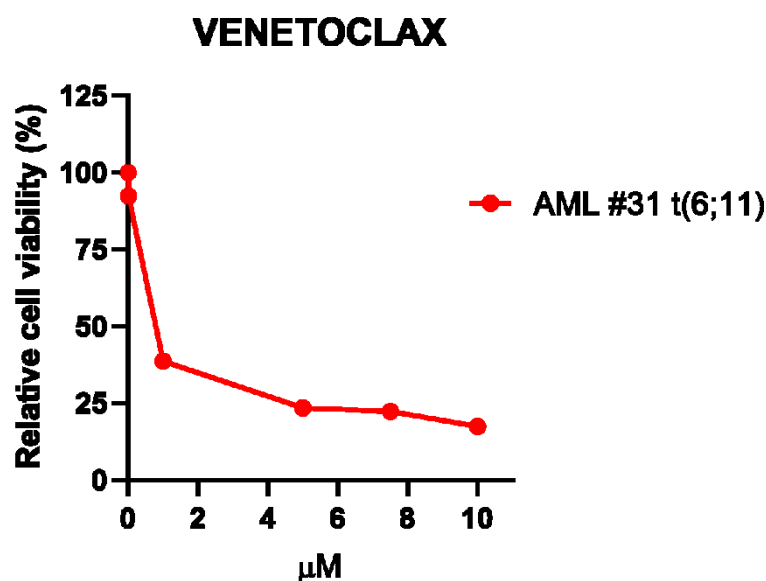


Figure 37. Cell viability of *ex vivo* AML#31 cells after 72h of Venetoclax treatment.

We observed that the combinations of venetoclax with Disulfiram and Asparaginase significantly reduced cell viability, compared with drugs used as single agents. Differently, IACS-010759 did not boost Venetoclax effect, whereas Gallein resulted highly effective as single agent thus not permitting to evaluate an additive effect when combined to Venetoclax (Figure 38).

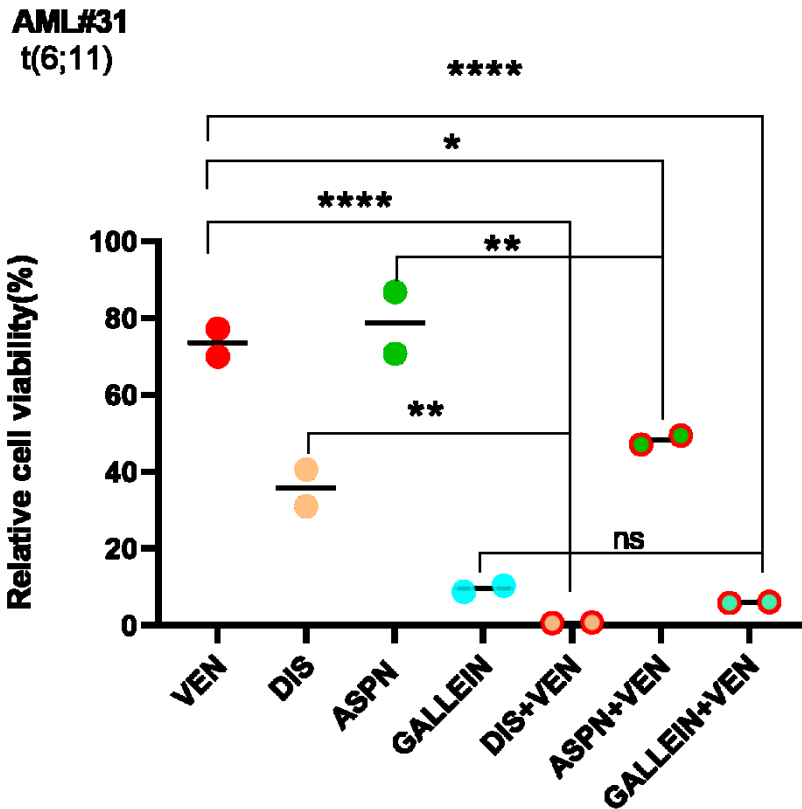


Figure 38. Cell viability of 3D system, evaluated 72h after treatment with Venetoclax(VEN) (0.01 μ M), Disulfiram(DIS) (36 μ M), Asparaginase(ASPN)(4.5 U/ml) and Gallein (130 μ M) normalized with respect to control scaffolds in *ex vivo* AML cells (AML #31) derived from PDX#31. p-value <0.05(*), <0.01(**), 0.0001(****).

4.3.3 *In vivo* testing of the most promising drugs combinations

According to results of 3D drug screening, the combination of Venetoclax with Disulfiram or Asparaginase emerged as a promising strategy to be finally validated in PDXs. Considering that in clinical setting new therapeutic strategies are predominantly used to treat refractory or relapsed disease, we set up an AML-PDX model of relapse to generate more predictive preclinical data, following the schema in Figure 39.

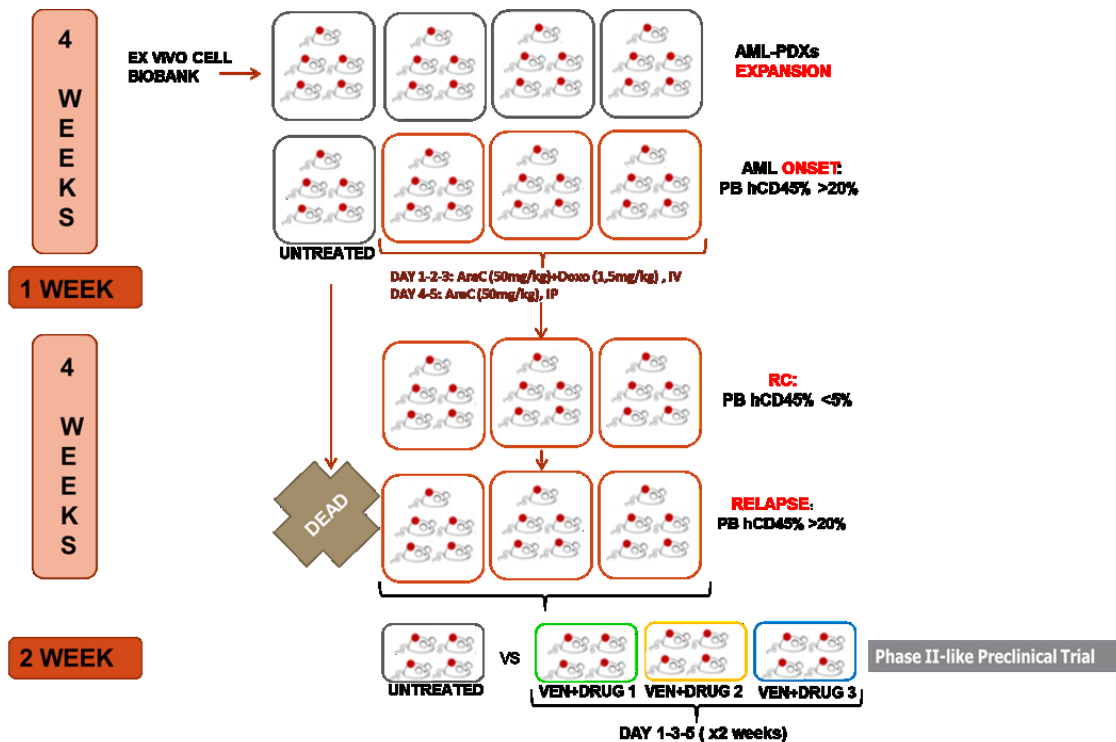


Figure 39. Workflow for the generation of AML-PDX relapse models, suitable to test innovative therapeutic approaches in Phase II-like preclinical trials.

After AML#31 inoculation in mice, PDXs were weekly monitored for engraftment by peripheral blood (PB) evaluation of hCD45+ cells. When hCD45 reached at least 20%, animals were treated with a chemotherapy induction cycle based on three days of intravenous injection of Cytarabine (50mg/kg) + Doxocyclin (1.5mg/kg), followed by two days of intraperitoneal injection of Cytarabine (50mg/kg) alone³⁷. As reported in Figure 39, after treatment discontinuation we assessed the complete remission (hCD45<5%) from day 12 to 24 from chemotherapy treatment (Figure 40). After one month, we measured AML relapse, starting from day 38, mice were randomized into 3 groups, namely DMSO, Venetoclax+Asparaginase, Venetoclax+Disulfiram (for further details see Material and Method “PDXs treatment”). Mice have been treated at day 1-3-5 for two weeks with combo treatments. At the end, combo treatment mice reached a second complete remission with both combinations (Figure 40), and will be further monitored for hCD45+ cells in PB and for survival.

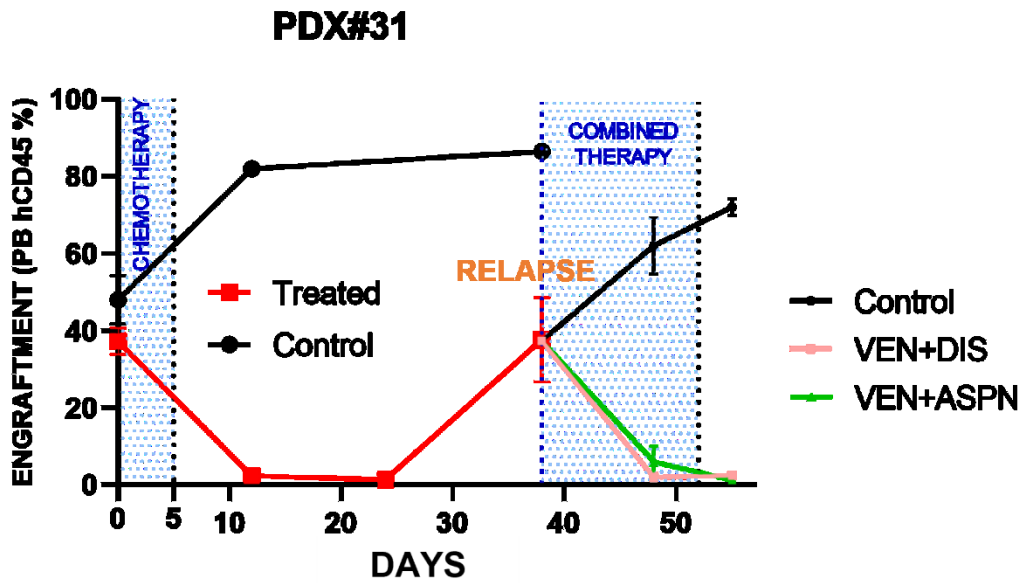


Figure 40. Percentage of hCD45+ AML cells detected in peripheral blood (PB) of PDXs#31 treated with chemotherapy from day 0 to 5 (red line) with respect to control PDXs (black line). Monitoring of hCD45 before treatment start (day 0), and after treatment discontinuation at day 12, 24 and 38: remission from day 12 to 24 and relapse at day 38 is shown in treated group; (n = 5 control group, n= 15 treated group). At relapse (day 38) mice were treated with Venetoclax(50mg/kg)+Disulfiram(50mg/kg) or Venetoclax(50mg/kg)+Asparaginase(ASPEN, 10.000 U/kg) at day 1-3-5 per two weeks. PB monitoring at day 48 and 52 showed second remission in treated mice.

CHAPTER 3

APPLICATION OF ESTABLISHED PRECLINICAL AML MODELS

The AML mice models generated during my PhD represent a powerful tool for studying AML, being the model that most closely resembles patients' disease. Indeed, the use of these models to test the results obtained *in vitro* can be widely applied with a strong translational significance.

During my PhD I was involved in a number of studies where the *in vivo* AML mice models had been used to validate working hypothesis and strengthen results, by performing the *in vivo* experiments. These studies have been recently published.

In detail:

- 1) **“Targeting the plasticity of mesenchymal stromal cells to reroute the course of acute myeloid leukemia”** by Borella G., Da Ros A. et al, published in ***Blood*, 2021** (manuscript available online at DOI 10.1182/blood.2020009845).

In this study we investigated the complex events occurring in the leukemia BM niche, deeply characterizing mesenchymal stromal cells (MSCs) relationship with AML blasts. We dissected roles and differences between mesenchymal stromal cells (MSCs) derived from healthy donors (h-MSCs) or from AML patients (AML-MSCs), reporting a different transcriptomic profile of the AML-MSCs or h-MSCs when co-cultured with primary AML cells, suggesting that when AML occurs, blasts remodel the stromal component of the microenvironment. Moreover, we documented an enhanced secretion of proinflammatory factors by MSCs when co-cultured with AML cells in a three-dimensional (3D) scaffold made of collagen and hydroxyapatite, that closely resemble the composition and the trabecular structure of bone marrow niche. Overall, we showed that when leukemia occurred the microenvironment is reprogrammed and by targeting it AML progression can be disadvantaged. In this paper, we identified Lercanidipine as a compound that selectively targeted AML-MSCs, and demonstrated that it synergized

with other AML-targeted drugs in the 3D system, unveiling the potential of a dual targeting approach that combined AML and MSCs targeting. This latter finding has been validated *in vivo* by using the *in loco* 3D-AML models, where the 3D system resembled a humanized leukemic BM niche in murine host.

In detail, we pre-seeded scaffolds *in vitro* with 0.4×10^6 AML-MSCs, and after 24 hours of culture we implanted them in the back of NSG mice. Three weeks later, a time lapse that was previously assessed for niche vascularization, we injected 1×10^6 luciferase-transduced AML cells directly inside the scaffold. In these mice model, leukemia progression was monitored by luciferase signals through living imaging techniques. Once luciferase signal was detectable in mice (8 days later), animals were intraperitoneally treated with Lercanidipine (3mg/kg) and with low-dose Ara-C (12.5mg/kg) as single agents or in combination. During the 5 weeks of treatment, we observed a strong reduction of leukemia burden by the dual targeting approach with respect to single agents; the higher effect of the combination was maintained up to 5 weeks after treatment discontinuation (Figure 1A-B), supporting the use of lercanidipine as an agent that synergizes with chemotherapy to boost a cytotoxic effect over cancer cells. Moreover, we confirmed lercanidipine to selectively targets stromal cells *in vivo*, as reported in Figure 1C by hCD73 and human-osteopontin staining, markers for MSC and MSC-derived osteoblasts respectively, in scaffolds harvested from mice at the end of treatment.

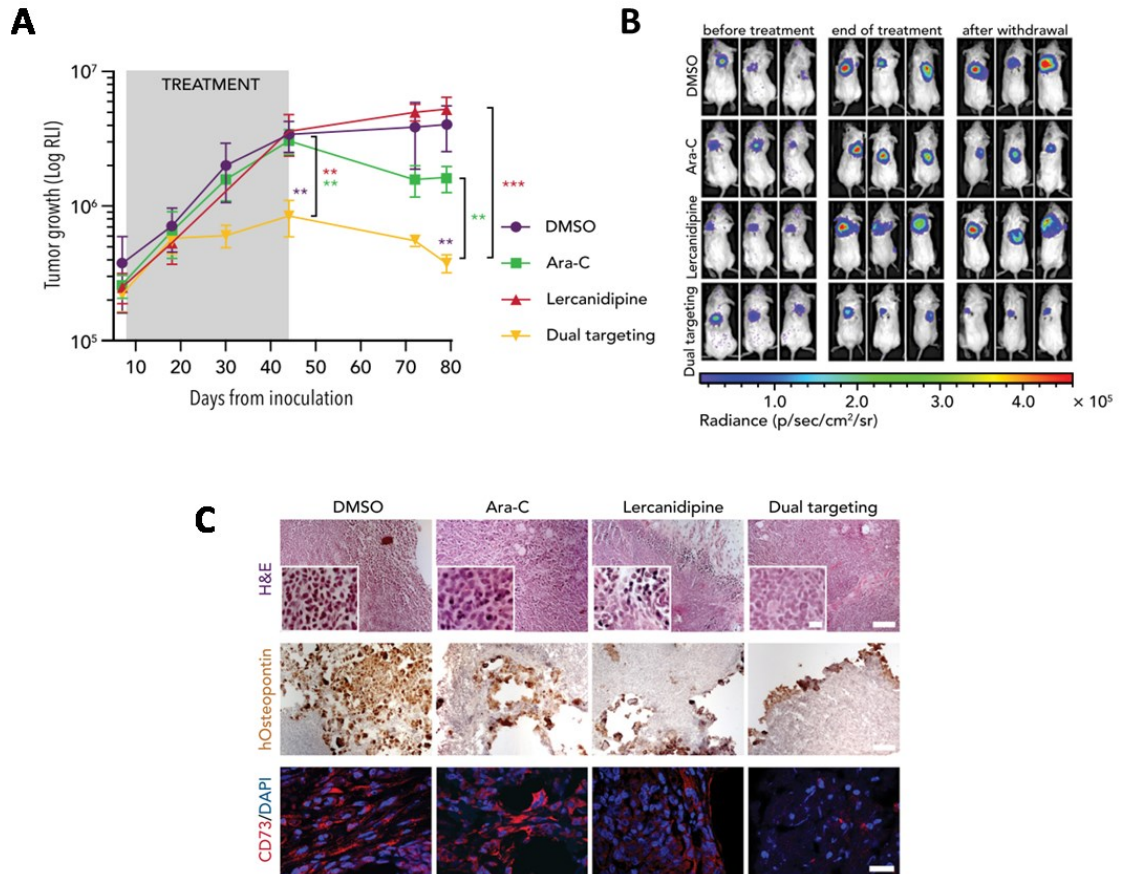


Figure 1. A) Tumor growth of luciferase-transduced primary AML cells in 3D scaffold in NSG mice, measured by luminescence activity during treatment with Ara-C (12.5 mg/kg) and lercanidipine (3 mg/kg), as single agents or in combination (dual targeting approach). Combination index (CI) = 0.1 at the end of treatment (day 44). CI = 0.5 after treatment withdrawal (day 79). CI < 1 = synergistic effect. B) Representative images of bioluminescence in differently treated mice before (at day 7) and after treatment (at day 44) and at treatment withdrawal (at day 79). n = 5 mice per group. C) Representative images of H&E (X 10 magnification; scale bar, 100 mm; scale bar of images at higher magnitude, 2 mm), human osteopontin immunohistochemical analysis (X 10 magnification; scale bar, 100 mm), and hCD73 immunofluorescence (X 60 magnification; scale bar, 40 mm) staining of scaffolds harvested from mice at the end of treatment. *p < 0.05, **p < 0.01, ****p < 0.0001.

In conclusion, in this manuscript we described a novel humanized 3D *in loco* model for AML that, by recapitulating human BM niche, resulted as a powerful tool to conduct innovative drug testing studies that combine AML and MSC targeting, opening for dual targeting approaches to cure pediatric AML.

2) **The long non-coding RNA CDK6-AS1 overexpression impacts on acute myeloid leukemia differentiation and mitochondrial dynamics”** published in *iScience*, 2021 (manuscript available online at DOI 10.1016/j.isci.2021.103350).

In this study we identified the high expression of the lncRNA *CDK6-AS1* as a robust marker of a specific AML subgroup with peculiar features of early myeloid differentiation arrest and enhanced mitochondria biogenesis. *CDK6-AS1* depletion increased differentiation of AML blasts, suggesting *CDK6-AS1* importance in regulating the balance between differentiation potential and self-renewal capacity. This finding supports the concept that aberrant *CDK6-AS1* expression during haematopoiesis could provide a key transforming event inducing the block of myeloid differentiation. In addition, we observed an association between high *CDK6-AS1* levels and mitochondrial biogenesis pathway activation. Collectively, our *in vitro* studies revealed an increased AML cell vulnerability for the majority of mitochondrial drugs used as single agent when *CDK6-AS1* was silenced, whereas for AML cell with the highest level of *CDK6-AS1* we combined chemotherapy and mitochondrial targeting observing synergistic improvement in their eradication. Since *CDK6-AS1* levels correlated with mitochondrial mass, we assigned to *CDK6-AS1* the role of an AML determinant of drug sensitivity. This approach enables the identification of those patients who can benefit from a mitochondrial targeting combined with chemotherapy, supporting a mitochondrial-oriented approach for a specific pediatric AML subgroup.

We tested this hypothesis by combining Tigecycline (TIGE, a mitochondrial translation inhibitor) with Cytarabine (ARA-C) in a pilot *in vivo* experiment. We characterized *CDK6-AS1* expression level on different ex vivo AML cells derived from our established PDXs. Then, we selected one model with low and one with high-*CDK6-AS1* expression. These

PDXs were expanded by intravenously injecting 1×10^6 ex vivo cells from our biobank in NSG mice. After PDXs engraftment (hCD45+ >5% in peripheral blood) mice were treated for 3 weeks with TIGE (75 mg/kg) or ARA-C (25 mg/kg) or in combination therapy (COMBO) by intraperitoneal injections 5 days per week.

ARA-C and COMBO strategies were found highly effective in reducing AML burden in mice (Figure 2A). After treatment discontinuation both high and low *CDK6-AS1* models relapsed, but high-*CDK6-AS1* PDXs treated with ARA-C as single agent relapsed faster with respect to mice treated with COMBO, that delayed leukemia progression thanks to mito-mass targeting (Figure 2A, right). Survival analysis confirmed the benefit of COMBO treatment in high-*CDK6-AS1* mice as demonstrated by prolonged survival (Figure 2B). These results provide the rationale for further studies on the efficacy of mitochondrial drugs, either alone or in combination with conventional chemotherapy. AML-PDX models represent a crucial preclinical tool to be exploited in the drug screening and confirmation studies for their ability to generate robust preclinical data.

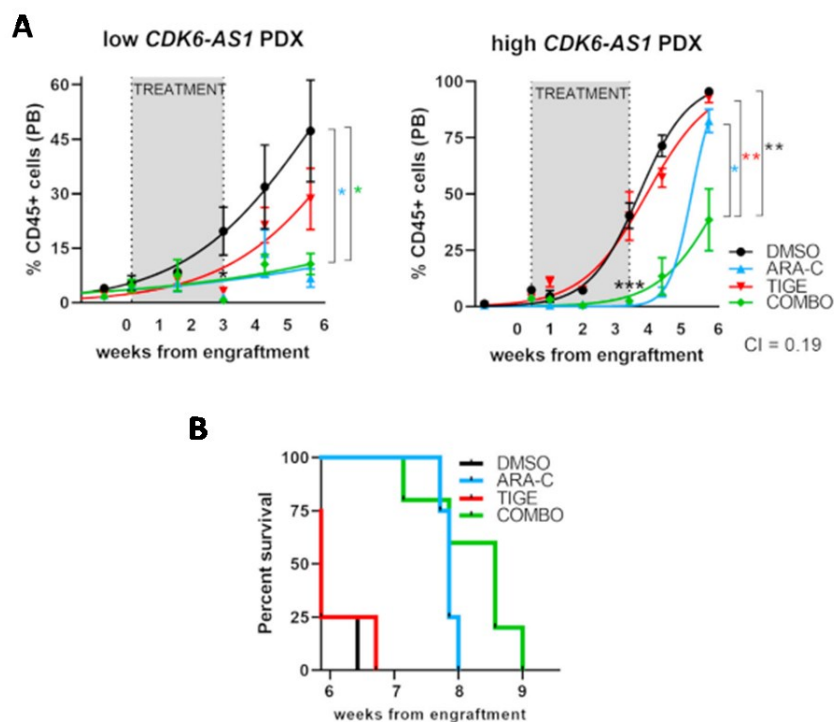


Figure 2. TIGE sensitization to chemotherapy in high-*CDK6-AS1* AML: A) Percentage of hCD45+ AML cells detected in peripheral blood (PB) of low- (left) and high- (right) *CDK6-AS1* PDXs with

TIGE, ARA-C, or COMBO (after 3-week treatment *p value<0.05, ***p value<0.001 of treated mice with respect to DMSO). Monitoring of hCD45 during 3 weeks after treatment discontinuation (mice n = 4/5 per group; *p value<0.05, **p value<0.01). Synergistic effect of COMBO in high-*CDK6-AS1* PDX (CI = 0.19). B) Overall survival Kaplan-Meier analysis. Median survival in days from end of treatment: DMSO 19.5, TIGE 20, ARA-C 34, COMBO 39 (log rank Mantel-Cox test: p value DMSO versus ARA-C = 0.0062 **, DMSO versus TIGE = ns, TIGE versus ARA-C = 0.0069 **, DMSO versus COMBO = 0.0025 **, COMBO versus TIGE = 0.0029 **).

- 3) Ex vivo primary AML cells derived from PDXs have been used in the context of the work entitled **“Novel Compounds Synergize With Venetoclax to Target *KMT2A*-Rearranged Pediatric Acute Myeloid Leukemia”** published on **Frontiers in Pharmacology** in **2022** (manuscript available online at DOI 10.3389/fphar.2021.820191).

This study arose thanks to the establishment of a large panel of AML-PDXs, representative of different genetic subtypes, and to the availability of huge number of *ex vivo* primary AML cells. Since we characterized AML-PDXs confirming a strong similarity between PDXs and patient’s AML, we suggested that *ex vivo* cells faithfully recapitulate the original AML, and are high predictive for AML studies *in vitro*.

In this study we tested the possible use of Venetoclax, a promising and studied BCL-2 inhibitor, in pediatric AML setting. By evaluating *BCL-2* levels in a cohort of pediatric AML samples, we found the majority of *KMT2A*-rearranged AML patients having statistically significant high levels of BCL-2, phospho-BCL-2 S70, and MCL-1, indicating the anti-apoptotic pathway activation. Limited activity of Venetoclax as single agent in high-risk AML has been reported, encouraging the investigation of rationally designed combinations to increase its activity in particular in *KMT2A*-r AML subgroups. Therefore we attempted to identify new compounds that could synergize with Venetoclax in particular in t(9;11) *KMT2A-MLL3*, being the most recurrent, and in t(6;11) *KMT2A-AFDN*, mediating the worst prognosis. High throughput screening of chemical compounds, allowed to select drugs specific for the *KMT2A* rearranged AML. The selected compounds were tested on AML cell lines in combination with Venetoclax to

assess drugs synergy. Most promising compounds resulted I-BET151 and sunitinib, moreover we identified Thioridazine (TDZ), a specific compound for *KMT2A-AFDN* rearranged AML, being synergic with Venetoclax. To validate our results in primary AML cells we took advantage of the *ex vivo* cells thanks to the large expansion of AML blasts in PDXs. We firstly demonstrated the synergistic effect of TDZ and Venetoclax being specific for t(6;11) *ex vivo* AML cells with respect to non t(6;11) *ex vivo* blasts (Figure 3).

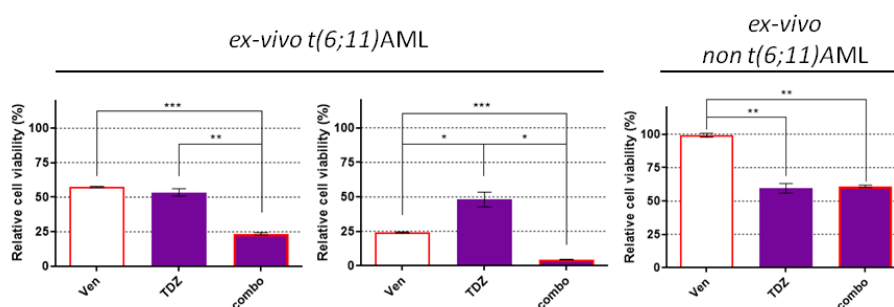


Figure 3. Cell viability of PDX-derived *ex vivo* t (6; 11) and non-t (6; 11) AML after treatment with venetoclax (1 μ M), thioridazine (10 μ M) or the combination at 24 h after treatment. ANOVA test was performed by applying Bonferroni correction for multiple statistical hypotheses testing. *p < 0.05; **p < 0.01.

In addition, all combinations found to be synergistic in *KMT2A*-rearranged AML cell line were tested in our recently developed 3D *in vitro* model that allowed long-term primary AML cells co-culture with AML-MSCs, recapitulating the crucial physiological aspects of leukemia niche (Figure 4). Also in this experimental setting we used *ex vivo* AML cells t(6;11) or t(9;11) rearranged. 3D co-cultures confirmed the synergistic effect of TDZ, I-BET151 and sunitinib with Venetoclax in primary AML cells.

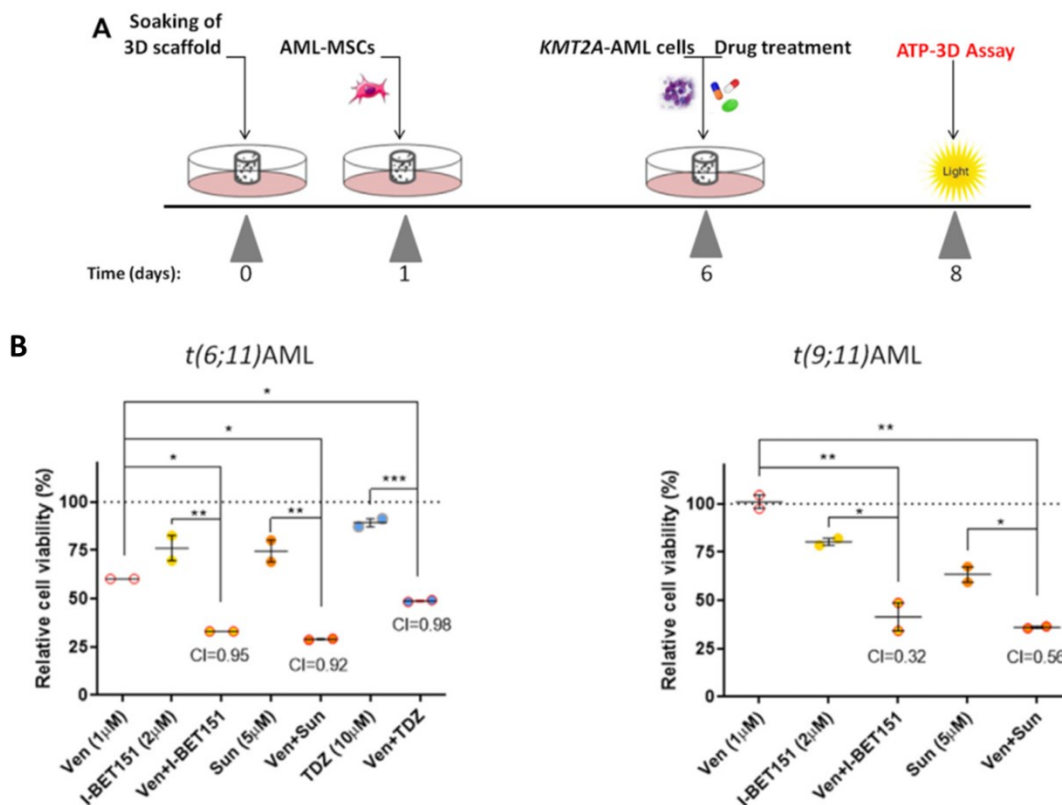


Figure 4. Combination treatments in *in vitro* 3D model. (A) Scheme of the *in vitro* 3D culture setup procedure: hydroxyapatite/collagen scaffolds were allowed to soak for 24 h, then seeded with acute myeloid leukemia (AML-MSCs) and cultured for a further 5 days prior to adding of *KMT2A*-rearranged AML cells and performing the drug treatment. Cell viability was evaluated in the 3D system at 48 h after treatment, by ATP 3D assay. (B) Cell viability of 3D system analyzed at 48 h after drug treatment with venetoclax (1 μ M), I-BET151 (2 μ M), sunitinib (5 μ M), and thioridazine (10 μ M) normalized to the respective controls (dimethyl sulfoxide; n=3) in *ex vivo* AML primary samples. CI, combination index; synergy when CI < 1. ANOVA test was performed by applying Bonferroni correction for multiple statistical hypotheses testing. *p < 0.05; **p < 0.01; ***p < 0.001; ****p < 0.0001.

In conclusion the investigation of established AML-PDXs accordingly to different biological questions may be accomplished; these models are crucial to perform key *in vivo* experiment in AML studies, confirming and giving strength to *in vitro* results. In parallel the possibility given by the PDXs to generate a biobank of *ex vivo* primary AML cells enables to conduct relevant studies by using primary cells, otherwise not feasible due to the low number on primary cells available from AML patients

CHAPTER 4

DISCUSSION AND CONCLUSIONS

In this study, we aimed at generating pediatric AML-PDXs to perform more robust drug screenings, since most of new drugs are not currently adopted in children with cancer because of their failure in efficacy and safety in human clinical trials, despite their promising preclinical results. Patient derived xenografts (PDXs) have emerged as predictive tools for cancer modelling and for the development of new therapeutic strategies. Previous studies demonstrated that generating PDXs for acute myeloid leukemia (AML) is complicated^{38,39}, and the use of highly immunocompromised mouse strains and their pre-conditioning by irradiation before transplant is highly recommended, documenting an improved engraftment success and the possibility to conduct long-term studies of leukemia growth, evolution and treatment response^{17,18,40-43}.

During my PhD I faced several old issues but I also explored novel strategies for generating a panel of pediatric AML models for improving drug portfolio for children suffering from AML. At first, I focused on the bone marrow microenvironment since in the recent years the three-dimensional modelling of several tissues and malignancies is considered an emerging investigational revolution for cancer research, including leukemia⁴⁴⁻⁵¹. The BM microenvironment plays a crucial role in the regulation of hematopoietic homeostasis, maintaining an accurate balance between differentiation and self-renewal of Hematopoietic Stem Cells (HSCs)⁵². Emerging evidences confirm that BM niche is not only involved in the regulation of normal hematopoiesis, but it can also contribute to malignant transformation and can be itself remodeled to support the uncontrolled proliferation of blasts through the secretion of molecules (cytokines and chemokines) and specific cell-cell interactions^{45,47}. The most influenced niche component by leukemia cells to promote their own survival are mesenchymal stromal cells (MSCs) that, after blasts occurrence, remodel the niche providing a sort of sanctuary in which leukemic cells acquire a drug-resistance phenotype^{36,53-55} evading chemotherapy-induced cell death, which may represent an important cue related to

children's relapse. The interaction between leukemic cells and the bone marrow niche represents one of the main causes of the low predictivity of traditional 2D cell cultures, unable to mimic these important crosstalk, and it might explain the failure of most of the new drugs entering in clinical trials. For these reasons, we generated a three-dimensional (3D) model mimicking the bone marrow niche and we use it to set up long primary cell cultures showing its ability to predict drug sensitivity and to perform new therapeutic targeting and test novel combination treatments³⁶. Thanks to these results, we explored the possibility of the 3D-AML model implanted *in vivo* to improve the AML engraftment in mice, thus enhancing PDXs generation. We showed that scaffolds resulted in a functional human hematopoietic microenvironment integrated in the murine host, where AML cells survived and proliferate, however blasts preferentially resided in the scaffold, and rarely disseminated outside. In order to dissect this issue we focused on the scaffold composition which is made up of collagen (30%) and hydroxyapatite (70%) mimicking bone; considering that hydroxyapatite has high adhesive properties, as documented also *in vitro*, we conclude that blasts preferentially colonized the 3D structure and the absence of paracrine stimuli in the NSG mouse reduce blasts migration also when stimulated by pharmacological treatments. Indeed, we conducted treatment studies in *in loco* 3D-AML mice model as presented in a recently publication³⁶. We reported that the AML-3D model *in vivo* allowed innovative drug screenings targeting blasts and the BM microenvironment, such as the MSCs, showing that combining the AML and MSCs targeting in a 3D artificial model that recapitulates crucial physiological aspects of leukemia niche, appears promising for accelerating the achievement of robust pre-clinical results that are instrumental for identifying innovative therapeutic approaches in childhood AML³⁶. Despite the implantation of this scaffold in mice was feasible and will be a useful tool for further drug selection and refinement *in vivo*, it was ineffective for the AML-PDXs establishment.

Thus, other inoculation methods were used, such as the intravenous or intrafemoral injections and the intrahepatic injection⁴¹ in pups, reaching the establishment of 22 PDX models that cover a wide genetic AML spectrum. We obtained an engraftment success of 36%, as previously reported by others⁴². To deepen into these models we found a

high grade of inter-tumoral heterogeneity among them. In particular, we noticed that PDXs models harbouring the *inv(16)CBFB-MYH11* showed a lower engraftment in terms of blasts percentage into the mice BM (average 19.3%) and timing, with a disease latency of 1 year, with respect to other AML cases (most of them harbouring a *KMT2A-r* AML) that increased blasts at >80% in the BM and engrafted in a median time of 4 months. These findings confirmed that AML-PDXs resembled typical features of standard and high AML risk classes⁵⁶. In line with these results, we showed a strong correlation between engraftment success and patients' outcome, as demonstrated by survival analysis, and according to genetic subtypes we confirmed the major engraftment success of the AML at high or intermediate risk with respect to those of standard risk^{38,57}. According to these results, we may consider the successful establishment of AML-PDX as a predictive result of an increased relapse risk and dismal outcome of the patient, suggesting that these models could represent those patient at very high risk of disease recurrence as an alert for surveillance or treatment consolidations.

This latter observation, correlating mice engraftment and patients' clinical outcome, highlights the difficult to generate PDXs representative of less aggressive AML subtypes^{38,57}. One hypothesis could be that in NSG mice the hematopoietic niche is reduced in its ability to produce most of haematopoietic cells and factors, thus influencing also leukemia sustainment due to reduced cell-cell interactions and to the absence of human cytokines and stromal cells^{36,47,50,51}. In order to overcome to this limitation of the NSG strains, novel mice strains expressing human cytokines^{39,40} are suggested to enhance engraftment of standard risk leukemia samples to improve the success in generating AML-PDX models.

At this point of our research, we are considering several refinements to establish a large number of PDXs with one main aim of reducing the long disease latency that costs time but also a lot of efforts for the engraftment monitoring. We observed that mean engraftment time of established PDXs is 6 months from inoculation, suggesting this timing as suitable endpoint for the majority of the high risk AML, but unsuitable for standard risk AML cases. These important remarks could be useful to plan different endpoints according to AML genetics, with the aim to enlarge the panel of PDXs to represent as much as possible the different AML subtypes.

This bottleneck is observed for the first passage from original AML to P0-PDX, whereas we had an impressive success from first to secondary and tertiary mouse recipients, increased up to 92% of engraftment at P2 mice generation, suggesting the maintenance of self-renewing leukemia initiating cells (LIC) during passages⁴² and indicating that NSG mice provide a favourable environment for proliferation and survival of these cancer cells.

As a matter of fact the blasts highly proliferated in engrafted mice suggesting PDXs as “bioreactors” for the expansion of leukemia cells, allowing primary AML expansion up to 50-fold⁴², useful for biobanking of cells to be further used for *in vitro* and *in vivo* experiments in the context of phase II- like preclinical trials. PDX models have been introduced to overcome the limitation of conventional preclinical models with the great advantage to expand the limited patient tumor materials. As a matter of fact, this is possible if PDXs retain the characteristics of patients’ tumor, such as tumor heterogeneity and tumor biological features, giving the opportunity for biomarker and drug discovery and novel treatment regimen testing. A substantial number of reports have suggested that PDX models could be used as robust preclinical tools either for drug efficacy testing or for the development of new therapeutic strategies¹³, however, their potential utility in preclinical phase II like studies has not been extensively studied at a large scale, particularly in the pediatric setting. Recent studies investigated PDXs models to characterize them at genomic and transcriptomic level assessing their robustness^{15,17,30,58}.

We characterized our established PDXs for immunophenotypic profile and genetic marker of the original patients’AML at diagnosis. In particular, we confirmed the maintenance of the genetic and of the immunophenotype, with slight recurrent differences in the expression levels of some surface markers such as the CD34 and CD117 being downregulated, and CD15 and CD11A/B expression upregulated in mice. Overall the characteristic phenotype of patients’ leukemic cells was largely preserved in paired P0-P1 and P2-PDX-derived blasts, harvested from mice BM or spleen.

Of more interest we investigated our models at omics level to study how blasts modify their proliferative and self-renewal capabilities during *in vivo* expansion¹⁸. Considering

that leukemia stem cells are postulated to initiate a developmental hierarchy in which LSCs give rise to more differentiated non-self-renewing myeloid lineage blasts that exhibit varying degrees of maturation arrest through the acquisition of multiple genetic and/or epigenetic changes, understanding the mechanisms that control self-renewal and lineage commitment during *in vivo* expansion is of fundamental importance to treat AML. This process may be reflected in a modification of clonal cancer composition in *in vivo* models with respect to AML at diagnosis and this evolution could suggest important findings. By Whole Exome Sequencing (WES) analysis we found that the majority of predicted pathogenic mutations found in patients' AML were preserved in PDXs AML (95,7%) thus resuming a perfect model of the disease. To note, in all analyzed AML samples we identified mutations in at least one "driver" gene³¹, that probably represent the first event initiating leukemogenesis and together with other variants constitute the founder clone. The characterized leukemia founder clone has been maintained in all mouse passages. Interestingly, the original AML showed other mutations defining several minor clones (allelic frequency (AF) <40%), thus suggesting that the founder clone evolved by acquiring new variants generating independent subclones. Then, by a comparison of AF of variants in patient AML and in engrafted PDX we observed a partial correlation (PCC=0.52) highlighting that the AML evolve *in vivo*. On the contrary, the AF correlation analysis between of the variants detected in P0 and in P2-PDX revealed genetic stability in mice (PCC=0.9) suggesting that the clonal evolution occurred from patient's AML to the first mice passage.

In light of these data, considering clones characterized by variants with specific AF, we delineated a clonal dynamics pattern in each model¹⁸. Briefly, AML#30 and AML#41 had a "monoclonal pattern" characterized by a founder clone with variants having AF = 50% in *NRAS* (AML#30) and *KRAS+TET2* (AML#41) driver genes, being propagated at the same AF in all mice passages. In these two models we identified other clones characterized by variants with AF <40% or AF>60% but not involving driver genes, thus defining both models as "monoclonal". The three models AML#20, AML#45 and AML#34 had an "expansion pattern", indicated in AML#20 by a clone harbouring *WT1* mutation that increase AF in mice models (from 50% to 100%); in AML#34 by an increase in the AF of a *FLT3* variant suggesting its clonal expansion in the PDXs (AF from 23 to 70%) and finally

in AML#45 by an *RB1* variant which was undetectable in patient's AML but increased at 50% in the PDXs. In the meanwhile, we recognized also a "loss pattern" of clonal dynamics¹⁸ characterized by the disappearance of the clones with variants in driver genes for AML#20 (original clone characterized by *WT1* and *NUP98* mutations has been lost) and for AML#34 (loss of subclone characterized by *KRAS* mutation). Noteworthy, all subclones lost in the AML#45 model were not characterized by mutations in driver genes.

This latter "loss pattern" observed in PDXs suggested those non functional AML clones that may be irrelevant in the disease relapse event. On the contrary, the "expansion pattern" enabled to detect minor rare clones, in some cases otherwise undetectable in patient's sample at diagnosis, that may play a critical role in leukemia progression. However further targeting studies *in vivo* will appoint specific roles to the propagated clones. In this scenario, clonal evolution studies in AML-PDXs could suggest targeted therapeutic interventions focused on the variants of selected clones, rather than focusing on targeting strategies specific for clones present only in the original AML at diagnosis.

In general, the detected genetic variants were not recurrent in our models but we underline recurrently mutated driver genes, known in AML, such as *RAS* (*KRAS* in AML#34 and AML#41 and *NRAS* in AML#30), *TET1* (AML#20 and AML#41), *TET2* (AML#20 and AML#34). Mutation in *RAS* gene are frequently reported in cancers and Ras proteins are essential components of signaling networks controlling cellular proliferation, differentiation, and survival⁵⁹. In particular, we identified canonical G13D (AML#34) and Q61A (AML#41) and Q61R (AML#30) Ras alterations. Mutations at Glycine 12-Glycine 13 (G12-G13) account for about 99% of the mutations described in cancer, and mutations affecting Glutamic acid 61 (Q61), account for the remaining 1%⁵⁹. In a recent work on pediatric AML, *NRAS* and *KRAS* mutations have been detected in 44% and 12% of patients respectively, and *NRAS* mutations have been reported mutually exclusive with *FLT3ITD* and *CKIT* mutations⁶⁰. Noteworthy, due to the difficult to directly hit Ras proteins for the lack of pockets for drug binding, researchers' focus upstream and downstream the Ras proteins trying to suppress its oncogenic signal⁶¹. Hence, recent

studies revealed new insights on the development of RAS targeting strategies⁶¹, such as the use of MEK or ERK inhibitors that will be further tested in our PDXs.

Regarding *TET* variants, it is a regulator of DNA methylation and in particular it converts 5mC to 5hmC, starting demethylation process. Notably, aberrations in genes related to DNA methylation are closely associated with tumor progression especially in blood cancers and in AML⁶². Deregulated methylation leads to hypermethylated CpG islands in the promoter region of different genes, causing the silencing of suppressor genes, the loss of cell apoptosis, proliferation, and differentiation control. On the contrary, hypomethylation of oncogenes enhances the tumorigenic potential of normal cells⁶³. *TET2* is the most frequently mutated gene in myelodysplastic syndromes (MDS)⁶⁴ and mutations in this gene have been reported in adult AML (7-23%), but resulted less frequent in pediatric AML (1.4%), with patient prognosis associated with *TET2* mutations requiring further studies to be dissected⁶⁵. Most of *TET2* mutations described in adult AML are inactivating mutations suggesting a possible role of this gene as tumor suppressor altering hematopoietic stem cell functions inducing epigenetic modifications⁶⁶. To note, Tet2 knockout in mice hematopoietic compartment has been associated with an expansion of stem cells with increased self-renewal capacity and a progressive myeloproliferation and defects in hematopoiesis⁶⁷. Interestingly, *TET2* mutations in adult AML have been often associated to *NPM1*, *FLT3-ITD*, *FLT3-TKD*, *JAK2*, *RUNX1*, *CEBPA*, *CBL*⁶⁶ and *KRAS* mutations as occurred in our samples that *TET2* mutation was associated to *CBL* in AML#45, and to *TET2*, *KRAS* and *FLT3* in AML#34. In light of these observations, a deeper investigation of identified *TET2* mutations to assess putative functional effects will drive further therapeutic strategy, including DNA Methyltransferases (DNMT) inhibitor (5-Azacitidine/Decitabine) or Histone deacetylases (HDAC) inhibitor (Vorinostat)¹ to be tested in PDXs.

Variants not detected in patients' AML but identified in PDXs are on *ARID1A* (AML#41 and AML#30) and *SLAIN1* (AML#41 and AML#45) genes. ARID family genes encodes for members of a large ATP-dependent chromatin remodeling complex, SNF/SWI, which is required for transcriptional activation of genes normally repressed by chromatin and it has been reported to be associated to hematopoietic process⁶⁸ and to cancer progression⁶⁹. *ARID1A* has been found mutated in a large number of patients with

ovarian cancer, and BET inhibitors have been reported to target *ARID1A* mutated cell lines and PDXs of ovarian cancer⁷⁰. To note, mutations in genes *ARID1A-ARID1B* and *ARID2* have been detected in PDXs expanded clones (AML#41 and AML#30) but also in AML founding clone (AML#41, AML#45 and AML#30), suggesting these genes as novel candidates to be investigated as potentially involved in AML. In light of these results, selected mutations are under investigation for their functional role and for the possibility to use novel targeted treatments. As a matter of fact, *ARID* variants have been detected in 3 *KMT2A* rearranged AML-PDXs opening for the possibility to perform a retrospective screening in a larger cohort of *KMT2A* rearranged samples to dissect this putative association.

Another interesting gene found recurrently mutated in clones expanded in PDXs is *SLAIN1* (PDX#41 and PDX#45). *SLAIN1* is a gene coding for microtubules end-tracking proteins, underlying important implication in cell cycle-specific regulation of microtubule dynamics^{71,72}. *SLAIN1* has not been previously associated to cancers but its role in controlling cell cycle push toward further characterization in AML⁷³.

A part from variants, transcriptomic profile of original AML was found clustering with profiles of paired PDXs. RNA sequencing allowed to find differential gene expression and to identify altered pathways in samples, or from patient' AML to matched PDXs, or among the PDXs. These comparisons will generate a lot of interesting results that will contribute to characterize our model and to detect AML vulnerabilities. In a preliminary differential gene expression analysis we identified an altered expression of genes of the G protein, SLC transporter, calcium homeostasis and mitochondrial electron transport chain, pathways that opened for tailored AML drug targeting. Drugs for targeting these pathways have been selected by using a refinement approach based on *in vitro* testing. At last, the predictive 3D co-cultures, previously set up in our laboratory³⁶, allowed to identify synergistic drug combinations with new agents and current drugs used for AML treatment (such as Cytarabine, Doxorubicine, and Venetoclax)^{36,74-76} that proceeded to AML-PDXs *in vivo* testing.

Here, we are proposing results of two new combination strategies for AML by using Asparaginase, Disulfiram, compounds little or never discussed in the pediatric AML

context^{34,77-80}, combined with Venetoclax, a drug that is not currently adopted in children with cancer, but that exerted a high interest for novel second line therapies⁸¹. We also successfully established a model of AML relapse *in vivo* by inducing the complete remission in AML-PDXs by a standard chemotherapy treatment, and waiting for an increase of the hCD45+ cells after treatment discontinuation, that identify the occurrence of a relapse event. Drug combinations here proposed have been tested in these models, supporting the use of AML-PDXs as a reliable and promising tool for further studies, where a large number of new drugs can be explored not only in the context of pediatric AML-PDXs at diagnosis, but also at relapse.

Overall, during my PhD, we aimed to identify and develop novel treatment strategies for AML and we required valid preclinical models. Thus, we obtained the successful establishment of AML-PDXs, able to faithfully recapitulate patients' AML complexity. These models represent a robust tool to test new therapeutic alternatives, that may be proposed in clinical trials in humans, and to perform a comprehensive understanding of disease biology.

In the next future, the possibility to obtain a larger panel of AML-PDXs and to perform more detailed multilevel genomic and epigenomic analysis will open for functional precision medicine approaches^{82,83}, and for tailoring therapies based on genomic characteristics to be exploited in "Basket trials", where patients with a specific genetic lesion, across a variety of tumor types, can be enrolled in the same trial.

REFERENCES

1. Kuhlen, M., Klusmann, J. H. & Hoell, J. I. Molecular Approaches to Treating Pediatric Leukemias. *Front. Pediatr.* **7**, 1–12 (2019).
2. de Rooij, J., Zwaan, C. & van den Heuvel-Eibrink, M. Pediatric AML: From Biology to Clinical Management. *J. Clin. Med.* **4**, 127–149 (2015).
3. Conneely, S. E. & Stevens, A. M. Acute Myeloid Leukemia in Children: Emerging Paradigms in Genetics and New Approaches to Therapy. *Curr. Oncol. Rep.* **23**, 16 (2021).
4. Fiorentini, A. *et al.* The Time Has Come for Targeted Therapies for AML: Lights and Shadows. *Oncol. Ther.* **8**, 13–32 (2020).
5. Elgarten, C. W. & Aplenc, R. Pediatric acute myeloid leukemia: Updates on biology, risk stratification, and therapy. *Curr. Opin. Pediatr.* **32**, 57–66 (2020).
6. Pearson, A. D. J. *et al.* Paediatric Strategy Forum for medicinal product development for acute myeloid leukaemia in children and adolescents: ACCELERATE in collaboration with the European Medicines Agency with participation of the Food and Drug Administration. *Eur. J. Cancer* **136**, 116–129 (2020).
7. Li, A. J., Dhanraj, J. P., Lopes, G. & Parker, J. L. Clinical trial risk in leukemia: Biomarkers and trial design. *Hematol. Oncol.* **39**, 105–113 (2021).
8. Dimasi, J. A., Reichert, J. M., Feldman, L. & Malins, A. Clinical approval success rates for investigational cancer drugs. *Clin. Pharmacol. Ther.* **94**, 329–335 (2013).
9. Horvath, P. *et al.* Screening out irrelevant cell-based models of disease. *Nat. Rev. Drug Discov.* **15**, 751–769 (2016).
10. Johnson, J. I. *et al.* Relationships between drug activity in NCI preclinical in vitro and in vivo models and early clinical trials. *Br. J. Cancer* **84**, 1424–1431 (2001).

11. Okada, Vaeteewoottacharn & Kariya. Application of Highly Immunocompromised Mice for the Establishment of Patient-Derived Xenograft (PDX) Models. *Cells* **8**, 889 (2019).
12. Fujii, E., Kato, A. & Suzuki, M. Patient-derived xenograft (PDX) models: Characteristics and points to consider for the process of establishment. *J. Toxicol. Pathol.* **33**, 153–160 (2020).
13. Hidalgo, M. *et al.* Europe PMC Funders Group Patient Derived Xenograft Models : An Emerging Platform for Translational Cancer Research. **4**, 998–1013 (2015).
14. Kunz, J. B. *et al.* PDX models recapitulate the genetic and epigenetic landscape of pediatric T-cell leukemia. 1–13 (2018). doi:10.15252/emmm.201809443
15. Wang, K. *et al.* Patient-derived xenotransplants can recapitulate the genetic driver landscape of acute leukemias. 151–158 (2017). doi:10.1038/leu.2016.166
16. Shi, J., Li, Y., Jia, R. & Fan, X. The fidelity of cancer cells in PDX models: Characteristics, mechanism and clinical significance. *Int. J. Cancer* **146**, 2078–2088 (2020).
17. Belderbos, M. E. *et al.* Clonal selection and asymmetric distribution of human leukemia in murine xenografts revealed by cellular barcoding. *Blood* **129**, 3210–3220 (2017).
18. Sandén, C. *et al.* Clonal competition within complex evolutionary hierarchies shapes AML over time. *Nat. Commun.* **11**, 1–10 (2020).
19. Byrne, A. T. *et al.* Interrogating open issues in cancer precision medicine with patient-derived xenografts. *Nat. Rev. Cancer* **17**, 254–268 (2017).
20. Masetti, R. *et al.* Genomic complexity and dynamics of clonal evolution in childhood acute myeloid leukemia studied with whole-exome sequencing. *Oncotarget* **7**, 56746–56757 (2016).
21. Bertuccio, S. N. *et al.* Exploiting clonal evolution to improve the diagnosis and treatment efficacy prediction in pediatric aml. *Cancers (Basel)*. **13**, 1–10 (2021).

22. Duque-Afonso, J. & Cleary, M. L. The AML salad bowl. *Cancer Cell* **25**, 265–267 (2014).
23. Morita, K. *et al.* Clonal evolution of acute myeloid leukemia revealed by high-throughput single-cell genomics. *Nat. Commun.* **11**, 1–17 (2020).
24. Farrar, J. E. *et al.* Genomic profiling of pediatric acute myeloid leukemia reveals a changing mutational landscape from disease diagnosis to relapse. *Cancer Res.* **76**, 2197–2205 (2016).
25. Petti, A. A. *et al.* Genetic and Transcriptional Contributions to Relapse in Normal Karyotype Acute Myeloid Leukemia. *Blood Cancer Discov.* **3**, 32–49 (2022).
26. Klco, J. M. *et al.* Functional heterogeneity of genetically defined subclones in acute myeloid leukemia. **25**, 379–392 (2015).
27. Wang, K. *et al.* Patient-derived xenotransplants can recapitulate the genetic driver landscape of acute leukemias. *Leukemia* **31**, 151–158 (2017).
28. Schmitz, M. *et al.* Xenografts of highly resistant leukemia recapitulate the clonal composition of the leukemogenic compartment. *Blood* **118**, 1854–1864 (2011).
29. Dworzak, M. N. *et al.* AIEOP-BFM consensus guidelines 2016 for flow cytometric immunophenotyping of Pediatric acute lymphoblastic leukemia. *Cytom. Part B - Clin. Cytom.* **94**, 82–93 (2018).
30. Kunz, J. B. *et al.* PDX models recapitulate the genetic and epigenetic landscape of pediatric T-cell leukemia. 1–13 (2018). doi:10.15252/emmm.201809443
31. Papaemmanuil, E. *et al.* Genomic Classification and Prognosis in Acute Myeloid Leukemia. **374**, 2209–2221 (2016).
32. Jaskulska, A., Janecka, A. E. & Gach-Janczak, K. Thapsigargin—from traditional medicine to anticancer drug. *Int. J. Mol. Sci.* **22**, 1–12 (2021).
33. Starling, A. P., East, J. M. & Lee, A. G. Stimulation of the Ca²⁺-ATPase of sarcoplasmic reticulum by disulfiram. *Biochem. J.* **320**, 101–105 (1996).

34. Chan, W. K. *et al.* Glutaminase activity of L-asparaginase contributes to durable preclinical activity against acute lymphoblastic leukemia. **18**, 1587–1592 (2020).
35. Heinz, S. *et al.* Mechanistic Investigations of the Mitochondrial Complex i Inhibitor Rotenone in the Context of Pharmacological and Safety Evaluation. *Sci. Rep.* **7**, 1–13 (2017).
36. Borella, G. *et al.* Targeting the plasticity of mesenchymal stromal cells to reroute the course of acute myeloid leukemia. *Blood* **138**, 557–570 (2021).
37. Wunderlich, M. *et al.* AML cells are differentially sensitive to chemotherapy treatment in a human xenograft model. *Blood* **121**, e90–e97 (2013).
38. Pearce, D. J. *et al.* AML engraftment in the NOD / SCID assay reflects the outcome of AML : implications for our understanding of the heterogeneity of AML. *Blood* **107**, 1166–73 (2006).
39. Wunderlich, M. *et al.* AML xenograft efficiency is significantly improved in NOD/SCID-IL2RG mice constitutively expressing human SCF, GM-CSF and IL-3. *Leukemia* **24**, 1785–1788 (2010).
40. Theocharides, A. P. A., Rongvaux, A., Fritsch, K., Flavell, R. A. & Manz, M. G. Humanized hemato-lymphoid system mice. *Haematologica* **101**, 5–19 (2016).
41. Her, Z. *et al.* An improved pre-clinical patient-derived liquid xenograft mouse model for acute myeloid leukemia. 1–14 (2017). doi:10.1186/s13045-017-0532-x
42. PV Sanchez¹, RL Perry, J. S. *et al.* A robust xenotransplantation model for acute myeloid leukemia. *Leukemia*
43. Miles, L. A. *et al.* Single-cell mutation analysis of clonal evolution in myeloid malignancies. *Nature* **587**, (2020).
44. Abarrategi, A. *et al.* Versatile humanized niche model enables study of normal and malignant human hematopoiesis. *J. Clin. Invest.* **127**, 543–548 (2017).
45. Schepers, K., Campbell, T. B. & Passegué, E. Normal and leukemic stem cell niches: Insights and therapeutic opportunities. *Cell Stem Cell* **16**, 254–267 (2015).

46. Bray, L. J. *et al.* A three-dimensional ex vivo tri-culture model mimics cell-cell interactions between acute myeloid leukemia and the vascular niche. *Haematologica* **102**, 1215–1226 (2017).
47. Krause, D. S. & Scadden, D. T. A hostel for the hostile: The bone marrow niche in hematologic neoplasms. *Haematologica* **100**, 1376–1387 (2015).
48. Crippa, S. & Bernardo, M. E. Mesenchymal Stromal Cells: Role in the BM Niche and in the Support of Hematopoietic Stem Cell Transplantation. *HemaSphere* **2**, e151 (2018).
49. Blanco, T. M., Mantalaris, A., Bismarck, A. & Panoskaltsis, N. The development of a three-dimensional scaffold for ex vivo biomimicry of human acute myeloid leukaemia. *Biomaterials* **31**, 2243–2251 (2010).
50. Hoggatt, J., Kfoury, Y. & Scadden, D. T. Hematopoietic Stem Cell Niche in Health and Disease. *Annu. Rev. Pathol. Mech. Dis.* **11**, 555–581 (2016).
51. Morrison, S. J. & Scadden, D. T. The bone marrow niche for haematopoietic stem cells. *Nature* **505**, 327–334 (2014).
52. Ugarte, F. & Forsberg, E. C. Haematopoietic stem cell niches: new insights inspire new questions. *EMBO J.* **32**, 2535–2547 (2013).
53. Wong, R. S. Y. & Cheong, S. K. Role of mesenchymal stem cells in leukaemia: Dr. Jekyll or Mr. Hyde? *Clin. Exp. Med.* **14**, 235–248 (2014).
54. Battula, V. L. *et al.* AML-induced osteogenic differentiation in mesenchymal stromal cells supports leukemia growth. *JCI Insight* **2**, (2017).
55. Corradi, G. *et al.* Mesenchymal stromal cells from myelodysplastic and acute myeloid leukemia patients display in vitro reduced proliferative potential and similar capacity to support leukemia cell survival. *Stem Cell Res. Ther.* **9**, (2018).
56. Pession, A. *et al.* Results of the AIEOP AML 2002/01 multicenter prospective trial for the treatment of children with acute myeloid leukemia. *Blood* **122**, 170–178 (2013).

57. Woiterski, J. *et al.* Engraftment of low numbers of pediatric acute lymphoid and myeloid leukemias into NOD/SCID/IL2Rc γ null mice reflects individual leukemogenecity and highly correlates with clinical outcome. *Int. J. Cancer* **133**, 1547–1556 (2013).
58. Choi, Y. Y. *et al.* Establishment and characterisation of patient-derived xenografts as preclinical models for gastric cancer. *Sci. Rep.* **6**, 1–12 (2016).
59. Fernández-Medarde, A. & Santos, E. Ras in cancer and developmental diseases. *Genes and Cancer* **2**, 344–358 (2011).
60. Kaburagi, T. *et al.* Clinical significance of RAS pathway alterations in pediatric acute myeloid leukemia. *Haematologica* **106**, 2624–2632 (2021).
61. Chen, K., Zhang, Y., Qian, L. & Wang, P. Emerging strategies to target RAS signaling in human cancer therapy. *J. Hematol. Oncol.* **14**, 1–23 (2021).
62. Thiede, C. Mutant DNMT3A: Teaming up to transform. *Blood* **119**, 5615–5617 (2012).
63. Wajed, S. A., Laird, P. W. & DeMeester, T. R. DNA methylation: An alternative pathway to cancer. *Ann. Surg.* **234**, 10–20 (2001).
64. Langemeijer, S. M. C. *et al.* Acquired mutations in TET2 are common in myelodysplastic syndromes. *Nat. Genet.* **41**, 838–842 (2009).
65. Li, M. J. *et al.* Tet oncogene family member 2 gene alterations in childhood acute myeloid leukemia. *J. Formos. Med. Assoc.* **115**, 801–806 (2016).
66. Weissmann, S. *et al.* Landscape of TET2 mutations in acute myeloid leukemia. *Leukemia* 934–942 (2012). doi:10.1038/leu.2011.326
67. Moran-Crusio, K. *et al.* Tet2 Loss Leads to Increased Hematopoietic Stem Cell Self-Renewal and Myeloid Transformation. *Cancer Cell* **20**, 11–24 (2011).
68. Han, L. *et al.* Chromatin remodeling mediated by ARID1A is indispensable for normal hematopoiesis in mice. *Leukemia* **33**, 2291–2305 (2019).

69. Xu, S. & Tang, C. The Role of ARID1A in Tumors: Tumor Initiation or Tumor Suppression? *Front. Oncol.* **11**, 1–18 (2021).
70. Berns, K. *et al.* ARID1A mutation sensitizes most ovarian clear cell carcinomas to BET inhibitors. *Oncogene* **37**, 4611–4625 (2018).
71. van der Vaart, B. *et al.* Microtubule plus-end tracking proteins SLAIN1/2 and ch-TOG promote axonal development. *J. Neurosci.* **32**, 14722–14728 (2012).
72. van der Vaart, B. *et al.* SLAIN2 links microtubule plus end-tracking proteins and controls microtubule growth in interphase. *J. Cell Biol.* **193**, 1083–1099 (2011).
73. Schnerch, D. *et al.* Cell cycle control in acute myeloid leukemia. *Am. J. Cancer Res.* **2**, 508–28 (2012).
74. Ma, C. *et al.* Leukemia-on-a-chip: Dissecting the chemoresistance mechanisms in B cell acute lymphoblastic leukemia bone marrow niche. *Sci. Adv.* **6**, (2020).
75. Tao, C., Zhang, G., Xiong, Y. & Zhou, Y. Functional dissection of synaptic circuits : in vivo patch-clamp recording in neuroscience. **9**, 1–8 (2015).
76. Zhang, B. *et al.* Altered microenvironmental regulation of leukemic and normal stem cells in chronic myelogenous leukemia. *Cancer Cell* **21**, 577–92 (2012).
77. Willems, L. *et al.* Inhibiting Glutamine uptake represents an attractive new strategy for treating acute myeloid leukemia. *Blood* **122**, 3521–3532 (2013).
78. Xu, B. *et al.* Disulfiram/copper selectively eradicates AML leukemia stem cells in vitro and in vivo by simultaneous induction of ROS-JNK and inhibition of NF- κ B and Nrf2. *Cell Death Dis.* **8**, e2797 (2017).
79. Panina, S. B., Pei, J., Baran, N., Konopleva, M. & Kirienko, N. V. Utilizing Synergistic Potential of Mitochondria-Targeting Drugs for Leukemia Therapy. *Front. Oncol.* **10**, (2020).
80. Liu, F. *et al.* Cotargeting of mitochondrial complex i and bcl-2 shows antileukemic activity against acute myeloid leukemia cells reliant on oxidative phosphorylation. *Cancers (Basel)*. **12**, 1–19 (2020).

81. Tregnago, C. *et al.* Novel Compounds Synergize With Venetoclax to Target KMT2A-Rearranged Pediatric Acute Myeloid Leukemia. *Front. Pharmacol.* **12**, 1–14 (2022).
82. Letai, A., Bholá, P. & Welm, A. L. Functional precision oncology: Testing tumors with drugs to identify vulnerabilities and novel combinations. *Cancer Cell* **40**, 26–35 (2022).
83. Chantal Pauli^{1, 2, 10,†}, Benjamin D. Hopkins^{5,†}, Davide Prandi⁶, Reid Shaw⁷, Tarcisio Fedrizzi⁶, Andrea Sboner^{1, 4, 5}, Verena Sailer^{1, 2}, Michael Augello^{1, 5}, Loredana Puca¹, Rachele Rosati⁷, Terra J. McNary¹, Yelena Churakova¹, Cynthia Cheung¹, Joanna Tr, and M. A. R. Personalized In Vitro and In Vivo Cancer Models to Guide Precision Medicine. *Cancer Discov IF 26* **47**, 549–562 (2017).

ABOUT THE AUTHOR

Publications

1. Tregnago C, Benetton M, **Da Ros A**, Borella G, Longo G, Polato K, Francescato S, Biffi A and Pigazzi M. “Novel compounds synergize with venetoclax to target KMT2A-rearranged acute myeloid leukemia” *Frontiers in Pharmacology* (2021)-doi.org/10.3389/fphar.2021.820191. *Frontiers in Pharmacology* IF 2020: 5.810

2. Borella G, **Da Ros A**, Borile G, Porcù E, Tregnago C, Benetton M, Marchetti A, Bisio V, Montini B, Michielotto B, Cani A, Leszl A, Campodoni E, Sandri M, Montesi M, Bresolin S, Cairo S, Buldini B, Locatelli F, Pigazzi M. “Targeting mesenchymal stromal cells plasticity to reroute acute myeloid leukemia course” *Blood* (2021) PMID: 34010415. *Blood* IF 2020: 23.62

3. Porcù E*, Benetton M*, Bisio V*, (*Authors contributed equally to the manuscript) **Da Ros A**, Tregnago C, Borella G, Zanon C, Bordi M, Germano G, Manni S, Campello S, Rao DS, Locatelli F, Pigazzi M. “The long non-coding RNA CDK6-AS1 overexpression impacts on acute myeloid leukemia differentiation and mitochondrial dynamics” *iScience*(2021) PMID: 34816103. *iScience* IF 2020: 5.458

4. Tregnago C, **Da Ros A**, Porcu E, Benetton M, Simonato M, Simula L, Borella G, Polato K, Minuzzo S, Borile G, Cogo P, Campello S, Massi A, Romagnoli R, Buldini B, Locatelli F and Pigazzi M. “Thioridazine requires calcium influx to induce MLL-AF6 rearranged AML cell death” *.Blood Adv* (2020) PMID: 32931582. *Blood Adv* IF 2021: 6.799

5. Tregnago C, Benetton M, Padrin D, Polato K, Borella G, **Da Ros A**, Marchetti A, Porcù E, Del Bufalo F, Mecucci C, Locatelli F, Pigazzi M. “NPM1 Mutational Status Underlines Different Biological Features in Pediatric AML” *Cancers* (2021) PMID: 34298672 *Cancers* IF 2020: 6.639

Abstract

2022:

SIES

A. Da Ros , V. Indio , E. Porcù, G. Borella , M. Benetton , C. Tregnago , S. Cairo , B. Michielotto, S. Bresolin , B. Buldini , A. Pession, F. Locatelli, M. Pigazzi . Pediatric Acute Myeloid Leukemia Patient Derived Xenografts:development and characterization of preclinical *in vivo* models for the identification and testing of new therapeutic approaches. XVII Congresso Nazionale SIES. Roma, 31 March-2 April 2022. **Oral Presentation**

2021:

CLLS:

Tregnago C, Porcù E, **Da Ros A**, Benetton M, Simonato M, Borella G, Borile G, Buldini B, Locatelli F, Pigazzi M. Thioridazine induces calcium overload being toxic for KDM2A-AFDN rearranged acute myelogenous leukemia. The 12th Biennial Childhood Leukemia and Lymphoma Symposium. 11-12 March 2021. Virtual.

Benetton M, Porcù E, **Da Ros A**, Bordi M, Borella G, Germano G, Tregnago C, Campello S, Locatelli F, Pigazzi M. The CDK6-AS1 controls a novel transcriptional circuit involved in myeloid differentiation and chemotherapy sensitivity of pediatric acute myeloid leukemia (AML). The 12th Biennial Childhood Leukemia and Lymphoma Symposium. 11-12 March 2021. Virtual.

AIEOP:

Tregnago C , Benetton M, Padrin D, Polato K, Borella G, **Da Ros A**, Marchetti A, Porcù E, Del Bufalo F, Mecucci C, Locatelli F, Pigazzi M. Lo stato mutazionale di NPM1 media caratteristiche biologiche peculiari della LAM, e può contribuire a una ulteriore sottoclassificazione dei pazienti. XLVI Congresso Nazionale AIEOP. 3-8 ottobre 2021. Virtual.

Oral presentation: Best Five Abstract 3 ottobre 2021, Brescia,Italy

Da Ros A, Indio V, Porcù E, Borella G, Benetton M, Tregnago C, Cairo S, Michielotto B, Bresolin S, Buldini B, Pession A, Locatelli F, Pigazzi M. LAM-patient derived xenograft (PDX): sviluppo e caratterizzazione di modelli preclinici in vivo per l'identificazione e la sperimentazione di nuovi approcci terapeutici. XLVI Congresso Nazionale AIEOP. 3-8 ottobre 2021. Virtual.

2020:

ASH:

Pigazzi M, Benetton M, Walter C, Hansen M, Skou A, **Da Ros A**, Marchetti A, Polato K, Belloni M, Tregnago C, Abrahamsson J, Fogelstrand L, Von Neuhoff N, Reinhardt D, Hasle H, Locatelli F, Merli P. Impact of minimal residual disease (MRD) assessed before transplantation on the outcome of children with acute myeloid leukemia given an allograft: a retrospective study by the I-BFM study group. 62nd ASH Annual Meeting. December 5-8, 2020. Virtual.

AIEOP:

Benetton M, Marchetti A, Tregnago C, **Da Ros A**, Polato K, Borella G, Porcù E, Varotto E, Lo Nigro L, Masetti R, Buldini B, Rizzari C, Fagioli F, Biffi A, Locatelli F, Pigazzi M. Nuove mutazioni ricorrenti possono migliorare la stratificazione dei pazienti alla diagnosi di leucemia mieloide acuta. XLV Congresso Nazionale AIEOP. Brescia,Italy. 25-27 ottobre 2020.

Marchetti A, Benetton M, Polato K, **Da Ros A**, Borella G, Porcù E, Francescato S, Tregnago C, Menna G, Santoro N, Merli P, Zecca M, Pession A, Biffi A, Locatelli F, Pigazzi M. La malattia residua minima molecolare come strumento di identificazione precoce di recidiva nella leucemia acuta mieloide. XLV Congresso Nazionale AIEOP. Brescia,Italy. 25-27 ottobre 2020.

Porcù E, Benetton M, Bisio V, **Da Ros A**, Tregnago C, Borella G, Zanon C, Montini B, Marchetti A, Germano G, Campello S, Locatelli F, Pigazzi M. L'overespressione del lncRNA CDK6-AS1 identifica un nuovo sottotipo di LAM altamente sensibile a farmaci anti-mitochondriali. XLV Congresso Nazionale AIEOP. Brescia,Italy. 25-27 ottobre 2020.

Borella G, **Da Ros A**, Porcù E, Borile G, Benetton M, Marchetti A, Montini B, Cani A, Bresolin S, Tregnago C, Michielotto B, Leszl A, Buldini B, Locatelli F, Pigazzi M. Caratterizzazione di cellule mesenchimali stromali derivate da pazienti pediatrici con leucemia mieloide acuta in un modello tridimensionale. XLV Congresso Nazionale AIEOP. Brescia,Italy. 25-27 ottobre 2020.

Pigazzi M, Benetton M, Walter C, Hansen M, Skou A, **Da Ros A**, Marchetti A, Polato K, Belloni M, Tregnago C, Abrahamsson J, Fogelstrand L, Von Neuhoff N, Reinhardt D, Hasle H, Locatelli F, Merli P. Impatto della malattia residua minima pre-trapianto sull'outcome dei bambini affetti da leucemia mieloide acuta: uno studio retrospettivo del gruppo di studio I-BFM. XLV Congresso Nazionale AIEOP. Brescia,Italy. 25-27 ottobre 2020. Oral presentation.

EHA:

Benetton M. , Porcù E , Da Ros A , Bisio V , Bordi M , Zanon C, Borella G, Germano G , Manni S, Tregnago C , Campello S , Rao D , Locatelli F, Pigazzi M The CDK6-AS1 controls a novel transcriptional circuit involved in myeloid differentiation and chemotherapy sensitivity of pediatric acute myeloid leukemia (AML). 25th EHA congress – Virtual. June 11-21, 2020.

Porcù E, Tregnago C, Da Ros A, Benetton M, Simonato M, Simula L, Borella G, Polato K, Minuzzo S, Borile G, Cogo P, Campello S, Massi A, Romagnoli R, Buldini B, Locatelli F, Pigazzi M. Thioridazine induces calcium overload being toxic for KDM2A-AFDN rearranged acute myelogenous leukemia. 25th EHA congress – Virtual. June 11-21, 2020.

2019:

ASH:

Bisio V, Benetton M, Porcù E, Bordi M, Zanon C, Borella G, **Da Ros A**, Germano G, Manni S, Tregnago C, Campello S, Rao DS, Locatelli F, Pigazzi M. The Long Noncoding RNA BALR2 Controls Novel Transcriptional Circuits Involved in Chemotherapy Sensitivity of

Pediatric Acute Myeloid Leukemia (AML) Blasts. 61 st ASH Annual Meeting, Orlando, FL. December 07-10, 2019.

Borella G, Da Ros A, Porcù E, Tregnago C, Benetton M, Bisio V, Campodoni E, Panseri S, Sandri M, Montesi M, Cairo S, Locatelli F, Pigazzi M. Acute Myeloid Leukemia (AML) In A 3D Bone Marrow Niche Showed High Performance For In Vitro And In Vivo Drug Screenings. 61 st ASH Congress Orlando, FL. December 07-10, 2019. Oral presentation.

AIEOP:

Benetton M, Tregnago C, **Da Ros A**, Polato K, Merli P, Buldini B, Rizzari C, Fagioli F, Pession A, Biffi A, Locatelli F, Pigazzi M. Studio del ruolo della Malattia Residua Minima Molecolare nei pazienti con leucemia mieloide acuta arruolati nel protocollo LAM2013/01. XLIV Congresso Nazionale AIEOP. Catania, Italy. 13 ottobre 2019. Oral presentation among the 5 best abstracts.

Tregnago C, Benetton M, Porcù E, **Da Ros A**, Borella G, Masetti R, Merli P, Zecca M, Santoro N, Biffi A, Locatelli F, Pigazzi M. Tioridazina: farmaco efficace e selettivo per la leucemia mieloide acuta con riarrangiamento t(6;11). XLIV Congresso Nazionale AIEOP. Catania, Italy. 13 ottobre 2019.

Da Ros A, Porcù E, Borella G, Benetton M, Tregnago C, Cairo S, Michielotto B, Buldini B, Masetti R, Mastronuzzi A, Biffi A, Locatelli F, Pigazzi M. Sviluppo di modelli preclinici in vivo di Leucemia Acuta Mieloide pediatrica per lo screening di nuovi farmaci. XLIV Congresso Nazionale AIEOP. Catania, Italy. 13 ottobre 2019.

EHA:

Borella G, Bisio V, **Da Ros A**, Tregnago C, Benetton M, Campodoni E, Panseri S, Sandri M, Montesi M, Cairo S, Locatelli F, Pigazzi M. Development of Innovative Preclinical in Vitro and In Vivo Tools for an Effective therapeutic strategy in pediatric acute myeloid leukemia. 24th EHA meeting. Amsterdam, Netherlands. June 13-16, 2019.

ESH:

Borella G, Bisio V, **Da Ros A**, Tregnago C, Benetton M, Panseri S, Montesi M, Cairo S, Locatelli F, Pigazzi M. Development of innovative preclinical in vitro and in vivo tools for an effective therapeutic strategy in pediatric acute myeloid leukemia. 3rd Scientific Workshop on Tumor Microenvironment in the Hematological Malignancies and its Therapeutic Targeting. London, England. February 24-26, 2019.

ACKNOWLEDGEMENTS

I would like to express my gratitude to my supervisor Martina Pigazzi, who guided me throughout my PhD project.

I wish to extend my sincere thanks to all her team members for their contributions to this study.

This work was possible thanks to the important contribution of AIRC (Associazione Italiana per la Ricerca sul Cancro, project AIRC-IG Martina Pigazzi), and AIL (Associazione italiana contro le leucemie-linfomi e mieloma, sezione di Treviso).